Technische Universität München
Institut für Energietechnik

Professur für Thermofluiddynamik

On the efficient numerical modeling of nonlinear self-excited thermoacoustic oscillations

Stefan Jaensch

Vollständiger Abdruck der von der Fakultät für Maschinenwesen der Technischen Universität München zur Erlangung des akademischen Grades eines

DOKTOR – INGENIEURS

genehmigten Dissertation.

Vorsitzender:
Prof. Dr.-Ing. Florian Holzapfel
Prüfer der Dissertation:
Prof. Wolfgang Polifke, Ph.D.
Prof. Dr.-Ing. habil. Boris Lohmann

Die Dissertation wurde am 21.11.2016 bei der Technischen Universität München eingereicht und durch die Fakultät für Maschinenwesen am 23.02.2017 angenommen.

Abstract

This thesis discusses the modeling of self-excited thermoacoustic oscillations. On the one hand two different types of hybrid CFD/low-order models are investigated. These models resolve the flame and its immediate vicinity with reactive flow simulations. The acoustic field is modeled via a coupled acoustic low-order model. One of the hybrid CFD/low-order models resolve the flame with a fully compressible and reactive CFD simulation. So called Characteristic Based State-Space Boundary Conditions (CBSBC), which have been developed within this thesis, are used to couple the simulation via characteristic wave amplitudes to the acoustic low-order model. The other hybrid CFD/low-order model investigated resolves the flame with a low-Mach CFD simulation. Here, the coupling is based on the fluctuations of a reference velocity and of the global heat release rate. A cross-validation in terms of a bifurcation analysis shows good agreement between the two models. This corroborates that premixed flame respond predominantly to fluctuations of the upstream velocity and that the most important nonlinearities can be attributed to hydrodynamic effects and flame kinematics.

Hybrid CFD/low-order models describe thermoacoustic oscillations accurately and reduce the computational costs significantly compared to fully compressible simulations of the whole domain. However, the computational effort is still considerable. Therefore, on the other hand, nonlinear extensions of the CFD/system identification (SI) approach are investigated. The CFD simulation is forced with a broadband, high-amplitude signal and the time series of the fluctuations of the reference velocity and of the global heat release rate are collected. Thereafter, system identification is applied in order to obtain nonlinear low-order models. Artificial neural networks are used as nonlinear model structure. It is found that these models can reproduce the forced response up to a certain amplitude level. The nonlinear low-order models are then combined with a thermoacoustic network model in order to model the self-excited thermoacoustic oscillations. Unfortunately, the oscillations predicted differ significantly from the ones pre-

dicted by the hybrid models. Theoretically, good agreement can be achieved, if sufficiently long time series are available. Our analysis indicates that generating sufficiently long time series is prohibitively expensive. Hybrid CFD/low-order models, such as those developed in the present thesis, appear to be more promising. It is expected that with this methodology it is possible to simulate self-excited thermoacoustic oscillations with high accuracy and reasonable computational effort.

Contents

Abstract **ii**

Acknowledgment **vi**

List of supervised Students **vii**

1 Introduction **1**

2 A few words on systems theory **5**
2.1 Continuous-time models 6
2.2 Discrete-time models 10

3 System identification **13**
3.1 Setting up the CFD simulation 14
3.2 Running the simulation 14
3.3 Post-processing of the time series collected 14
3.4 Fit a model to the data 15
3.5 Validation of the model 16

4 Modeling of thermoacoustic oscillations **19**
4.1 Modeling of the acoustics 20
4.2 Modeling of the flame dynamics 22

5 Summary of achievements and papers **25**
5.1 PAPER-GREYBOX 26
5.2 PAPER-CBSBC 27
5.3 PAPER-HYBRID 28
5.4 PAPER-ANN 29

6 Outlook **31**

Bibliography **33**

Appendices

A.1 PAPER-GREYBOX 41
A.2 PAPER-CBSBC 51
A.3 PAPER-HYBRID 66
A.4 PAPER-ANN 74

Acknowledgment

The financial support from the Research Association for Combustion Engines (Forschungsvereinigung Verbrennungskraftmaschinen e. V. – FVV, project number: 6011150) is gratefully acknowledged. The author gratefully acknowledge the Gauss Center for Supercomputing e.V. (www.gauss-centre.eu) for funding this project by providing time on the GCS Supercomputer SuperMUC at Leibniz Supercomputing Centre (LZZ, www.lrz.de).

List of supervised Students

Student	Type	Year	Topic
Tristan Fehling	Term Paper	2013	Implementation and analysis of linear system identification methods
Anna Kohl	Term Paper	2013	Application of linear parameter varying systems for the identification of the flame transfer function
Max Meindl	Term Paper	2014	Parameter study on the identifiability of thermoacoustic network models
Yupeng Qin	Term Paper	2015	Parameter study of the direct numerical simulation of a laminar premixed flame
Diqing Chang	Term Paper	2015	Investigation of the influence of the excitation signal on the identification of thermoacoustic systems
Johannes Probst	Diploma thesis	2014	Implementation of an adaptive mesh refinement algorithm for the simulation of laminar premixed flames with OpenFOAM
Michael Redhead	Bachelor thesis [1]	2014	System identification of Wiener-models using BFGS updated strategy
Estefania Vila Lusquinos	Master thesis [2]	2015	Design of unknown input observers for acoustic network models
Dongjing Xu	Internship	2015/2016	Simulation of thermoacoustic oscillations with OpenFOAM
Hajer Ben Charrada	HiWi	2013/2014	–
Igor Tominec	HiWi	2015	–
Arvind Bharathi	Internship	2012	–
Max Meindl	HiWi	2014/2015	–
Michael Leipold	Internship	2015	–

1 Introduction

"Thermoacoustic instabilities are a cause for concern in combustion applications as diverse as small household burners, gas turbines and rocket engines" [1–10]. A self-amplifying feedback between an unsteady heat source and the surrounding acoustic field yields large oscillations of the flow variables. These oscillations can reach amplitude levels at which they cause serious damage to the engine. For the case of a perfectly premixed flame, the fundamental mechanism is illustrated and explained in Fig. 1.1. As noted by Culick et al. [11], thermoacoustic instabilities have been observed during the development of practically all rocket engines. In gas turbine combustion chambers thermoacoustic oscillations limit the operational flexibility [12, 13]. Giacomazzi [12] discuss the problems occurring when gas turbines are used as backup solution for renewable power plants, such as wind turbines or solar power plants. For this purpose gas turbines have to compensate the unsteady power generation of the renewable power plants and therefore, have to adjust their operating condition quickly and flexibly.
A well established method to describe thermoacoustic instabilities is linear stability analysis [14–18]. This methodology allows to predict stable and unstable operating ranges. A generic stability map is shown in Fig. 1.2. Typically, it is assumed that the stable operating range is acceptable and that the unstable operating range should be avoided. This, however, is a very conservative assumption. As indicated in Fig. 1.2, according to the linear analysis small perturbations decay exponentially in the stable regime and grow exponentially in the unstable regime. Theoretically, according to the linear stability analysis, small perturbations grow to infinity in the unstable regime. Obviously, this is unphysical. In real engines nonlinear effects will become important and the engine exhibits a thermoacoustic oscillations with a finite amplitude. If this amplitude is below a certain threshold, the oscillation will not damage the engine. Hence, knowing the oscillation amplitude allows to extend the operating range of the engine. Therefore, the main objective of this thesis is the development of methods to predict the amplitude of self-excited thermoacoustic oscillations.

Thermoacoustic oscillation can be very complex. Kabiraj et al. [19] observed periodic, aperiodic and chaotic oscillations as well as hysteresis while studying a laminar premixed flame. Such complex oscillations can only be described with nonlinear models. For gas turbine engines the two most important nonlinear effects are the nonlinear flame dynamics [20–22] and nonlinear acoustic damping [23, 24]. The present thesis focuses on modeling the nonlinear flame dynamics. The most common model is the flame describing function[3] (FDF) proposed by Dowling [25]. Noiray et al. [26] demonstrated that an FDF combined with a linear model for the acoustics can predict limit cycle amplitudes, mode switching and instability triggering with good accuracy. The configuration investigated was a laminar matrix burner. With the FDF it is also possible to model thermoacoustic oscillations of turbulent combustors (see e.g. [27, 28]). The FDF framework has two significant drawbacks: (1) It can describe only harmonic limit cycles, i.e. thermoacoustic oscillations with a single dominant frequency. More complex types of oscillations cannot be predicted. (2) It is very expensive to determine an FDF. Commonly, a given configuration is forced with harmonic signals at a large number of frequencies and amplitudes [26]. This procedure can in principle be applied to experimental [26, 27] as well as to simulated flames [29–32]. However, this approach is prohibitively expensive for large parameter studies in industrial applications. A detailed discussion on other nonlinear models proposed is provided in Sec. 4.2.

The methods investigated in this thesis aim to overcome both issues. On the one hand, in PAPER-CBSBC and PAPER-HYBRID, hybrid CFD/low-order models are investigated: The flame is simulated with a computational fluid dynamics (CFD) solver, which is coupled to a linear model of the acoustics. These models can describe self-excited thermoacoustic oscillations accurately, and reduce the effort compared to a CFD simulation of the whole configuration significantly. The novelty of the hybrid formulations developed in the present thesis is their consistency, (no spurious waves are generated), and their robustness and flexibility (complex impedances can be imposed and the formulation works for laminar as well as for turbulent flows). However, the hybrid models are still expensive. Therefore, on the other hand, CFD/system identification (SI) [33] approach is investigated: a transient simulation is forced with a broadband signal and time series are collected from which low-order model are deduced via system identification. In PAPER-GREYBOX linear grey-box models are discussed,

[3] A describing function is a frequency response which depends on the amplitude of the excitation signal (see also Sec. 4.2).

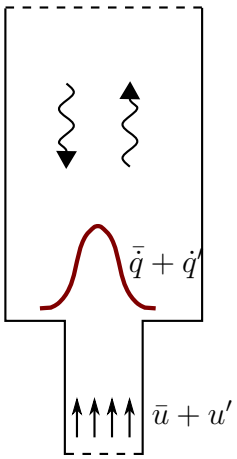

Figure 1.1: Thermoacoustic coupling: A perturbation u' of the mean flow velocity $\bar{u}$ causes a fluctuation $\dot{q}'$ of the mean heat release rate $\bar{\dot{q}}$. The additional heat yields an expansion of the gas surrounding the flame. Thus, the flame acts as an unsteady volume source and consequently as a sound source. The acoustic waves emitted, are reflected at the combustion chamber walls and again cause a perturbation u' of the mean flow at the flame base. This closes the feedback.

which allow among other things to estimate the heat release rate fluctuations from acoustic measurements only. Following the work of Selimefendigil et al. [34–36] in PAPER-ANN a nonlinear extension of the CFD/SI approach is investigated. Artificial neural networks (ANN) are used to model the nonlinear dynamics of a laminar premixed flame. In theory, when very long time series are available, the ANN identified should represent the CFD model accurately. The uncertainty of the prediction made by the models identified is assessed. The results indicated that generating sufficiently long time series is prohibitively expensive and that more sophisticated models are required.
The remainder of this thesis is organized as follows: In Chap. 2 some fundamental properties of dynamical systems are derived and discussed. System identification is discussed in detail in Chap. 3. Chap. 4 focuses on the modeling of thermoacoustic oscillations. In Chap. 5 the publications contributing to this thesis are summarized.

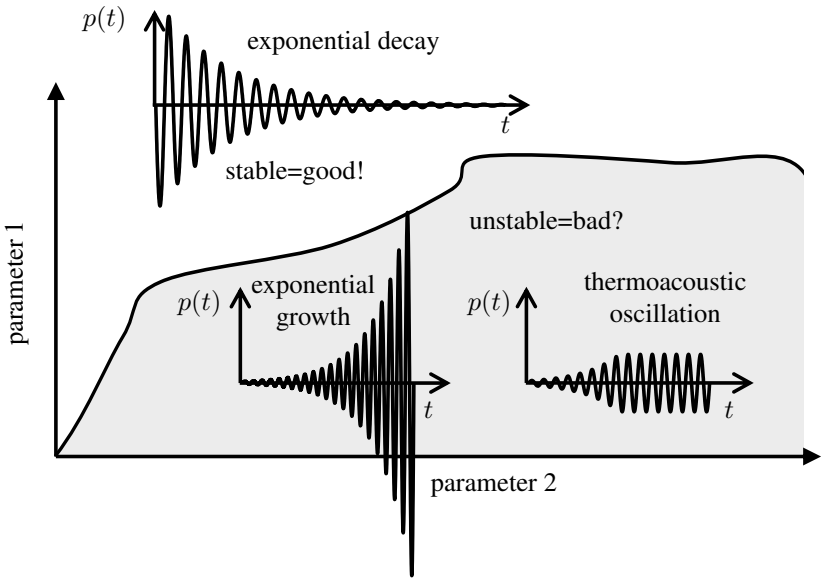

Figure 1.2: Generic example of a linear stability map and possible types of oscillations occurring in the stable and in the unstable regime.

2 A few words on systems theory

The present thesis builds on a system theoretic perspective of the modeling of thermoacoustic oscillations. This perspective has been developed over the last decades by several authors. The most important results of systems theory are discussed in the present chapter. A detailed review of the literature related to thermoacoustics is provided in Chap. 4. The material discussed in the present chapter is well known to the systems theory community and can be found in a large number of books. The author of the present thesis used the books by Lunze [37, 38].
In Fig. 2.1 a generic dynamical system $\mathbf{G}$ is shown. It connects m *inputs* $\mathbf{u}(t) = [u_1(t), \ldots, u_m(t)]^T$ and p *outputs* $\mathbf{y}(t) = [y_1(t), \ldots, y_p(t)]^T$. Mathematically, we write this as

$$\mathbf{y}(t) = \mathbf{G} \circ \mathbf{u}(t).$$

$\mathbf{G}$ denotes the *operator* of the system and t the time. The symbol "$\circ$" describes the dynamic mapping of the inputs $\mathbf{u}$ to the outputs $\mathbf{y}$ via the operator $\mathbf{G}$.
The most general classification of systems is between *linear* and *nonlinear* systems. Linear systems fulfill the principle of additivity

$$\mathbf{G} \circ (\mathbf{u}_1 + \mathbf{u}_2) = \mathbf{G} \circ \mathbf{u}_1 + \mathbf{G} \circ \mathbf{u}_2,$$

and the principle of homogeneity

$$\mathbf{G} \circ (\alpha \mathbf{u}) = \alpha \left(\mathbf{G} \circ \mathbf{u} \right).$$

If at least one of these principles is violated the system is called *nonlinear*. This is the only common feature of nonlinear systems and thus, these systems are hard to characterize in general. Indeed, an large eddy simulation (LES) solver can be considered as a nonlinear system. In the present work, we will discuss the flame dynamics as a specific type of nonlinear systems in Sec. 4.2. Within the present chapter we focus the discussion on linear systems.

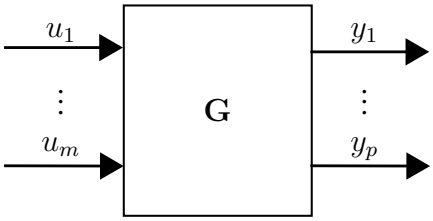

Figure 2.1: Generic dynamical system

2.1 Continuous-time models

A linear system can be represented without loss of generality in state-space form:

$$\dot{\mathbf{x}} = \mathbf{A}\mathbf{x} + \mathbf{B}\mathbf{u}, \tag{2.1}$$

$$\mathbf{y} = \mathbf{C}\mathbf{x} + \mathbf{D}\mathbf{u}, \tag{2.2}$$

with the *system matrices* $\mathbf{A} \in \mathbb{R}^{n\times n}, \mathbf{B} \in \mathbb{R}^{n\times m}, \mathbf{C} \in \mathbb{R}^{p\times n}, \mathbf{D} \in \mathbb{R}^{p\times m}$ and the *state-vector* $\mathbf{x} \in \mathbb{R}^{n\times 1}$. Here, n is the *order* of the system. The system matrices can be determined in manifold ways. In PAPER-CBSBC an overview of the most appropriated approaches to obtain these matrices for thermoacoustic systems is provided, written by the author of the present thesis.
A state-space model is not a unique representation of a specific system. We can introduce a transformation matrix $\mathbf{T} \in \mathbb{R}^{n\times n}$ with full rank and define the transformation

$$\mathbf{x} = \mathbf{T}\mathbf{z}.$$

Inserted in (2.1) this yields

$$\dot{\mathbf{z}} = \mathbf{T}^{-1}\mathbf{A}\mathbf{T}\mathbf{z} + \mathbf{T}^{-1}\mathbf{B}\mathbf{u},$$
$$\mathbf{y} = \mathbf{C}\mathbf{T}\mathbf{z} + \mathbf{D}\mathbf{u}.$$

For example, such a transformation can represent a transformation of units or a reordering of equations. All system matrices are changed, while the system still describes the same physics. Consequently, many properties (e.g. stability, transfer behavior) of the model are preserved. Please note that although the system describes the same physics, the transformation can change its numerical properties significantly.
A linear state-space model is essentially a system of ordinary differential equations (ODE). A large number of properties can be deduced from this perspective. The solution of the ODE can be found with the matrix exponential function

given as

$$e^{\mathbf{A}t} = I_n + \mathbf{A}t + \frac{\mathbf{A}^2}{2!}t^2 + \frac{\mathbf{A}^3}{3!}t^3 + \ldots,$$

with the identity matrix $\mathbf{I}_n \in \mathbb{R}^{n\times n}$. An important property of the matrix exponential function is that for a diagonal matrix $\mathbf{\Lambda}$ with the values λ_i on the diagonal the matrix exponential function can be calculated according to

$$e^{\mathbf{\Lambda}t} = \begin{bmatrix} e^{\lambda_1} & & \\ & \ddots & \\ & & e^{\lambda_n} \end{bmatrix}.$$

Its inverse is

$$\left(e^{\mathbf{A}t}\right)^{-1} = e^{-\mathbf{A}t},$$

and the temporal derivative is given as

$$\frac{d}{dt}e^{\mathbf{A}t} = \mathbf{A}e^{\mathbf{A}t} = e^{\mathbf{A}t}\mathbf{A}.$$

In order to solve the ODE we use the ansatz

$$\mathbf{x}(t) = e^{\mathbf{A}t}\mathbf{k}(t). \tag{2.4}$$

Inserting this expression in Eq. (2.1) yields

$$\begin{aligned} \dot{\mathbf{x}} &= \mathbf{A}e^{At}\mathbf{k} + \mathbf{B}\mathbf{u} = \mathbf{A}e^{\mathbf{A}t}\mathbf{k} + e^{\mathbf{A}t}\dot{\mathbf{k}} \\ &\Rightarrow \dot{\mathbf{k}} = \left(e^{\mathbf{A}t}\right)^{-1}\mathbf{B}\mathbf{u} = e^{-\mathbf{A}t}\mathbf{B}\mathbf{u}(t) \\ &\Rightarrow \mathbf{k}(t) = \mathbf{k}(0) + \int_0^t e^{-\mathbf{A}\tau}\mathbf{B}\mathbf{u}(\tau)d\tau. \end{aligned}$$

Together with Eq. (2.4) and the initial condition $\mathbf{k}(0) = \mathbf{x}_0$ we obtain

$$\mathbf{x}(t) = e^{\mathbf{A}t}\mathbf{x}_0 + \int_0^t e^{\mathbf{A}(t-\tau)}\mathbf{B}\mathbf{u}(\tau)d\tau + \mathbf{D}\mathbf{u}(t).$$

Considering the output equation (2.2) of the state-space model this yields the general solution of (2.1)

$$\mathbf{y}(t) = \mathbf{C}e^{\mathbf{A}t}\mathbf{x}_0 + \int_0^t \mathbf{C}e^{\mathbf{A}(t-\tau)}\mathbf{B}\mathbf{u}(\tau)d\tau + \mathbf{D}\mathbf{u}(t). \tag{2.6}$$

The system matrix $\mathbf{A}$ can be decomposed according to

$$\mathbf{A} = \mathbf{V}\mathbf{\Lambda}\mathbf{V}^T.$$

Here, $\mathbf{V}$ is a matrix containing the eigenvectors of $\mathbf{A}$. In the scope of this tutorial we restricted the discussion to eigenvalues with an algebraic multiplicity of one. Thus, $\mathbf{\Lambda}$ is a diagonal matrix with the eigenvalues λ_i on the diagonal. Using $\mathbf{V}$ as transformation matrix, the general solution (2.6) of the state-space model becomes

$$\begin{aligned}\mathbf{y}(t) &= \mathbf{C}\mathbf{V}e^{\mathbf{V}^T\mathbf{A}\mathbf{V}t}V\mathbf{x}_0 + \int_0^t \mathbf{C}\mathbf{V}e^{\mathbf{V}^\mathbf{T}\mathbf{A}\mathbf{V}(t-\tau)}\mathbf{V}^T\mathbf{B}\mathbf{u}(\tau)d\tau + \mathbf{D}\mathbf{u}(t) \\ &= \mathbf{C}\mathbf{V}e^{\mathbf{\Lambda}t}\mathbf{V}^T\mathbf{x}_0 + \int_0^t \mathbf{C}\mathbf{V}e^{\mathbf{\Lambda}(t-\tau)}\mathbf{V}^T\mathbf{B}\mathbf{u}(\tau)d\tau + \mathbf{D}\mathbf{u}(t). \end{aligned} \tag{2.7}$$

Thus, the response of the system can be described in terms of a sum of exponential functions. The response will decay if and only if all real parts of the eigenvalues λ_i are smaller than zero. In this case the response to an arbitrary initial excitation of the model will decay exponentially. Such models are called *asymptotically stable*.
For an impulse excitation, i.e. $\mathbf{u}(t) = \delta(t)$ one obtains

$$\begin{aligned}\mathbf{y}(t) &= \int_0^t \mathbf{C}e^{\mathbf{A}(t-\tau)}\mathbf{B}\delta(\tau)d\tau + \mathbf{D}\delta(t) \\ &= \underbrace{\mathbf{C}e^{\mathbf{A}t}\mathbf{B}}_{\mathbf{h}(t)} + \mathbf{D}\delta(t)\end{aligned}$$

Here, $\mathbf{h}(t)$ is the impulse response. Inserting this expression in (2.6) one obtains

$$\mathbf{y}(t) = \int_0^t \mathbf{h}(t-\tau)\mathbf{u}(\tau)d\tau + \mathbf{D}u(t) \tag{2.9}$$

If $\mathbf{h}(t)$ is known, the output of the system to an arbitrary input signal can be computed. In that sense the system is characterized by its impulse response. The representation (2.9) is also known is infinite impulse response (IIR) model. Please note that according to Eq. (2.7) the impulse response can be described by exponential functions. For a stable system these functions will decay exponentially and thus, never be exactly zero. Therefore, the impulse response of a continuous-time model is always infinite in time.
To model thermoacoustic systems the response of the model to harmonic forcing signals is of particular importance. Therefore, we consider the response of the state-space model (2.1) to the input signal

$$\mathbf{u}(t) = \mathbf{u}_0 e^{st}.$$

Here, $\mathbf{u}_0$ is the vector of amplitudes of the signal and s is the Laplace variable

$$s = \sigma + j\omega,$$

with the angular frequency ω, the growth rate σ. The response to an harmonic input signal oscillating at frequency ω corresponds to $s = j\omega$. Inserting this ansatz in Eq. (2.7) yields

$$\mathbf{y}(t,\omega) = \mathbf{C}\mathbf{V}e^{\mathbf{\Lambda}t}\mathbf{V}^T\mathbf{x}_0 + \int_0^t \mathbf{C}\mathbf{V}e^{\mathbf{\Lambda}(t-\tau)}\mathbf{V}^T\mathbf{B}\mathbf{u}_0 e^{s\tau}d\tau + \mathbf{D}\mathbf{u}_0 e^{st}.$$

The first term represents the transient response and will vanish for long times.

$$\begin{aligned}
\mathbf{y}(t,\omega) &= \mathbf{C}\mathbf{V}\left(\int_0^t e^{\mathbf{\Lambda}(t-\tau)}e^{s\tau}d\tau\right)\mathbf{V}^T\mathbf{B}\mathbf{u}_0 + \mathbf{D}\mathbf{u}_0 e^{st} \\
&= \mathbf{C}\mathbf{V}\left(\int_0^t e^{\mathbf{\Lambda}\tau}e^{s(t-\tau)}d\tau\right)\mathbf{V}^T\mathbf{B}\mathbf{u}_0 + \mathbf{D}\mathbf{u}_0 e^{st} \\
&= \mathbf{C}\mathbf{V}\left(\int_0^\infty e^{\mathbf{\Lambda}\tau}e^{s(t-\tau)}d\tau - \int_t^\infty e^{\mathbf{\Lambda}\tau}e^{s(t-\tau)}d\tau\right)\mathbf{V}^T\mathbf{B}\mathbf{u}_0 + \mathbf{D}\mathbf{u}_0 e^{st},
\end{aligned}$$

for $t \to \infty$ the second integral tends to zero as the size of the integration interval decreases.

$$\begin{aligned}
\mathbf{y}(t,s) &= \mathbf{C}\mathbf{V}\left(\int_0^\infty e^{\mathbf{\Lambda}\tau}e^{-s\tau}d\tau\right)e^{st}\mathbf{V}^T\mathbf{B}\mathbf{u}_0 + \mathbf{D}\mathbf{u}_0 e^{st} \\
&= \mathbf{C}\mathbf{V}\left(\int_0^\infty e^{-(s\mathbf{I}_n-\mathbf{\Lambda})\tau}d\tau\right)e^{st}\mathbf{V}^T\mathbf{B}\mathbf{u}_0 + \mathbf{D}\mathbf{u}_0 e^{st} \\
&= \mathbf{C}\mathbf{V}\left[-\left(s\mathbf{I}_n-\mathbf{\Lambda}\right)^{-1}e^{-(s\mathbf{I}_n-\mathbf{\Lambda})\tau}\right]_0^\infty e^{st}\mathbf{V}^T\mathbf{B}\mathbf{u}_0 + \mathbf{D}\mathbf{u}_0 e^{st} \\
&= \mathbf{C}\mathbf{V}\left(s\mathbf{I}_n-\mathbf{\Lambda}\right)^{-1}e^{st}\mathbf{V}^T\mathbf{B}\mathbf{u}_0 + \mathbf{D}\mathbf{u}_0 e^{st} \\
&= \left[\mathbf{C}\mathbf{V}\left(s\mathbf{I}_n-\mathbf{\Lambda}\right)^{-1}\mathbf{V}^T\mathbf{B} + \mathbf{D}\right]\mathbf{u}_0 e^{st} \\
&= \left[\mathbf{C}\left(s\mathbf{I}_n-\mathbf{V}\mathbf{\Lambda}\mathbf{V}^T\right)^{-1}\mathbf{B} + \mathbf{D}\right]\mathbf{u}_0 e^{st} \\
&= \underbrace{\left[\mathbf{C}\left(s\mathbf{I}_n-\mathbf{A}\right)^{-1}\mathbf{B} + \mathbf{D}\right]}_{=\mathbf{G}(s)}\mathbf{u}_0 e^{st}.
\end{aligned}$$

$\mathbf{G}(s)$ is called the *transfer matrix* of the state-space model (2.1)

$$\mathbf{G}(s) = \begin{bmatrix} G_{11}(s) & \cdots & G_{1m}(s) \\ \vdots & & \vdots \\ G_{p1}(s) & \cdots & G_{pm}(s) \end{bmatrix} = \mathbf{C}\left(s\mathbf{I}_n-\mathbf{A}\right)^{-1}\mathbf{B} + \mathbf{D}.$$

The elements $G_{ij} = Y_i(s)/U_j(s)$ of the transfer matrix $\mathbf{G}(s)$ are the *transfer functions* from the j-th input to the i-th output of the state-space model. Please note, this result can be obtained in a much simpler manner via the Laplace transform.
With the modal transformation it can also be shown that each transfer function is a rational polynomial function

$$\begin{aligned}
\mathbf{G}(s) &= \mathbf{C}\left(s\mathbf{I}_n - \mathbf{A}\right)^{-1}\mathbf{B} + \mathbf{D} \\
&= \mathbf{C}\mathbf{V}\left(s\mathbf{I}_n - \mathbf{\Lambda}\right)^{-1}\mathbf{V}^T\mathbf{B} + \mathbf{D} \\
&= \mathbf{C}\mathbf{V}\begin{bmatrix} s-\lambda_1 & & \\ & \ddots & \\ & & s-\lambda_n \end{bmatrix}^{-1}\mathbf{V}^T\mathbf{B} + \mathbf{D} \\
&= \begin{bmatrix} \tilde{c}_{11} & \cdots & \tilde{c}_{1n} \\ \vdots & & \vdots \\ \tilde{c}_{p1} & \cdots & \tilde{c}_{pn} \end{bmatrix}\begin{bmatrix} \frac{1}{s-\lambda_1} & & \\ & \ddots & \\ & & \frac{1}{s-\lambda_n} \end{bmatrix}\begin{bmatrix} \tilde{b}_{11} & \cdots & \tilde{b}_{1m} \\ \vdots & & \vdots \\ \tilde{b}_{n1} & \cdots & \tilde{b}_{nm} \end{bmatrix} + \mathbf{D} \\
&= \sum_{i=1}^{n}\frac{1}{s-\lambda_i}\begin{bmatrix} \tilde{b}_{i1}\tilde{c}_{1i} & \cdots & \tilde{b}_{im}\tilde{c}_{1i} \\ \vdots & & \vdots \\ \tilde{b}_{i1}\tilde{c}_{pi} & \cdots & \tilde{b}_{im}\tilde{c}_{pi} \end{bmatrix}.
\end{aligned}$$

Expanding the sum yields

$$\begin{aligned}
\mathbf{G}(s) = &\frac{1}{s^n + \alpha_{n-1}s^{n-1} + \cdots + \alpha_0} \\
&\begin{bmatrix} \beta_{11}^{n-1}s^{n-1} + \cdots + \beta_{11}^0 & \cdots & \beta_{1m}^{n-1}s^{n-1} + \cdots + \beta_{1m}^0 \\ \vdots & & \vdots \\ \beta_{p1}^{n-1}s^{n-1} + \cdots + \beta_{p1}^0 & \cdots & \beta_{pm}^{n-1}s^{n-1} + \cdots + \beta_{pm}^0 \end{bmatrix}.
\end{aligned}$$

with the coefficients α and β of the rational polynomials.

2.2 Discrete-time models

Discretizing the continuous-time state-space model (2.1) in time yields a discrete-time state-space model

$$\begin{aligned}
\mathbf{x}(k\Delta t) = \mathbf{x}_{k+1} &= \mathbf{A}_d\mathbf{x}_k + \mathbf{B}_d\mathbf{u}_k \\
\mathbf{y}_k &= \mathbf{C}_d\mathbf{x}_k + \mathbf{D}_d\mathbf{u}_k.
\end{aligned} \tag{2.13}$$

Here, k is the discrete time increment defined as $t = k\Delta t$ with the time step Δt.
The general solution of the discrete-time state-space model is given as

$$\mathbf{y}(k) = \mathbf{C}_d \mathbf{A}_d^k \mathbf{x}_0 + \sum_{i=0}^{k-1} \mathbf{C}_d \mathbf{A}_d^{k-1-i} \mathbf{B}_d \mathbf{u}(i) + \mathbf{D}_d \mathbf{u}(i) \tag{2.14}$$

This solution can be found by inserting Eq. (2.13) iteratively into itself. A discrete-time state-space model is stable if all eigenvalues of $\mathbf{A}_d$ have a magnitude smaller than 1.
As for continuous-time models, the impulse response model of a discrete-time time model can be deduced imposing an impulse excitation, i.e.

$$\delta_d(k) = \begin{cases} 1/\Delta t & \text{for } k = 0 \\ 0 & \text{else} \end{cases}$$

This yields

$$\mathbf{y}(k) = \underbrace{\mathbf{C}_d \mathbf{A}_d^{k-1} \mathbf{B}_d / \Delta t}_{\mathbf{h}_d(k)} + \mathbf{D}_d \delta_d(k).$$

Inserted into Eq. (2.14) yields

$$\mathbf{y}(k) = \sum_{i=0}^{k-1} \mathbf{h}_d(k-i) \Delta t \mathbf{u}(i) + \mathbf{D}_d \mathbf{u}(i)$$

Thus, as for the continuous-time models, knowing the impulse response is sufficient to calculate the output of a discrete-time model for an arbitrary input signal. The impulse response of discrete-time models has one significant difference compared to the impulse response of continuous-time models: If the matrix A is Nilpotent[4] the impulse response will be finite. The corresponding model is called finite impulse response (FIR) model.
Applying the z-transform to Eq. (2.2) yields the frequency response of the model

$$\mathbf{G}(z) = \mathbf{C}_d \left(z\mathbf{I}_n - \mathbf{A}_d \right)^{-1} \mathbf{B}_d + \mathbf{D}_d. \tag{2.15}$$

As for continuous-time models it can be shown that the z-transfer matrix can be represented as rational polynomial function. In order to calculate the response of the model to a harmonic excitation at frequency ω we set

$$z = e^{j\omega\Delta t}.$$

[4] i.e. it exists a $k \in \mathbb{N}$ such that $A^k = 0$. All eigenvalues of a Nilpotent matrix are equal to zero.

The z-transfer matrix of a discrete-time model can be converted in to a continuous-time transfer matrix. For this we first discretize the continouse-time state-space model (2.1) in time using a forward Euler scheme:

$$\begin{aligned}\mathbf{x}_{k+1} &= \underbrace{(\mathbf{I} + \Delta t\mathbf{A})}_{\mathbf{A}_d}\mathbf{x}_k + \underbrace{\Delta t\mathbf{B}}_{\mathbf{B}_d}\mathbf{u}_k \\ \mathbf{y}_k &= \underbrace{\mathbf{C}}_{\mathbf{C}_d}\mathbf{x}_k + \underbrace{\mathbf{D}}_{\mathbf{D}_d}\mathbf{u}_k\end{aligned}$$

inserting these expressions for the system matrices of the discrete-time model into Eq. (2.15) yields

$$\begin{aligned}\mathbf{G}(z) &= \mathbf{C}\left(z\mathbf{I}_n - (\mathbf{I} + \Delta t\mathbf{A})\right)^{-1}\Delta t\mathbf{B} + \mathbf{D} \\ &= \mathbf{C}\left(\underbrace{\frac{z-1}{\Delta t}}_{=s}\mathbf{I}_n - \mathbf{A}\right)^{-1}\mathbf{B} + \mathbf{D}\end{aligned}$$

Thus by choosing

$$s = \frac{z-1}{\Delta t} \;\Leftrightarrow\; z = 1 + s\Delta t$$

a continuous time transfer matrix can be transformed into a discrete-time transfer matrix and vise versa. This transformation is an approximation and introduces the error made by the use of the forward Euler scheme. The methodology can be extended for other schemes. As shown in [39], applying a Crank-Nicholson discretization of Eq. (2.1) yields the famous Tustin transformation.

3 System identification

The most common way to build models is to use the relations provided by fundamental principles, such as mass or energy conservation etc.. This, however, is a very challenging task and the agreement with validation data is often insufficient. One way to overcome this issue is to fit some or even all of the model parameters to measured data. This creates the risk of over-fitting. Nevertheless, the quality of the predictions made by such *empirical* models is often significantly higher than models built entirely on fundamental principles. System identification (SI) provides a general framework to build empirical models in an efficient and consistent manner. Dependent on the data available different methods are needed. Experimental data is often provided in terms of a frequency response. Bothien et al. [18] and PAPER-CBSBC discuss, with a focus on thermoacoustic problems, how to use this kind of data to build models. Typically, frequency responses are determined by forcing a given system at several distinct frequencies and by post-processing the data collected with a Fourier transform. Applying the same procedure to a CFD simulation is extremely expensive, as it requires a large number of simulations. In the present chapter we discuss system identification methods that allow to deduce a model from a CFD simulation efficiently. The key idea is to force the simulation with a broadband signal. This signals excites all frequencies simultaneously and allows to deduce an empirical low-order model from data generated by a single simulation. The procedure is called CFD/SI approach. Polifke [33] provides an overview of this approach. Overall, the method can be divided into four steps: Setting up the CFD simulation, running the simulation, pre-processing the data, fitting the model to the data and validating the model. A schematic overview of the method is shown in Fig. 3.1. In the remainder of this chapter these steps are discussed in detail.

3.1 Setting up the CFD simulation

The first step is to setup a CFD simulation. This step does not differ from any other CFD simulation, except that one has to be able to impose a forcing signal and to collect the output signal. For example. if, as in the present case, one wants to obtain a low-order model for the flame dynamics, one has to be able to force the inflow velocity with an arbitrary signal and to collect the resulting fluctuations of the global heat release rate. Many CFD solvers provide this functionality out of the box, otherwise the necessary modifications are minimal. This makes the CFD/SI approach applicable to a large number of problems.

3.2 Running the simulation

The second step is to run the simulation with an appropriate excitation signal. A general method to create signals well suited for the CFD/SI approach was proposed by Föller et al. [40]. The most important property of the signal is the cutoff frequency. It should be chosen such that all frequencies of interest are excited. Besides this the excitation amplitude is to be selected. For the linear CFD/SI approach a constant amplitude with a value as large as possible without exciting nonlinear effects should be chosen. For the nonlinear CFD/SI approach larger amplitudes and preferably non-constant amplitudes should be used. Additionally, the time series have to be significantly longer. Indeed, in PAPER-ANN time series that are up to 30 times longer than time series sufficient for the linear CFD/SI approach are used. It is found that even for these extremely long time series the variance of results is significant.

3.3 Post-processing of the time series collected

After running the simulation, the time series collected have to be pre-processed before the system identification methods can be applied. On the one hand this means to normalize the data. On the other hand the data is sampled down. This step is necessary, as discrete time models are commonly used for the identification. Consequently, the time steps of the model and of the data have to be equal. The down sampling rate is an additional parameter which has to be chosen. This step can be avoided if continuous-time models are used for the identifications (see e.g. [41]). To the best of our knowledge continuous time system identification has not yet been applied to thermoacoustic problems.

3.4 Fit a model to the data

The next step is to choose a suitable model structure given as

$$\mathbf{y}(t, \boldsymbol{\Theta}) = \mathbf{G}(\boldsymbol{\Theta}) \circ \mathbf{u}(t),$$

with the vector of unknown parameters $\boldsymbol{\Theta}$. In the linear regime a state-space model (see Eq. (2.2)) provides a general model structure[5]. In the nonlinear regime a large number of different model structures are available. At this point we refer to Isermann et al. [49] and Nelles [50]. Nonlinear models suitable to model the flame dynamics are discussed in Sec. 4.2.
The vector of unknown parameter can be determined by solving a least squares optimization problem

$$\hat{\boldsymbol{\Theta}} = \underset{\boldsymbol{\Theta}}{\operatorname{argmin}} \left\{ \sum_{i=0}^{N} \|\mathbf{y}(t_i) - \hat{\mathbf{y}}(t_i, \boldsymbol{\Theta})\|_2^2 \right\}.$$

Here, $\hat{\boldsymbol{\Theta}}$ is the identified parameter vector, N is the number of sampled data points, $\mathbf{y}$ denotes the measured output signal and $\hat{\mathbf{y}}$ the output predicted by the model. Depending on the model structure, different algorithms are used to solve the optimization problem. Using a fully parametrized state-space model as given in Eq. (2.2), which provides a general structure for linear models, however, yields numerical difficulties [51]. This is because a state-space model has a large number of redundant parameters. As discussed in the previous chapter a state-space model can be transformed into a transfer function described by rational polynomial functions. This transformation preserves the input-output behavior of the model. However, the state-space model has $n^2 + (m+p)n + pm$ parameters while, the corresponding transfer function only $n - 1 + npm$. Thus, the parameters of the state-space models are linearly dependent in respect to the transfer behavior of the state-space model. This results in a poorly conditioned optimization problem, which is why for a long time only transfer functions were used for identification. The Wiener-Hopf inversion [33, 52] used frequently to identify the flame transfer function is one of these techniques. Robust algorithms for the identification of fully parametrized state-space models are the subspace identification methods [53–55] and gradient based algorithms, which calculate the search direction according to the data-driven local coordinates (DDLC) parametrization [51]. These algorithms are expected to be advantageous for problems with a large number of input and output signals. For

[5]Note, in this work only a deterministic model is discussed. The CFD/SI approach can be extended in such a way that model of the noise source is identified. This is extensively discussed by Sovardi et al. [42–48].

nonlinear system identification the parameters used depend strongly on the nonlinear model structure. The algorithm used to identify artificial neural networks is called error back propagation [50]. Using an Volterra series[6] yields an linear optimization problems. A variety of algorithms has been proposed to identify Hammerstein-Wiener models (see e.g. [56–59]). A discussion from a thermoacoustic perspective for some model structures can be found in [34–36] and in PAPER-ANN.

As LES requires a huge computational effort, the time series used for the CFD/SI approach are often very short. In this limit regularization can improve the quality of the models identified. The idea is to add constraints to the optimization problem:

$$\hat{\boldsymbol{\Theta}} = \underset{\boldsymbol{\Theta}}{\operatorname{argmin}} \left\{ \sum_{i=0}^{N} \|\mathbf{y}(t_i) - \hat{\mathbf{y}}(t_i, \boldsymbol{\Theta})\|_2^2 + \boldsymbol{\Theta}^T R \boldsymbol{\Theta} \right\},$$

with the regularization matrix R. This allows to use assumptions e.g. that the impulse response of the model identified is smooth and decays exponentially. An overview on the methods available can be found in [52, 60].

3.5 Validation of the model

The final step is to validate the models identified. Here, experimental data can be used to validate the CFD simulation only. A comparison of the models identified and experimental data should only be done if one is sure that the model identified represents the CFD simulation accurately. In order to investigate this a number of strategies and methods are available. The most reliable methods require to generate additional data. For example one compares the FDF deduced directly from the CFD simulation against the one predicted by the nonlinear model identified. When self-excited thermoacoustic oscillations are to be modeled, it is ideal to compare the oscillations predicted by the CFD simulation against the one predicted by the nonlinear model identified. In order to avoid additional error sources the CFD simulation and the nonlinear model should be coupled with the same model for the acoustics. This was done within the scope of the present thesis in PAPER-ANN. Other methods are residual analysis or Akaike's information criterion (AIC) [61]. These methods do not require additional data. However, their reliability is much lower and they can be used only in the linear regime.

[6] This model structure is also called nonlinear auto regressive (NLARX) models.

The validation of the model can fail for several reasons. In order to find the error source in a systematic manner one may follow the steps shown in Fig. 3.1 from bottom to top. A possible error source is the identification algorithms used [50]. As non-deterministic algorithms are used to identify artificial neural networks, simply restarting the optimization can yield a better model. For the Wiener-Hopf inversion the regularization can be changed. The next possible error is the model structure. Here, one can e.g. change the number of the impulse response coefficients or the structure of an artificial neural network. Another error source is the pre-processing of the data used for the identification. This kind of error is most often related to an incorrect down sampling rate. However, one should also check the normalization of the data. If all these possible errors sources can be excluded, the issue is related to the CFD simulation. At best the time series are too short. In this case one should simple continue the simulation. In order to obtain a continuous time series, it is necessary that the broadband excitation signal is long enough. Therefore, it is best practice to create an excitation signal, which is at least ten times longer than the required simulation time expected. Obviously, this signal should be created before the first simulation is started. In the linear regime confidence intervals allow to estimate the uncertainty of the model with respect to the length of the time series used. Sovardi et al. [42] discuss this strategy and use it to identify the scattering matrix of an orifice. With sufficiently long time series one should always be able to identify a proper model. Please note, as shown in PAPER-ANN in the nonlinear regime one may not be able to create sufficiently long time series. Another possible issue with the excitation signal is the amplitude. For the linear regime it should be as high as possible without exciting nonlinear effects. In the nonlinear regime the excitation signal should excite all amplitudes of interest. Additionally, the excitation signal should excite all frequencies of interest. Once all issues mentioned above have been solved, one has ensured that the model identified represents the CFD simulation accurately. The next step is to validate the model identified against experimental data. If no agreement is obtained the issue either caused by CFD simulation or by the experiment.

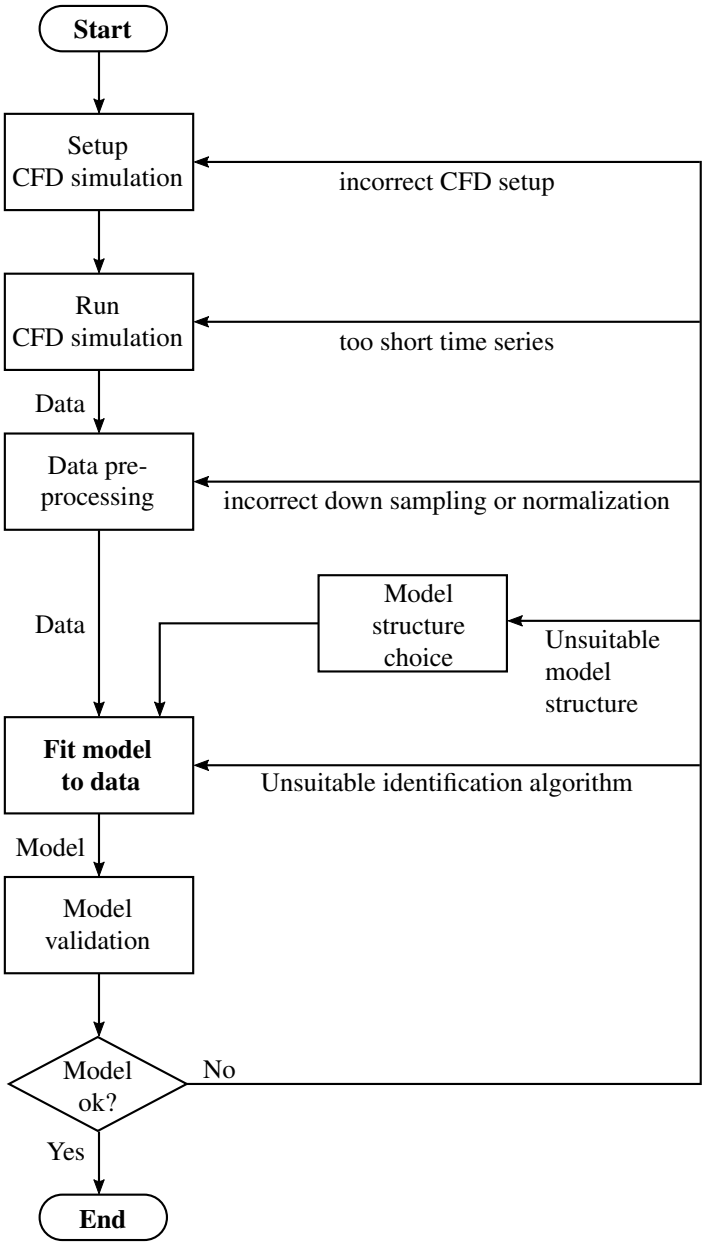

Figure 3.1: Schematic procedure of the CFD/SI approach. Adapted from [62]

4 Modeling of thermoacoustic oscillations

In Fig. 4.1 (top) a generic sketch of a premixed combustor is shown. At the left hand side premixed gas is injected into the plenum of the combustor. For swirl flames the swirler coincides with the area contraction. The flame stabilizes after the area expansion. For certain working conditions the combustor will exhibit thermoacoustic oscillations. The first step to model these oscillations is to separate the acoustics and the flame dynamics, as shown in Fig. 4.1 (middle).
In the present project only low-frequency oscillations are considered. In this limit the acoustic wave-lengths are much larger than the relevant length scales of the cross-sections. Therefore, all acoustic waves are plane and can be described in terms of the characteristic wave amplitudes f and g (see e.g. [63, 64])

$$f = \frac{1}{2}\left(\frac{p'_A}{\bar{\rho}\bar{c}} + u'_A\right), \quad g = \frac{1}{2}\left(\frac{p'_A}{\bar{\rho}\bar{c}} - u'_A\right),$$

with the density ρ, the speed of sound c and the acoustic fluctuation of pressure p'_A and of velocity u'_A. The symbol $(\bar{\cdot})$ denotes the temporal average. As shown in Fig. 4.1, f corresponds to the wave traveling in downstream direction and g to the one traveling in upstream direction.
In order to model thermoacoustic oscillations, a model which describes how an unsteady heat source $\dot{q}'$ generates acoustic waves is necessary. For low-frequency oscillations the minimal acoustic wave length is significantly smaller than the axial expansion of the flame. Thus, the flame is acoustically compact and can be considered to be infinitesimally thin. Evaluating the one dimensional momentum and energy equations over this infinitesimal flame yields the Rankine-Hugoniot equations. They are given in state-space form as [65–67]

$$\begin{bmatrix} g_u \\ f_d \end{bmatrix} = \frac{1}{\zeta+1}\begin{bmatrix} 1-\zeta & 2 & \theta\bar{u}_1 \\ 2\zeta & \zeta-1 & \theta\zeta\bar{u}_1 \end{bmatrix}\begin{bmatrix} f_u \\ g_d \\ \dot{q}' \end{bmatrix}, \tag{4.17}$$

with $\zeta = \bar{\rho}_3\bar{c}_3/\bar{\rho}_4\bar{c}_4$ and $\theta = \bar{T}_4/\bar{T}_1 - 1$. $\bar{T}$ is the temperature. The index u and d denote the position upstream and downstream of the flame front, respectively.

The Rankine-Hugoniot equation describe a static relationship. Therefore, the corresponding state-space model consists only of the matrix D. The matrices A, B and C are equal to zero.
With the Rankine-Hugoniot equations a model that describes how the unsteady heat source acts on the acoustics is available. In order to close the thermoacoustic feedback loop a model which describes how the acoustics acts on the unsteady heat source is necessary. Perfectly premixed flames react predominantly to fluctuations of the velocity upstream of the flame [68, 69]. Therefore, the flame dynamics can be represented as the dynamical system

$$\dot{q}' = \mathbf{G}_{\text{flame}} \circ u'. \tag{4.18}$$

In the remainder of this chapters we will first discuss the modeling of the acoustics and then the modeling of the flame dynamics. Finally, we discuss hybrid CFD/low-order modeling approaches of thermoacoustic oscillations.

4.1 Modeling of the acoustics

Plane acoustic waves can be described with acoustic network models [14–16]. As shown in Fig. 4.1 (bottom), the key idea is to divide the configuration into several elements. The elements are modeled separately from each other. In a final step, all models are interconnected in order to obtain a model for the whole configuration. The internal elements can be represented as scattering matrix

$$\begin{bmatrix} g_u \\ f_d \end{bmatrix} = \begin{bmatrix} S_{11}(s) & S_{12}(s) \\ S_{21}(s) & S_{22}(s) \end{bmatrix} \begin{bmatrix} f_u \\ g_d \end{bmatrix}.$$

The coefficient S_{11} describes the reflection of the wave f_u, which results in the wave g_u, and so on (compare Fig. 4.2). The boundary elements can be modeled as reflection coefficients $R_u(s)$ and $R_d(s)$.
Both the scattering matrix and the reflection coefficients describe linear dynamical systems and can be represented as linear state-space models. The models for the internal elements are given as

$$\begin{aligned} \dot{\mathbf{x}}_S &= A_S \mathbf{x}_S + B_S \begin{bmatrix} f_u \\ g_d \end{bmatrix}, \\ \begin{bmatrix} g_u \\ f_d \end{bmatrix} &= C_S \mathbf{x}_S + D_S \begin{bmatrix} f_u \\ g_d \end{bmatrix}. \end{aligned}$$

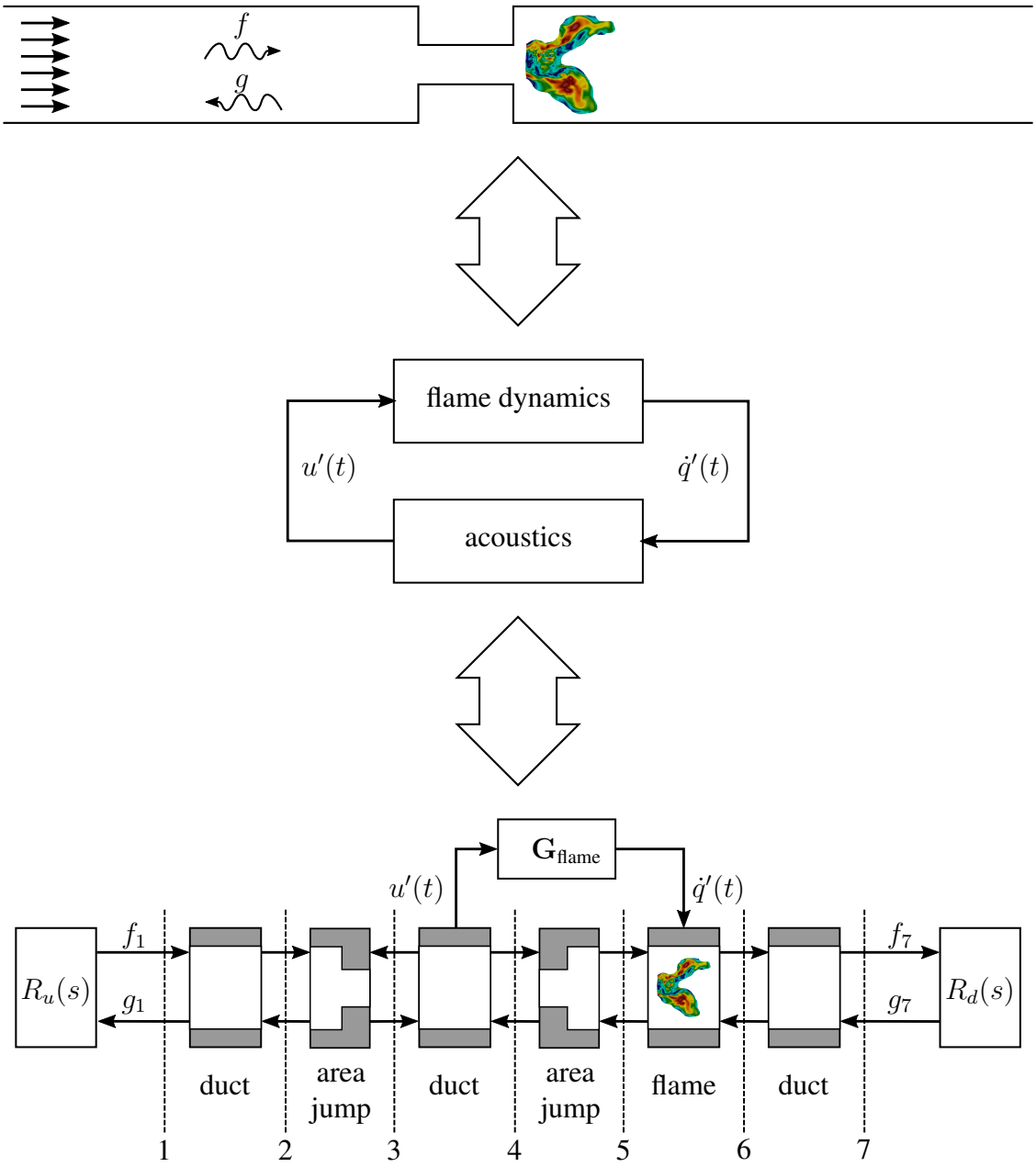

Figure 4.1: Top: Generic combustor, Middle: separation in acoustics and flame dynamics, Bottom: Corresponding network model

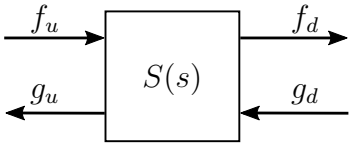

Figure 4.2: Sketch of a scattering matrix

The state-space representation allows a robust and general implementation. It was first proposed by Schuermans et al. [17]. The methodology was then generalized by Bothien et al. [18] and Emmert et al. [70].
A simple model for an area jump is given as (see e.g. [71])

$$\begin{bmatrix} g_u \\ f_d \end{bmatrix} = \underbrace{\begin{bmatrix} \frac{\alpha-1}{\alpha+1} & \frac{2}{\alpha+1} \\ \frac{2\alpha}{\alpha+1} & \frac{\alpha-1}{\alpha+1} \end{bmatrix}}_{=D_{\text{area jump}}} \begin{bmatrix} f_u \\ g_d \end{bmatrix},$$

with the area ratio $\alpha = A_2/A_3$. This is a static model and thus, its state-space representation consists of the feed through matrix, only.
For the duct sections a model based on the linearized one-dimensional Euler equations can be found. A detailed derivation by the author of this thesis is provided in PAPER-CBSBC. Emmert et al. [70] discuss how general geometries can be modeled via numerical discretization of linearized perturbation equations.
Within the scope of the dissertation of T. Emmert a thermoacoustic network framework called taX[7] was developed. The author of this thesis supported the development with a lot of discussions, some coding and by being the first user. All network models used for the present work were generated with taX.

4.2 Modeling of the flame dynamics

In the limit of small perturbation a linear model can capture the flame dynamics. This linear model is known as flame transfer function (FTF) [65]. Well established methods exist to obtain an FTF. It can be determined from experiment by harmonic forcing or from CFD via the CFD/SI approach, as discussed in the previous chapter. For higher levels of perturbations nonlinear models are necessary. Here, several modeling approaches have been proposed.
One model proposed is the flame describing function (FDF) [25]. The FDF is

[7] https://tax.wiki.tum.de/

an amplitude dependent FTF

$$\mathrm{FDF}(\omega, A) = \frac{\mathcal{F}\{\dot{q}'(\omega, A)\}}{\mathcal{F}\{u'(\omega, A)\}}$$

with the excitation amplitude A. $\mathcal{F}\{\cdot\}$ denotes the Fourier transform. It has been shown that the FDF in combination with a network model for the acoustics can predict thermoacoustic oscillations of laminar [26] and turbulent [27, 72, 73] flames. In order to obtain an FDF, a given flame is forced at different frequencies and amplitudes and the resulting fluctuations of the global heat release rate are recorded. With this information the FDF can be obtained via a Fourier transform of the signals. This procedure works for real flames in an experiment as well as for simulated flames. For the latter, however, the procedure is extremely expensive as a large number of simulations are necessary. Heckl [74] developed an analytic model based on the FDF. Unfortunately, it is not straight forward (and at the best of our knowledge not possible) to use the ideas behind the FDF in order to develop an identification algorithm. This is because the amplitude of a broadband excitation signal is not known in the time domain. Therefore, other model structures are necessary.

Another model structure proposed are Hammerstein-Wiener models. As shown in Fig. 4.3, the core of these models is a linear transfer function $\mathbf{G}(s)$. The nonlinearity is modeled via two static nonlinear functions $\gamma_1(t)$ and $\gamma_2(t)$. From the analysis of the FDF it is known that the response of the heat release rate saturates for high excitation amplitude. This effect can be modeled by using a saturation function for $\gamma_2(t)$ [17, 20]. In [75], system identification with a Hammerstein-Wiener model was used to determine low-order models of a flame modeled via the G-equation.

A very general nonlinear model structure are artificial neural networks [50]. A generic artificial neural networks is shown in Fig. 4.4. It consists of several neurons. The structure can be extended by increasing the number of layers and the number of neurons per layer. This allows to model complex nonlinearities. Selimefendigil et al. [34–36] used artificial neural networks to model the nonlinear dynamics of the heat transfer of an cylinder in pulsating cross-flow. The potential and limitations of artificial neural networks to model the dynamic of a laminar premixed flame are investigated in PAPER-ANN.

A model for laminar premixed flame is based on the G-equation [76]. The nonlinear dynamics of this model agrees qualitatively with experimental results [77, 78]. However, the results depend strongly on the velocity model used and therefore no quantitative agreement with experimental results is achieved.

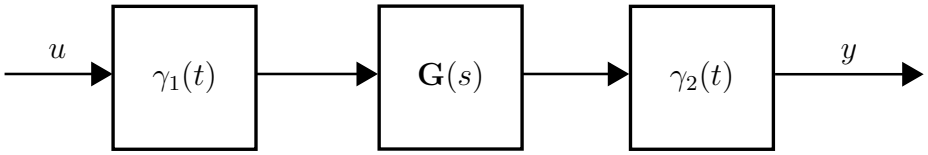

Figure 4.3: General Hammerstein-Wiener model structure.

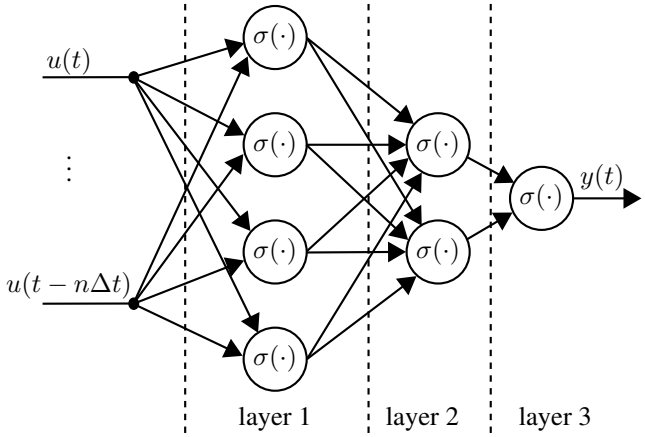

Figure 4.4: Generic artificial neural network (PAPER-ANN)

The most accurate, though most expensive, way to model the flame dynamics is a CFD simulation. For low frequencies, as discussed in the present work, the flame is compact. This allows us to utilize a low Mach [8] simulation. Kornilov et al. [79] modeled the linear dynamics of a laminar flame with a low Mach CFD solver and compared the results against experiment. Good agreement was reported. Moeck et al. [80] and Jaensch et al. (PAPER-HYBRID) coupled a low Mach simulation with an acoustic network model in order to model self-excited thermoacoustic oscillations. In [81] the coupling is based on the upstream and the downstream velocity. In PAPER-HYBRID the coupling is based on the upstream velocity and the global heat release rate. By inserting Eq. (4.18) into Eq. (4.17) one can easily show that both formulations are equal. If the flame is modeled with a fully compressible simulation, self-excited thermoacoustic oscillations can be captured without the need of an acoustic network model. Nevertheless, it can be advantageous to couple the simulation with an acoustic model: This allows to change the acoustic boundary conditions without changing the mesh. PAPER-CBSBC provide an overview over these so called time-domain impedance boundary conditions (TDIBC).

[8] I.e. the density depends on the temperature, but not on pressure.

5 Summary of achievements and papers

In this section the achievements and the papers of this doctoral research project are summarized. An overview of all papers is provided in Fig. 5.1. Major parts of the present manuscript were already submitted as final report of the FVV project *nonlinear flame dynamics* [82].

In PAPER-GREYBOX a grey-box identification approach for thermoacoustic network models was developed. This ansatz allows to use a priori knowledge of the physics of thermoacoustic oscillations (e.g. the Rankine-Hugoniot equations) for the results of the CFD/SI approach. This enables us to deduce the FTF and to the estimate fluctuations of the global heat release rate from acoustic measurements only. Furthermore, within this paper the modeling of thermoacoustic oscillations was analyzed from a system theoretic perspective. In that sense PAPER-GREYBOX can be considered as foundation of the present thesis.

In PAPER-CBSBC the system theoretic perspective, developed in PAPER-GREYBOX, was extended to a novel formulation of time-domain impedance boundary conditions (TDIBC). The so called "characteristics based state-space boundary conditions" (CBSBC) allows to impose almost arbitrary reflection coefficients or impedances at the inflow and outflow boundary conditions of large eddy simulations and direct numerical simulations. In contrast to other TDIBC formulations found in the literature, CBSBC is at the same time numerically robust, avoids drift of the mean flow variables *and* does not introduce artificial reflections at the boundary. It already has been decided to include the algorithm to the release version of AVBP [9] (Cerfacs and IFP). Furthermore, CBSBC forms the basis of the time-domain impedance BC implemented in LESLIE[10] (Computational Combustion Lab, Georgia Institute of Technology).

CBSBC made possible the coupling of a compressible CFD code to a low order acoustic model. In PAPER-HYBRID this was utilized to conduct a bifurcation analysis of self-excited thermoacoustic oscillations of a laminar premixed flame. As illustrated in Fig. 5.1, the results obtained with the model based on

[9] http://cerfacs.fr/en/computational-fluid-dynamics-softwares/

[10] http://www.ccl.gatech.edu/leslie

CBSBC were compared against a second model. The second model is based on a low-Mach CFD solver, which is coupled to an acoustic network model according to the Rankine-Hugoniot equations. Good agreement between the two models was observed. PAPER-HYBRID is the first bifurcation study of a laminar flame with high-fidelity models.
In PAPER-ANN an extension of the CFD/SI approach to the nonlinear regime is investigated. Artificial neural networks (ANNs) are utilized to model the nonlinear dynamics of a laminar flame. A large parameter study was conducted in order analyze the robustness of the method. The results from PAPER-HYBRID allowed us to compare self-excited thermoacoustic oscillations predicted by the ANNs identified directly with the oscillations predicted by the hybrid CFD/low-order models (compare Fig 5.1). Unfortunately, the agreement observed was poor. It is concluded that more sophisticated methods are needed. The main achievements of PAPER-ANN are the systematic way the quality of the nonlinear model was investigated and the direct comparison of the quantity of interest i.e. the amplitude of self-excited thermoacoustic oscillations. The procedure proposed should always be used to analyze the capability of novel nonlinear low-order models to predict self-excited thermoacoustic oscillations.

5.1 PAPER-GREYBOX

A GREY-BOX IDENTIFICATION APPROACH FOR THERMOACOUSTIC NETWORK MODELS
S. Jaensch, T. Emmert, C. F. Silva, and W. Polifke, GT2014-27034, in Proceedings of ASME Turbo Expo, Düsseldorf, Germany, 2014, 10.1115/GT2014-27034.
Abstract: This work discusses from a system theoretic point of view the low order modeling and identification of the acoustic scattering behavior of a ducted flame. In this context, one distinguishes between black-box and grey-box models. The former rely on time series data only and do not require any physical modeling of the system that is to be identified. The latter exploit prior knowledge of the system physics to some extent and in this sense are physically motivated. For the case of a flame stabilized in a duct, a grey-box model is formulated that comprises an acoustic part as well as sub-models for the flame dynamics and the jump conditions for acoustic variables across the region of heat release. Each of the subsystems can be modeled with or without physical a priori knowledge, in combination they yield a model for the scattering behav-

ior of the flame. We demonstrate these concepts by analyzing a CFD model of a laminar conical premixed flame. The grey-box approach allows to optimize directly the scattering behavior of the identified model. Furthermore, we show that the method allows to estimate heat release rate fluctuations as well as the flame transfer function from acoustic measurements only.
Contribution: I implemented the SI routines which are not part of Matlab's SI toolbox, applied the system identification methodology and analyzed the results. Additionally, I wrote most of the manuscript.

5.2 PAPER-CBSBC

ON THE ROBUST, FLEXIBLE AND CONSISTENT IMPLEMENTATION OF TIME DOMAIN IMPEDANCE BOUNDARY CONDITIONS FOR COMPRESSIBLE FLOW SIMULATIONS
S. Jaensch, C. Sovardi, and W. Polifke, Journal of Computational Physics, vol. 314, pp. 145–159, 2016, http://dx.doi.org/10.1016/j.jcp.2016.03.010.
Abstract: The accurate simulation of compressible flows requires the appropriate modeling of the reflection of acoustic waves at the boundaries. In the present study we discuss time domain impedance boundary conditions (TDIBC). The formulation proposed allows to impose a desired reflection coefficient at the inflow and outflow boundaries. Our formulation is an extension of the well known Navier-Stokes characteristic boundary conditions. The frequency dependent reflections at the boundaries are implemented with a state-space model in the time domain. We provide a comprehensive discussion on how such state-space models can be constructed and interpreted. This discussion shows that the state-space description allows a robust and flexible implementation. It allows to consider complex reflection coefficients and account for non constant CFD time steps in a straight forward manner. Furthermore, we prove analytically and demonstrate numerically that the formulation proposed is consistent, i.e. the formulation ensures that the flow simulation exhibits the reflection coefficient imposed accurately, as long as the waves impinging on the boundary are plane, and it prohibits drift of the mean flow variables. Finally, the boundary conditions are tested successfully for laminar and turbulent flows.
Contribution: I developed the method, implemented a first version of CB-SBC in LESLIE [11], conducted the validation simulations and wrote most of the manuscript.

[11] Computational Combustion Lab, Georgia Institute of Technology

5.3 PAPER-HYBRID

HYBRID CFD/ LOW-ORDER MODELING OF NONLINEAR THERMOACOUSTIC OSCILLATIONS

S. Jaensch, M. Merk, E. A. Gopalakrishnan, S. Bomberg, T. Emmert, R. I. Sujith, W. Polifke, Proceedings of the Combustion Institute, vol. 36, pp. 3827-3834, 2017, http://dx.doi.org/10.1016/j.proci.2016.08.006.

Abstract: This paper proposes and compares two nonlinear time-domain models of self-excited thermoacoustic instabilities of laminar premixed flames. The flame and its immediate vicinity are resolved with reactive flow simulations. Simultaneously, the acoustic field is modeled with low-order models which are coupled to the reactive flow simulations. On the one hand a model based on the fully compressible Navier-Stokes equations is investigated. Here, the low-order model is coupled to the simulation via the characteristic wave amplitudes at the inlet boundary. The other model resolves the flame with a weakly compressible reactive flow simulation. In order to include the thermoacoustic feedback, this model is coupled with an acoustic network model by the global heat release rate and the fluctuation of the axial velocity at a reference position upstream of the flame. A bifurcation analysis using the plenum length as bifurcation parameter is conducted. Both models exhibit complex nonlinear oscillations. A bifurcation analysis shows that both models are in good agreement with each other. Therefore, we conclude that the coupling of a linear acoustic model and a nonlinear flame model via reference velocity and global heat release rate is sufficient to accurately capture nonlinear oscillations of thermoacoustic instabilities. This implies that the most important nonlinearities can be attributed to hydrodynamic effects and the flame kinematics. Additionally, the study provides further evidence that premixed flames predominantly respond to fluctuations of the upstream velocity-pressure fluctuations and acoustic waves act on the flame only in an indirect manner, as they cause fluctuations of the upstream velocity.

Contribution: I implemented the coupling of the low Mach simulation and the acoustic network model. I conducted the low Mach simulations and wrote most parts of the manuscript.

Comment: A first version of this paper was published as a report for the SFB/TRR 40 summer program [83].

5.4 PAPER-ANN

UNCERTAINTY ENCOUNTERED WHEN MODELLING SELF-EXCITED THERMOACOUSTIC OSCILLATIONS WITH ARTIFICIAL NEURAL NETWORKS
S. Jaensch, W. Polifke, International Journal of Spray and Combustion Dynamics, 2017, http://dx.doi.org/10.1177/1756827716687583.

Abstract: Artificial neural networks are a popular nonlinear model structure and are known to be able to describe complex nonlinear phenomena. This article investigates the capability of artificial neural networks to serve as a basis for deducing nonlinear low-order models of the dynamics of a laminar flame from a Computational Fluid Dynamics (CFD) simulation. The methodology can be interpreted as an extension of the CFD/system identification approach: a CFD simulation of the flame is perturbed with a broadband, high-amplitude signal and the resulting fluctuations of the global heat release rate and of the reference velocity are recorded. Thereafter, an artificial neural network is identified based on the time series collected. Five data sets that differ in amplitude distribution and length were generated for the present study. Based on each of these data sets, a parameter study was conducted by varying the structure of the artificial neural network. A general fit-value criterion is applied and the 10 artificial neural networks with the highest fit values are selected. Comparing of these 10 artificial neural networks allows to obtain information on the uncertainty encountered. It is found that the methodology allows to capture the forced response of the flame reasonably well. The validation against the forced response, however, depends strongly on the forcing signal used. Therefore, an additional validation criterion is investigated. The artificial neural networks are coupled with a thermoacoustic network model. This allows to model self-excited thermoacoustic oscillations. If the training time series are sufficiently long, this coupled model allows to predict the trend of the root mean square values of fluctuations of the global heat release rate. However, the prediction of the maximal value of the fluctuation amplitude is poor. Another drawback found is that even if very long-time series are available, the behaviour of artificial neural networks cannot be guaranteed. It is concluded that more sophisticated nonlinear low-order models are necessary.

Contribution: I conducted the parameter study, implemented the coupling between artificial neural networks and the acoustic network models and wrote most of the manuscript.

Comment: A first version of this paper has been published as report at the FVV-

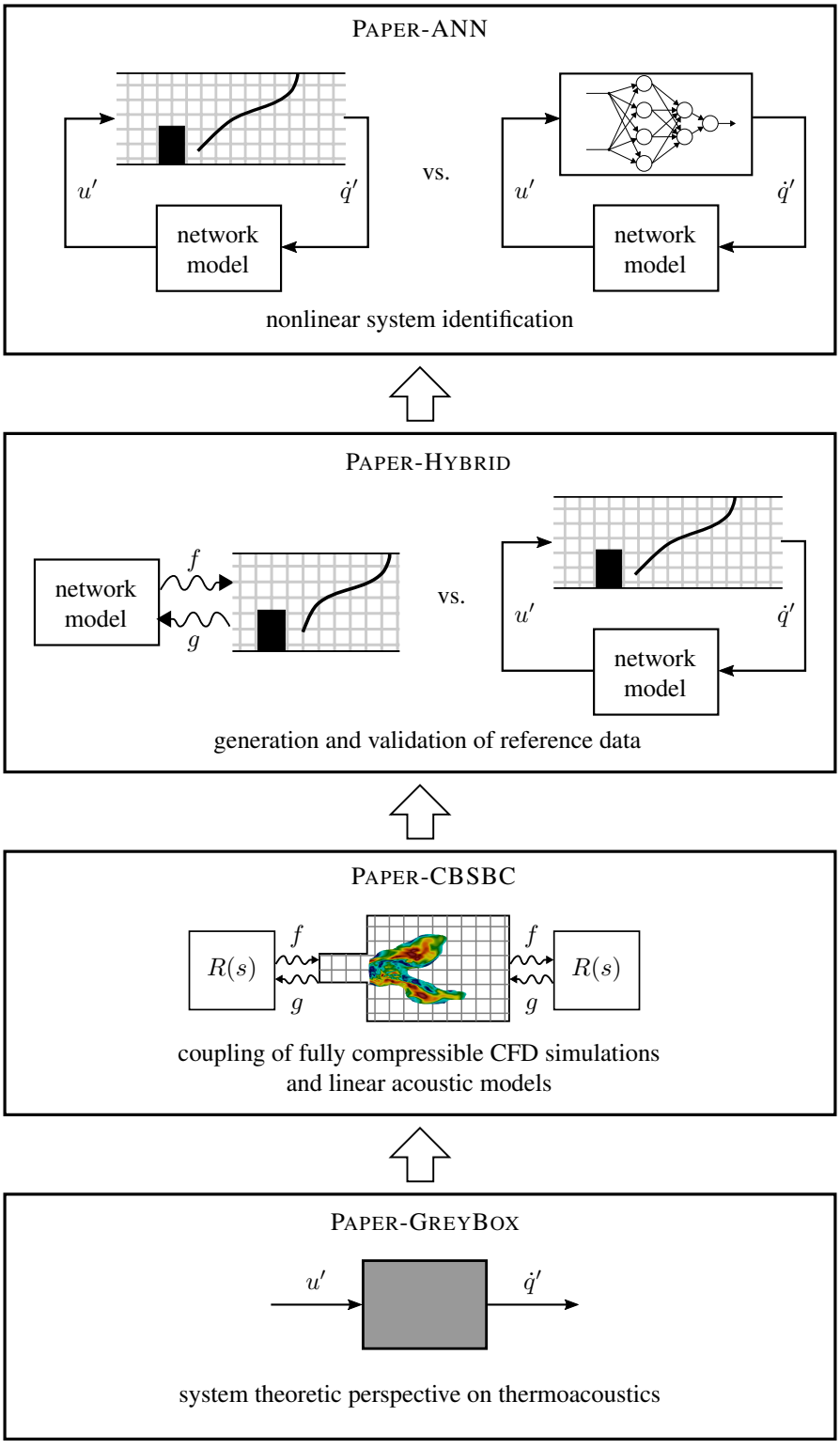

Figure 5.1: Overview of the papers contributing to this thesis.

Frühjahrstagung Turbomaschinen [84] and at the International Symposium on Thermoacoustic Instabilities in Gas Turbines and Rocket Engines [85].

6 Outlook

All methods developed in the present thesis are formulated in a very general way and can easily be applied to a variety of other problems. The laminar premixed flame investigated should be considered as an example application. Tudisco et al. [86] use CBSBC to investigate the Continuously Variable Resonance Combustor (CVRC) rig located at Purdue University. The rig is a single injector rocket engine type combustor. With CBSBC it should also be possible to model the influence of Helmholtz resonators and dissipative liners in LES of gas turbine combustion chambers. The methods are also expected to improve combustion noise simulations. The noise measured from a real flame depends strongly on the acoustic boundary conditions. This can be modeled via CBSBC. With the hybrid low-Mach formulation proposed it should, in theory, be possible to simulate combustion noise with an incompressible simulation. In the FVV follow-up project ROLEX[12] it is planned to use the hybrid formulations to model annular and multi-can combustors of modern gas turbines. Other possible applications are thermoacoustic engines or HVAC systems.
CBSBC can be applied as long as the waves impinging on the boundary conditions are plane. The limitation of the hybrid low-Mach model is the compactness assumption of the heat source. Further effort should be spent to overcome these limitations.
As the computational effort of the hybrid models is still considerable, methods to build nonlinear low-order models of the flame dynamics in a general and consistent way are required. In the scope of this thesis, in PAPER-ANN, artificial neural networks have been used to extend the CFD/SI approach to the nonlinear regime. Unfortunately, a high uncertainty of amplitudes of thermoacoustic oscillations predicted was observed. Hence, more sophisticated methods are required. One way to improve the results are white- or grey-box models, which account for the physics of the flame more accurately. Another idea is to use not only the time series of the input and output signal to identify the model, but also

[12] Hybrid **R**educed **O**rder / **L**ES Models of self-e**X**cited Combustion Instabilities in Multi-Burner Systems

field data [87]. This allows to use more information to build the models which should reduce the length of the time series required. These models should be validated in the systematic procedure proposed in PAPER-ANN.

Bibliography

[1] W. Polifke. "Divide et Impera – Combining CFD, system identification and system modelling to analyse thermo-acoustic combustion instabilities". In: *3. NAFEMS CFD-Seminar: "Simulation gekoppelter Strömungsvorgänge (Multifield FSI)"*. Wiesbaden, Germany: NAFEMS, 2006.

[2] W. Polifke, C. O. Paschereit, and K. Döbbeling. "Suppression of Combustion Instabilities through Destructive Interference of Acoustic and Entropy Waves". In: *6th. Int. Conf. on Sound and Vibration*. Copenhagen, Denmark, 1999.

[3] W Polifke, A Poncet, C. O. Paschereit, and K Döbbeling. "Determination of (Thermo-) Acoustic Transfer Matrices by Time-Dependent Numerical Simulation". In: *7th Int. Conference on Numerical Combustion*. York, UK, 1998.

[4] W. Polifke, C. O. Paschereit, and T. Sattelmayer. "A Universally Applicable Stability Criterion for Complex Thermoacoustic Systems". In: *18. Deutsch-Niederländischer Flammentag, emVDI Bericht*. 1313. Delft, NL: Verein Deutscher Ingenieure (VDI), 1997, pp. 455–460.

[5] W Polifke and C. O. Paschereit. "Determination of Thermo-Acoustic Transfer Matrices by Experiment and Computational Fluid Dynamics". In: *ERCOFTAC Bulletin* 38 (Sept. 1998).

[6] W. Polifke. "Mechanisms of flame-acoustics interaction in premix burners". In: *Combura 2004*. Nieuwegein, The Netherlands: STW, NVV, Dutch section of the Combustion Institute., Mar. 2004.

[7] W. Polifke and C. J. Lawn. "On the Low-Frequency Limit of Flame Transfer Functions". In: *Combust. Flame*. 3rd ser. 151.3 (Nov. 2007), pp. 437–451. DOI: 10.1016/j.combustflame.2007.07.005.

[8] W Polifke, C. O. Paschereit, and K Döbbeling. "Constructive and Destructive Interference of Acoustic and Entropy Waves in a Premixed Combustor with a Choked Exit". In: *International Journal of Acoustics and Vibration* 6.3 (2001), pp. 135–146. DOI: 10.20855/ijav.2001.6.382.

[9] W Polifke, A Poncet, C. O. Paschereit, and K Döbbeling. "Reconstruction of Acoustic Transfer Matrices by Instationary Computational Fluid Dynamics". In: *J. of Sound and Vibration* 245.3 (Aug. 2001), pp. 483–510. DOI: 10.1006/jsvi.2001.3594.

[10] W. Polifke and C. Wall. "Non-Reflecting Boundary Conditions for Acoustic Transfer Matrix Estimation with LES". In: *Proceedings of the Summer Program 2002*. Stanford, USA: Center for Turbulence Research, Stanford University, 2002, pp. 345–356.

[11] F. E. Culick and V. Yang. “Overview of Combustion Instabilities in Liquid-Propellant Rocket Engines”. In: *Liquid Rocket Engine Combustion Instability* 169 (1995), pp. 3–37. (Visited on 01/06/2016).

[12] E. Giacomazzi. “The Importance of Operational Flexibility in Gas Turbine Power Plants”. eng. In: *Energia, Ambiente e Innovazione* 6 (Feb. 2014), pp. 58–63. DOI: 10.12910/EAI2013-35. (Visited on 04/20/2016).

[13] T. Lieuwen and V. Yang, eds. *Combustion Instabilities in Gas Turbine Engines: Operational Experience, Fundamental Mechanisms, and Modeling*. Vol. 210. Progress in Astronautics and Aeronautics. AIAA, 2005. ISBN: 1-56347-669-X.

[14] A. P. Dowling. “The Calculation of Thermoacoustic Oscillation”. In: *Journal of Sound and Vibration* 180.4 (1995), pp. 557–581. DOI: 10.1006/jsvi.1995.0100.

[15] J. J. Keller. “Thermoacoustic Oscillations in Combustion Chambers of Gas Turbines”. In: *AIAA Journal* 33.12 (1995), pp. 2280–2287.

[16] D Bohn and E Deucker. “An Acoustical Model to Predict Combustion Driven Oscillations”. In: *20th Int’l Congress on Combustion Engines*. 20th International Congress on Combustion Engines. London, UK: CIMAC, 1993.

[17] B. Schuermans, V. Bellucci, and C. O. Paschereit. “Thermoacoustic Modeling and Control of Multi-Burner Combustion Systems”. In: *Int’l Gas Turbine and Aeroengine Congress & Exposition*. GT2003-38688. Atlanta, GA, U.S.A.: ASME, 2003, pp. 509–519. DOI: 10.1115/GT2003-38688.

[18] M. Bothien, J. Moeck, A. Lacarelle, and C. O. Paschereit. “Time Domain Modelling and Stability Analysis of Complex Thermoacoustic Systems”. In: *Proceedings of the Institution of Mechanical Engineers, Part A: Journal of Power and Energy* 221.5 (Jan. 2007), pp. 657–668. DOI: 10.1243/09576509JPE384.

[19] L. Kabiraj, R. Sujith, and P. Wahi. “Bifurcations of Self-Excited Ducted Laminar Premixed Flames”. In: *J. Eng. Gas Turb. Power* 134 (2012), p. 031502.

[20] A. P. Dowling. “Nonlinear Self-Excited Oscillations of a Ducted Flame”. In: *Journal of Fluid Mechanics* 346 (1997), pp. 271–290. (Visited on 12/17/2015).

[21] R. M. Murray, C. A. Jacobson, R. Casas, A. I. Khibnik, C. R. J. Jr, R. Bitmead, A. A. Peracchio, and W. M. Proscia. *System Identification for Limit Cycling Systems: A Case Study for Combustion Instabilities*. Tech. rep. Technical Report CDS97-012. Caltech, 1997.

[22] T Poinsot and S. M. Candel. “A Nonlinear Model for Ducted Flame Combustion Instabilities”. In: *Combust. Sci. Tech.* 61 (1988), pp. 121–153.

[23] A. Cummings and W. Eversman. “High Amplitude Acoustic Transmission through Duct Terminations: Theory”. In: *Journal of Sound and Vibration* 91.4 (1983), pp. 503 –518. ISSN: 0022-460X. DOI: http://dx.doi.org/10.1016/0022-460X(83)90829-5.

[24] T. Schuller, N. Tran, N. Noiray, D. Durox, S. Ducruix, S. Candel, and others. “The Role of Nonlinear Acoustic Boundary Conditions in Combustion/Acoustic Coupled Instabilities”. In: *ASME Turbo Expo*. Orlando, FL, 2009.

[25] A. P. Dowling. “A Kinematic Model of a Ducted Flame”. In: *J. Fluid Mech.* 394.394 (1999), pp. 51–72.

[26] N. Noiray, D. Durox, T. Schuller, and S. Candel. “A Unified Framework for Nonlinear Combustion Instability Analysis Based on the Flame Describing Function”. In: *J. Fluid Mech.* 615 (2008), pp. 139–167. DOI: 10.1017/S0022112008003613.

[27] B. Cosic, J. Moeck, and C. O. Paschereit. “Prediction of Pressure Amplitudes of Self-Excited Thermoacoustic Instabilities for a Partially Premixed Swirl Flame”. In: *Proceedings of ASME Turbo Expo 2013*. San Antonio, Texas, USA, 2013.

[28] C. F. Silva, F. Nicoud, T. Schuller, D. Durox, and S. Candel. “Combining a Helmholtz Solver with the Flame Describing Function to Assess Combustion Instability in a Premixed Swirled Combustor”. In: *Combustion and Flame* 160.9 (Sept. 2013), pp. 1743–1754.

[29] H. Krediet. *Prediction of Limit Cycle Oscillations in Gas Turbine Combustion Systems Using the Flame Describing Function*. 2012.

[30] H. J. Krediet, C. H. Beck, W. Krebs, S. Schimek, C. O. Paschereit, and J. B. W. Kok. “Identification of the Flame Describing Function of a Premixed Swirl Flame from LES”. In: *Comb. Sci. Tech.* (2012), pp. –. DOI: 10.1016/j.proci.2012.06.140.

[31] H. J. Krediet, C. H. Beck, W. Krebs, and J. B. W. Kok. “Saturation Mechanism of the Heat Release Response of a Premixed Swirl Flame Using LES”. In: *Proceedings of the Combustion Institute* 34.1 (2013), pp. 1223 –1230. ISSN: 1540-7489. DOI: 10.1016/j.proci.2012.06.140.

[32] X. Han and A. S. Morgans. “Simulation of the Flame Describing Function of a Turbulent Premixed Flame Using an Open-Source LES Solver”. In: *Combustion and Flame* 162.5 (May 2015), pp. 1778–1792. ISSN: 0010-2180. DOI: 10.1016/j.combustflame.2014.11.039. (Visited on 05/05/2015).

[33] W. Polifke. “Black-Box System Identification for Reduced Order Model Construction”. In: *Annals of Nuclear Energy*. Advanced stability analysis for nuclear reactors 67C (2014), pp. 109–128. ISSN: 0306-4549. DOI: 10.1016/j.anucene.2013.10.037. (Visited on 07/21/2014).

[34] F. Selimefendigil and W. Polifke. “A Nonlinear Frequency Domain System Model with Coupled Modes for Limit Cycle Prediction of Thermoacoustic Systems”. In: *Int. J. Spray Comb. Dynamics*. 4th ser. 3 (2011), pp. 303–330. ISSN: 1756-8277. DOI: 10.1260/1756-8277.3.4.303.

[35] F. Selimefendigil. “Identification and Analysis of Nonlinear Heat Sources in Thermo-Acoustic Systems”. PhD Thesis. TU München, 2010.

[36] F. Selimefendigil, S. Föller, and W. Polifke. “Nonlinear Identification of the Unsteady Heat Transfer of a Cylinder in Pulsating Crossflow”. In: *Computers and Fluids*. 0th ser. 53 (2012), pp. 1–14. DOI: 10.1016/j.compfluid.2011.08.012.

[37] J. Lunze. *Regelungstechnik. 1: Systemtheoretische Grundlagen, Analyse und Entwurf einschleifiger Regelungen: mit 64 Beispielen, 166 Übungsaufgaben sowie einer Einführung in das Programmsystem MATLAB*. ger. 5., neu bearb. und erw. Aufl. Springer-Lehrbuch. Berlin: Springer, 2006. ISBN: 978-3-540-28326-3.

[38] J. Lunze. *Regelungstechnik. 2: Mehrgrößensysteme, digitale Regelung: mit 55 Beispielen, 94 Übungsaufgaben sowie einer Einführung in das Programmsystem MATLAB*. ger. 5., neu bearb. Aufl. Springer-Lehrbuch. Berlin: Springer, 2008. ISBN: 978-3-540-78462-3 978-3-540-78463-0.

[39] G. F. Franklin, J. D. Powell, and M. L. Workman. *Digital Control of Dynamic Systems*. eng. 3. ed., [Nachdr.] Menlo Park, Calif.: Addison-Wesley, 2002. ISBN: 978-0-201-33153-0 978-0-201-82054-6.

[40] S. Föller and W. Polifke. "Advances in Identification Techniques for Aero-Acoustic Scattering Coefficients from Large Eddy Simulation". In: *18th International Congress on Sound and Vibration (ICSV18)*. Vol. 4. Rio de Janeiro, Brazil, 2011, pp. 3122–3129.

[41] N. K. Sinha and G. Prasada Rao, eds. *Identification of Continuous-Time Systems: Methodology and Computer Implementation*. International series on microprocessor-based systems engineering v. 7. Dordrecht ; Boston: Kluwer Academic, 1991. ISBN: 978-0-7923-1336-6.

[42] C. Sovardi, S. Jaensch, and W. Polifke. "Concurrent Identification of Aero-Acoustic Scattering and Noise Sources at a Flow Duct Singularity in Low Mach Number Flow". In: *Journal of Sound and Vibration* 377 (Sept. 2016), pp. 90–105. DOI: 10.1016/j.jsv.2016.05.025.

[43] C. Sovardi, Y. Aurégan, and W. Polifke. "Parametric LES/SI Based Aeroacoustic Characterization of Tandem Orifices in Low Mach Number Flows". In: *Acta Acustica united with Acustica* 102.5 (2016), pp. 793–803. DOI: 10.3813/AAA.918994.

[44] C. Sovardi and W. Polifke. "CFD-Based Modelling of Sound Generation in Ducted Discontinuities". In: *Progress in Simulation, Control and Reduction of Ventilation Noise*. Ed. by C. Schram. Vol. VKI LS 2016-02. VKI Lecture Series 2015. Rhode-St-Genèse, BE: VKI, 2016. ISBN: ISBN-13 978-2-87516-098-0.

[45] C. Sovardi and W. Polifke. "Acoustic Characterisation of Double-Orifice Configurations by Means of a LES-SI Approach". In: *Euronoise 2015 – 10th European Congress and Exposition on Noise Control Engineering*. Maastricht, The Netherlands: European Acoustics Association, 31st May to 3rd June, 2015.

[46] C. Sovardi and W. Polifke. "CFD-Based Modelling of Sound Generation in Ducted Discontinuities". In: *Progress in Simulation, Control and Reduction of Ventilation Noise*. VKI Lecture Series 2015. Rhode-St-Genèse, BE: VKI, Nov. 2015.

[47] C. Sovardi, S. Jaensch, C. Silva, and W. Polifke. "Identification of Sound Sources in Internal Ducted Flows: A Large Eddy Simulation–System Identification Approach." In: *21st International Congress on Sound and Vibration (ICSV21)*. 2014. (Visited on 11/18/2014).

[48] C. Sovardi and W. Polifke. "Identification of Sound Sources in Internal Non-Reactive Turbulent Flows". In: *DGLR/DEGA X-Noise Workshop Strömungsakustik*. München / Ottobrunn: DGLR / DEGA / X-Noise-Netzwerk, 20./21. November 2013.

[49] R. Isermann and M. Münchhof. *Identification of Dynamical Systems: An Introduction with Applications*. Advanced textbooks in control and signal processing. Berlin and Heidelberg: Springer-Verlag, 2010. ISBN: 978-3-540-78878-2.

[50] O. Nelles. *Nonlinear System Identification*. en. Berlin, Heidelberg: Springer Berlin Heidelberg, 2001. ISBN: 978-3-642-08674-8. (Visited on 10/07/2016).

[51] A. Wills and B. Ninness. “On Gradient-Based Search for Multivariable System Estimates”. In: *IEEE Transactions on Automatic Control* 53.1 (2008), pp. 298–306. DOI: 10.1109/TAC.2007.914953.

[52] T. Chen, H. Ohlsson, and L. Ljung. “On the Estimation of Transfer Functions, Regularizations and Gaussian Processes—Revisited”. In: *Automatica* 48.8 (Aug. 2012), pp. 1525–1535. DOI: 10.1016/j.automatica.2012.05.026.

[53] M. Verhaegen and P. Dewilde. “Subspace Model Identification Part 1. The Output-Error State-Space Model Identification Class of Algorithms”. In: *International Journal of Control* 56 (5) (1992), pp. 1187–1210.

[54] M. Verhaegen and P. Dewilde. “Subspace Model Identification Part 2. Analysis of the Elementary Output-Error State-Space Model Identification Algorithm”. In: *International Journal of Control* 56 (5) (1992), pp. 1211–1241.

[55] M. Verhaegen. “Subspace Model Identification Part 3. Analysis of the Ordinary Output-Error State-Space Model Identification Algorithm”. In: *International Journal of Control* 58,3 (1993), pp. 555–586.

[56] D. Westwick and M. Verhaegen. “Identifying MIMO Wiener Systems Using Subspace Model Identification Methods”. In: *Signal Processing* 52.2 (1996), pp. 235–258. ISSN: 0165-1684. DOI: 10.1016/0165-1684(96)00056-4.

[57] M. Schoukens, G. Vandersteen, and Y. Rolain. “An Identification Algorithm for Parallel Wiener-Hammerstein Systems”. In: 2013, pp. 4907–4912.

[58] M. Schoukens and Y. Rolain. “Parametric Identification of Parallel Wiener Systems”. In: *Instrumentation and Measurement, IEEE Transactions on* 61.10 (2012), pp. 2825–2832.

[59] J. Paduart, L. Lauwers, R. Pintelon, and J. Schoukens. “Identification of a Wiener–Hammerstein System Using the Polynomial Nonlinear State Space Approach”. In: *Control Engineering Practice* 0 (2012), pp. –. DOI: 10.1016/j.conengprac.2012.06.006.

[60] G. Pillonetto, F. Dinuzzo, T. Chen, G. D. Nicolao, and L. Ljung. “Kernel Methods in System Identification, Machine Learning and Function Estimation: A Survey”. In: *Automatica* 50.3 (2014), pp. 657–682. DOI: 10.1016/j.automatica.2014.01.001.

[61] H Akaike. “Modern Development of Statistical Methods. Á In: Eykhoff, P.(Ed.), Trends and Progress in Systems Identification”. In: (1981).

[62] M. Verhaegen and V. Verdult. *Filtering and System Identification: A Least Squares Approach*. Cambridge: Cambridge University Press, 2012. ISBN: 978-1-107-40502-8.

[63] S. W. Rienstra and A. Hirschberg. *An Introduction to Acoustics*. Tech. rep. IWDE 92-06. Eindhoven University of Technology, 2015.

[64] M. L. Munjal. *Acoustics of Ducts and Mufflers*. Second edition. Chichester, West Sussex, United Kingdom: Wiley, 2014. ISBN: 978-1-118-44312-5.

[65] T. Poinsot and D. Veynante. *Theoretical and Numerical Combustion*. 2nd ed. Edwards, R. T. Incorporated, 2012.

[66] B. T. Chu. “On the Generation of Pressure Waves at a Plane Flame Front”. In: *4th Symposium (International) on Combustion*. Vol. 4. Cambridge, Massachusetts, USA: Combustion Institute, 1953, pp. 603–612. DOI: 10.1016/S0082-0784(53)80081-0.

[67] J. Kopitz and W. Polifke. “CFD-Based Application of the Nyquist Criterion to Thermo-Acoustic Instabilities”. In: *J. Comp. Phys.* 14th ser. 227 (2008), pp. 6754–6778. DOI: doi:10.1016/j.jcp.2008.03.022.

[68] C. F. Silva, T. Emmert, S. Jaensch, and W. Polifke. “Numerical Study on Intrinsic Thermoacoustic Instability of a Laminar Premixed Flame”. In: *Combust. Flame* 162.9 (2015), pp. 3370 –3378. ISSN: 0010-2180. DOI: 10.1016/j.combustflame.2015.06.003.

[69] C. F. Silva, S. Jaensch, T. Emmert, and W Polifke. “On the Autoregressive Behavior of the Intrinsic Thermoacoustic Feedback Loop Observed in Premixed Flames”. In: *22nd International Congress on Sound and Vibration (ICSV22)*. Florence, Italy, 12-16 July 2015.

[70] T. Emmert, M. Meindl, S. Jaensch, and W. Polifke. “Linear State Space Interconnect Modeling of Acoustic Systems”. In: *Acta Acustica united with Acustica* 102.5 (2016), pp. 824–833. DOI: 10.3813/AAA.918997.

[71] W. Polifke. “System Identification for Aero- and Thermo-Acoustic Applications”. In: *Advances in Aero-Acoustics and Thermo-Acoustics*. Ed. by C. Schram. VKI LS 2011-01. Rhode-St-Genèse, BE: Von Karman Institute, 2011, pp. 1–46.

[72] A. Cuquel, C. Silva, F. Nicoud, D. Durox, and T. Schuller. “Prediction of the Nonlinear Dynamics of a Multiple Flame Combustor by Coupling the Describing Function Methodology with a Helmholtz Solver”. In: *Proceedings of ASME Turbo Expo 2013*. Glasgow, UK: ASME, 2013.

[73] C. Mirat, D. Durox, and T. Schuller. “Stability Analysis of a Swirl Spray Combustor Based on Flame Describing Function”. In: *Proceedings of the Combustion Institute* 35.3 (2015), pp. 3291 –3298. ISSN: 1540-7489. DOI: http://dx.doi.org/10.1016/j.proci.2014.08.020.

[74] M. Heckl. “A New Perspective on the Flame Describing Function of a Matrix Flame”. In: *International Journal of Spray and Combustion Dynamics* 7.2 (May 2015), pp. 91–112. ISSN: 1756-8277. DOI: 10.1260/1756-8277.7.2.91. (Visited on 07/10/2015).

[75] Z. Zhang, D. Guan, Y. Zheng, and G. Li. “Characterizing Premixed Laminar Flame–acoustics Nonlinear Interaction”. In: *Energy Conversion and Management* 98 (July 2015), pp. 331–339. ISSN: 0196-8904. DOI: 10.1016/j.enconman.2015.03.095. (Visited on 04/21/2015).

[76] T. Schuller, S. Ducruix, D. Durox, and S. Candel. “Modeling Tools for the Prediction of Premixed Flame Transfer Functions”. In: *Proc. Combust. Inst.* 29.1 (2002), pp. 107–113.

[77] K. Kashinath, I. C. Waugh, and M. P. Juniper. “Nonlinear Self-Excited Thermoacoustic Oscillations of a Ducted Premixed Flame: Bifurcations and Routes to Chaos”. In: *J. Fluid Mech.* 761 (Dec. 2014), pp. 399–430. ISSN: 1469-7645. DOI: 10.1017/jfm.2014.601. (Visited on 01/29/2015).

[78] K. Kashinath, S. Hemchandra, and M. P. Juniper. “Nonlinear Phenomena in Thermoacoustic Systems With Premixed Flames”. In: *Journal of Engineering for Gas Turbines and Power* 135 (2013), p. 061502.

[79] V. N. Kornilov, R. Rook, J. H. M. ten Thije Boonkkamp, and L. P. H. de Goey. "Experimental and Numerical Investigation of the Acoustic Response of Multi-Slit Bunsen Burners". In: *Combustion and Flame* 156.10 (Oct. 2009), pp. 1957 –1970. ISSN: 0010-2180. DOI: 10.1016/j.combustflame.2009.07.017. (Visited on 11/10/2014).

[80] J. Moeck, C. Scharfenberg, O. Paschereit, and R. Klein. "A Zero-Mach Solver and Reduced Order Acoustic Representations for Modeling and Control of Combustion Instabilities". In: *Active Flow Control II*. Vol. 108. Notes on Numerical Fluid Mechanics and Multidisciplinary Design. Springer, 2010, pp. 291–306. ISBN: 978-3-642-11735-0.

[81] J. P. Moeck, M. R. Bothien, S. Schimek, A. Lacarelle, and C. O. Paschereit. "Subcritical Thermoacoustic Instabilites in a Premixed Combustor". In: *14th AIAA/CEAS Aeroacoustics Conference (29th AIAA Aeroacoustics Conference)*. Vancouver, Canada: AIAA/CEAS, May 5 – 7 2008.

[82] S. Jaensch and W. Polifke. *CFD-Basierte, Niedrigdimensionale Modellierung Der Nichtlinearen Dynamik von Vormischflammen*. Vol. FVV-Heft Nr. 1098. 2016.

[83] S. Jaensch, M. Merk, E. Gopalakrishnan, S. Bomberg, T. Emmert, R. I. Sujith, and W. Polifke. "Hybrid CFD/ Low Order Modeling of Thermoacoustic Limit Cycles". In: *SFB/TRR 40 – Summer Program Report 2015*. Ed. by C. Stemmer, Adams, N. A., Haidn O.J., Radespiel, R., Sattelmayer, T., Schröder, W., and Weigand, B. Garching, Germany, 2015.

[84] S. Jaensch and W. Polifke. "CFD-Basierte, Niedrigdimensionale Modellierung Der Nichtlinearen Dynamik von Vormischflammen". In: *Informationstagung Motoren/Turbomaschinen*. R574 / R575. Bad Neuenahrt, Germany: FVV, 2016.

[85] S. Jaensch and W. Polifke. "On the Uncertainty Encountered When Modeling Self-Excited Thermoacoustic Oscillations with Artificial Neural Networks". In: *Int. Symp. on Thermoacoustic Instabilities in Gas Turbines and Rocket Engines*. GTRE-006. Garching, Germany, June 2016.

[86] P. Tudisco, R. Ranjan, S. Menon, S. Jaensch, and W. Polifke. "Application of the Time-Domain Admittance Boundary Condition to Large-Eddy Simulation of Combustion Instability in a Shear-Coaxial, High Pressure Combustor". In: *Flow, Turbulence and Combustion* (2017). DOI: 10.1007/s10494-017-9804-3.

[87] B. Peherstorfer and K. Willcox. "Data-Driven Operator Inference for Nonintrusive Projection-Based Model Reduction". en. In: *Computer Methods in Applied Mechanics and Engineering* 306 (July 2016), pp. 196–215. ISSN: 00457825. DOI: 10.1016/j.cma.2016.03.025. (Visited on 10/29/2016).

Appendices

Proceedings of ASME Turbo Expo 2014: Turbine Technical Conference and Exposition
GT2014
June 16-20, 2014, Düsseldorf, Germany

GT2014-27034

A GREY-BOX IDENTIFICATION APPROACH FOR THERMOACOUSTIC NETWORK MODELS

S. Jaensch, T. Emmert, C. F. Silva, W. Polifke
Lehrstuhl für Thermodynamik
Technische Universität München
D-85747 Garching, Germany
Email: polifke@td.mw.tum.de

ABSTRACT

This work discusses from a system theoretic point of view the low order modeling and identification of the acoustic scattering behavior of a ducted flame.

In this context, one distinguishes between black-box and grey-box models. The former rely on time series data only and do not require any physical modeling of the system that is to be identified. The latter exploit prior knowledge of the system physics to some extent and in this sense are physically motivated.

For the case of a flame stabilized in a duct, a grey-box model is formulated that comprises an acoustic part as well as sub-models for the flame dynamics and the jump conditions for acoustic variables across the region of heat release. Each of the subsystems can be modeled with or without physical a priori knowledge, in combination they yield a model for the scattering behavior of the flame.

We demonstrate these concepts by analyzing a CFD model of a laminar conical premixed flame. The grey-box approach allows to optimize directly the scattering behavior of the identified model. Furthermore, we show that the method allows to estimate heat release rate fluctuations as well as the flame transfer function from acoustic measurements only.

NOMENCLATURE

f_i	downstream traveling characteristic wave amplitude measured at position i
g_i	upstream traveling characteristic wave amplitude measured at position i
S_{ij}	element of the Scattering matrix
$\boldsymbol{G}$	general dynamical system
h	impulse response coefficient
$\boldsymbol{A}, \boldsymbol{B}, \boldsymbol{C}, \boldsymbol{D}$	state-space matrices
n	order of the state-space model
$\boldsymbol{x}$	state vector
$\boldsymbol{v}, v_i$	input signal
$\hat{\boldsymbol{y}}, \hat{y}_i$	output signal
q	time-shift operator
a, b	coefficients of polynomials
$\boldsymbol{\Theta}$	parameter vector
e	prediction error
$V(\boldsymbol{\Theta})$	cost function
λ	regularization parameter
u'	velocity fluctuation
p'	pressure fluctuation
$\dot{q}'$	heat release rate fluctuation
$\hat{q}'$	estimated heat release rate fluctuation
τ, σ	coefficient of the $n-\tau-\sigma$ model
Δt	sampling time
τ_c	characteristic time scale
f	frequency
$\omega^\star$	normalized frequency
$\bar{h}$	continues time impulse response
$\bar{\rho}$	mean density
$\bar{c}$	mean speed of sound
fit	fit-value

INTRODUCTION

Thermoacoustic instabilities are a cause for concern in combustion applications as diverse as domestic heaters, gas turbines, and rocket engines. They go along with high fluctuations of pressure and heat release rate and therefore, can lead to a significant reduction of the life time of the engine [1].

Due to the today limited computational capacities it is not possible to simulate a whole gas turbine with CFD in order to

S. Jaensch, T. Emmert, C. F. Silva, and W. Polifke, GT2014-27034, in Proceedings of ASME Turbo Expo, Düsseldorf, Germany, 2014, 10.1115/GT2014-27034.. Reprinted with permission from ASME.

analyze thermoacoustic instabilities. Instead, the gas turbine is divided into several subsystems and a low-order model for each of the subsystems is determined. Then, all low-order models are connected in order to predict the stability of the whole system. This type of models is called "thermoacoustic network model" [2–6].

Point of discussion of the present study is the low-order modeling of the acoustic scattering behavior of a flame stabilized in a duct. This is the relationship between acoustic waves that are impinging on a flame and the resulting reflected and transmitted acoustic waves. The state of the art ansatz is to combine the Rankine-Hugoniot jump conditions with the flame transfer function (FTF) [7]. Thereby, the Rankine-Hugoniot equations represent the linearized, one dimensional momentum and energy equations evaluated over the flame. They relate the incoming and outgoing acoustic waves with the fluctuation of the global heat release rate. The FTF closes the equations by relating the velocity fluctuation at a reference position with the fluctuation of the heat release rate. We can distinguish between two different types of models used for the FTF. On the one hand there are analytic models like the $n-\tau-\sigma$ model [8–10]. On the other hand the FTF can be determined with an approach that combines CFD simulations with system identification (SI) techniques. Thereby, at first the CFD model is excited with broadband signals in order to generate data. Afterwards, the SI methods are used to derive models from the time series. This approach is called CFD/SI approach and was originally proposed in [11]. The part of the identification does not require any physical assumptions and therefore, is a black-box approach. As we will see grey-box modeling establishes a connection between the analytical white-box models and the black-box modeling of the CFD/SI approach.

The rest of the paper is organized as follows. First an overview of thermoacoustic network models and the basic theory of system identification is provided. Then the modelling of the scattering matrix of an acoustic flame element is analyzed from a system theoretic perspective and different models of the flame dynamics are discussed. Finally, the approach is validated using a CFD model of a laminar premixed conical flame.

THERMOACOUSTIC NETWORK MODELS

This section gives a brief overview on the modeling of thermoacoustic networks, as it is used in the paper. The classical modeling of acoustic networks is in frequency domain [2,3,6]. An alternative way of the modeling is based on state-space models in the time domain [4,5]. It is possible to show that both formulations are equivalent. Further details on the implementation used in the present work are given in [12].

The modeling of the acoustic network is based on the assumption of plane waves. This is justified, as the cross section length of the acoustic elements is much smaller than the characteristic wavelength relevant in those systems. In order to obtain a causal formulation of the acoustic network, the acoustic perturbations are formulated throughout the paper in terms of the characteristic wave amplitudes f and g. They are defined as

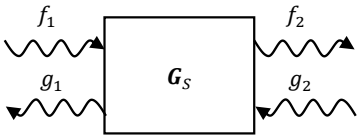

Figure 1: Up- and downstream acoustic waves of a general scattering system

$$f=\frac{1}{2}\left(\frac{p'}{\bar{\rho}\,\bar{c}}+u'\right),\ g=\frac{1}{2}\left(\frac{p'}{\bar{\rho}\,\bar{c}}-u'\right) \qquad (1)$$

with the fluctuation of pressure p' and of velocity u' and the mean density $\bar{\rho}$ and speed of sound $\bar{c}$.

Acoustic elements like ducts, area jumps and flames are described by their corresponding scattering systems. In an abstract way it is given as

$$\boldsymbol{G}_S:\begin{bmatrix}g_1\\f_1\end{bmatrix}\mapsto\begin{bmatrix}f_2\\g_2\end{bmatrix} \qquad (2)$$

As shown in Figure 1 it relates the acoustic waves upstream and downstream of the element. We omit entropy waves because entropy waves generated by the flame couple with acoustic perturbations only in regions of strong mean flow acceleration, which are not discussed in the present work [13]. However, the presented framework can be extended without essential difficulty to account for this effect. Commonly, a scattering system is expressed in terms of the scattering matrix. We use the terminology "system" to point out that we describe a dynamic relationship between the input output signals and that it is unnecessary to restrict oneself to the frequency domain or to a specific model structure. For elements like ducts and area jumps analytic expressions for the scattering systems exist [14]. Scattering systems of complex elements can be derived from experiments or from CFD. In the latter case two main approaches are used: On the one hand solvers based on a linearized formulation of the Navier-Stokes equations [15] and on the other hand solvers based on the full Navier-Stokes equations. The present study considers the determination of the scattering systems from fully compressible CFD simulations. Here, the computationally most efficient method is the CFD/SI approach [11,16–18]. The approach forms the basis for this work and therefore, is discussed in the subsequent sections.

SYSTEM IDENTIFICATION

With SI we can derive dynamical models from time series data. Within this section we explain the general procedure, which consists of three steps: collection of the time series data, selection of the model structure and the determination of the unknown parameters of the model [19–21].

S. Jaensch, T. Emmert, C. F. Silva, and W. Polifke, GT2014-27034, in Proceedings of ASME Turbo Expo, Düsseldorf, Germany, 2014, 10.1115/GT2014-27034.. Reprinted with permission from ASME.

Data Acquisition

The first step is the collection of the data. For a given experimental setup or, as in the present case, a CFD simulation one first defines the inputs and outputs of interest. When the scattering system is to be identified, the inputs and the outputs are the incoming and outgoing acoustic waves, respectively. Afterwards, input signals are designed in order to make the experiment as informative as possible. One requirement is to excite all frequencies of interest with an amplitude as high as possible, i.e. without bringing the amplitude to levels where non-linear effects are important. When the experiment has more than one input channel, the data is more informative if the correlation of the input signals of each channel is low. The input signals used for the present study are given in [22] and meet these requirements.

Selection of the Model Structure

The second step is the selection of the model structure. As shown in Figure 2, a dynamical model describes the relationship between the n_v input signals v_i and the estimates of the n_y output signals $\hat{y}_j$. The mapping is described by a function $f(\boldsymbol{v}, \boldsymbol{\Theta})$. Here, $\boldsymbol{\Theta}$ is the vector of unknown parameters that are to be determined during the identification process. Within this work we consider the function $f(\boldsymbol{v}, \boldsymbol{\Theta})$ to be linear.

A general description for linear models is given by the so called transfer function notation

$$\hat{y}_j(t) = \sum_{i=1}^{n_v} \frac{1 + a_{1,i,j} q^{-1} + \cdots + a_{n_a,i,j} q^{-n_{a_{i,j}}}}{b_{0,i,j} + b_{1,i,j} q^{-1} + \cdots + b_{n_b,i,j} q^{-n_{b_{i,j}}}} v_i(t) \qquad (3)$$

where q is the time-shift operator, and $a_{k,i,j}$ and $b_{k,i,j}$ are the coefficients of the polynomials. An equivalent formulation is the state space structure. It is given as

$$\begin{bmatrix} \boldsymbol{x}(t + \Delta t) \\ \hat{\boldsymbol{y}}(t) \end{bmatrix} = \begin{bmatrix} \boldsymbol{A} & \boldsymbol{B} \\ \boldsymbol{C} & \boldsymbol{D} \end{bmatrix} \begin{bmatrix} \boldsymbol{x}(t) \\ \boldsymbol{v}(t) \end{bmatrix} \qquad (4)$$

Here, $\boldsymbol{x}(t) \in \mathbb{R}^n$ is the state vector, $\hat{\boldsymbol{y}}(t)$ and $\boldsymbol{v}(t)$ are the vectorized output and input signals as given in Figure 2, Δt is the sampling time and $\boldsymbol{A}$, $\boldsymbol{B}$, $\boldsymbol{C}$,and $\boldsymbol{D}$ are the system matrices of appropriate size. The integer n denotes the order of the system. The parameters for this type of model are the coefficients of the system matrices.

A model structure commonly used for the CFD/SI approach is the finite impulse response (FIR) model, it is given as

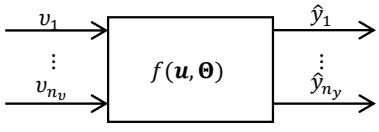

Figure 2: General dynamical model

$$\hat{y}_j(t) = \sum_{i=1}^{n_v} \sum_{k=0}^{L_{i,j}} h_{k,i,j} v_i(t - k\Delta t) \qquad (5)$$

The unknown parameters for this model structure are the coefficients of the impulse response $h_{k,j}$. L_i is the length of the impulse response. With $j = 1, \ldots, n_y$ equation (5) describes an FIR model with n_v inputs and n_y outputs. The FIR model (5) is a simplification of transfer function model (3) and the state space model (4). For the transfer function model this can easily be seen by setting the parameters to $a_{k,i,j} = h_{k,i,j}$, $b_{0,i,j} = 1$, $b_{k\neq 0,i,j} = 0$ and $L_{i,j} = n_{a_{i,j}}$. For the state-space model one can show that if all eigen values of the Matrix $\boldsymbol{A}$ are equal to zero, the state space model has a finite impulse response and hence, is an FIR model.

Throughout the paper we separate between black-box, grey-box and white box models as follows. When we use a black-box model, only the input and output signals of the model have a physical meaning and we do not have any insight regarding the mechanisms leading to the specific relationship between these signals. Mathematically the model can be described as a state-space model where all coefficients of the system matrices are to be estimated by system identification routines. A Grey-box models uses some physical knowledge to determine the model structure. This means that some of the parameters of the system matrices are known from physical considerations and the remaining parameters are identified. As we will show later on the $n - \tau - \sigma$ model may be considered as an example of a grey-box model. Accordingly, a white-box model is a model where all parameters are known from physical considerations and none of the parameters is identified.

Determination of the Parameters

The last step is to determine the unknown parameters of the model. Therefore, we define an optimization problem based on the least squares approach. The parameters are determined by minimizing the cost function

$$V(\boldsymbol{\Theta}) = \sum_{k=1}^{N} e(k\,\Delta t, \boldsymbol{\Theta})^2 \qquad (6)$$

with the length of the time series N and the prediction error $e(t) = y(t) - \hat{y}(t, \boldsymbol{\Theta})$. Hereby, $y(t)$ and $\hat{y}(t, \boldsymbol{\Theta})$ are the measured and the estimated output, respectively. If the model is an FIR filter, the resulting optimization problem can be solved analytically and is known as the Wiener-Hopf equation. For a general state-space model the optimization can only be solved using iterative algorithms. Wills and Ninness [23] give an overview over these algorithms.

As long simulation times are very expensive, the time series used in the CFD/SI approach are typically very short. In this case

S. Jaensch, T. Emmert, C. F. Silva, and W. Polifke, GT2014-27034, in Proceedings of ASME Turbo Expo, Düsseldorf, Germany, 2014, 10.1115/GT2014-27034.. Reprinted with permission from ASME.

the quality of the identified model can be improved by regularization. Thereby, the cost function $V(\boldsymbol{\theta})$ is extended to

$$V(\boldsymbol{\theta}) = \sum_{k=1}^{N} e(k\,\Delta t, \boldsymbol{\theta})^2 + \lambda \boldsymbol{\theta}^T \boldsymbol{\theta} \qquad (7)$$

with the regularization parameter λ. A study on the influence of the regularization to the CFD/SI approach is given in [22]. Chen et. al. [24] discuss different ways to interpret regularization using the example of the FIR model.

FROM BLACK-BOX TO WHITE-BOX MODELLING

In this section we analyze the modelling of a thermoacoustic flame element from a system theoretic perspective. We start with a black-box model that does not require any physical knowledge. Then we show that physical relationships allow us to split the black-box model into several subsystems with different physical interpretation. At first we model each of these subsystems again as black-box model. Afterwards, we discuss how the subsystem representing the flame dynamics can be modeled.

Black-box Modeling of the Scattering System

Using the black-box approach we see the scattering system as shown in Figure 1. We know the physical meaning of inputs and outputs and the black-box identification provides the transfer behavior between them. However, we do not get an understanding of the physical mechanisms that lead to the specific scattering behavior.

Grey-box Modeling of the Scattering System

The following derivation of the scattering system is motivated by the analysis in [12]. In the grey-box approach the scattering system of the flame is seen as shown in Figure 3. The schematic diagram in Figure 4 represents the same configuration in a more abstract way. Here, the whole system is separated into three subsystems: 1) the system $\boldsymbol{G}_F$ describing the dynamics of the flame, 2) the system $\boldsymbol{G}_A$ describing the acoustic part and 3) the system $\boldsymbol{G}_{JC}$ describing the jump condition over the flame.

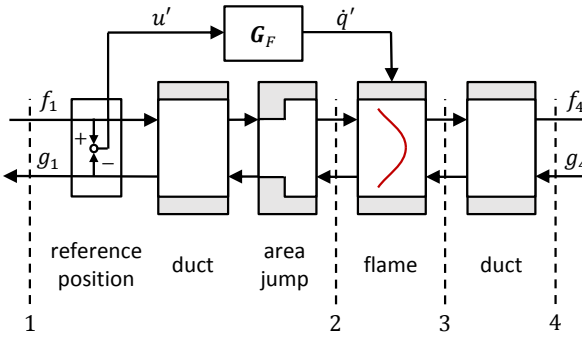

Figure 3: Grey-box model for the scattering behavior of a flame stabilized in a duct

Each of these subsystems is discussed in the remaining paragraphs of this section.

The system $\boldsymbol{G}_F$ represents the dynamics of the flame. It links the velocity fluctuation u' at a reference position to the fluctuation of the global heat release $\dot{q}'$. We define the corresponding system as

$$\boldsymbol{G}_F : u' \longmapsto \dot{q}' \qquad (8)$$

Secondly, the acoustic system $\boldsymbol{G}_A$ describes the dynamic behavior of the acoustic waves. Its main components are the scattering systems $\boldsymbol{G}_S^u$ and $\boldsymbol{G}_S^d$ of the acoustic elements upstream and downstream of the flame, respectively. The upstream scattering system $\boldsymbol{G}_S^u$, linking the acoustic waves upstream of the flame position, is given as

$$\boldsymbol{G}_S^u : \begin{bmatrix} f_1 \\ g_2 \end{bmatrix} \longmapsto \begin{bmatrix} g_1 \\ f_2 \end{bmatrix} \qquad (9)$$

According to Figure 3 this scattering system represents a duct/area-jump configuration. The corresponding transfer behavior of the system can be determined in manifold ways, e.g. by the CFD/SI approach or by analytical modelling.

In analogy the downstream scattering system

$$\boldsymbol{G}_S^d : \begin{bmatrix} f_3 \\ g_4 \end{bmatrix} \longmapsto \begin{bmatrix} g_3 \\ f_4 \end{bmatrix} \qquad (10)$$

relates the acoustic waves traveling on the downstream side of the flame.

For the reference velocity we define the following expression

$$u' = f_1 - g_1 \qquad (11)$$

Finally, the acoustic system $\boldsymbol{G}_A$ is retrieved by assembling (9) to (11) and is given as

$$\boldsymbol{G}_A : \begin{bmatrix} g_2 \\ f_3 \\ f_1 \\ g_4 \end{bmatrix} \longmapsto \begin{bmatrix} g_1 \\ f_4 \\ g_3 \\ f_2 \\ u' \end{bmatrix} \qquad (12)$$

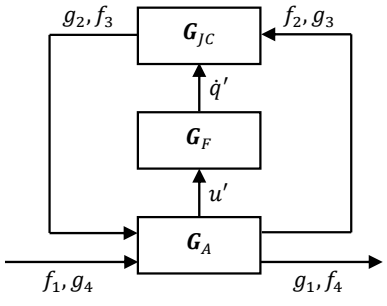

Figure 4: Schematic diagram of the configuration from Figure 3

S. Jaensch, T. Emmert, C. F. Silva, and W. Polifke, GT2014-27034, in Proceedings of ASME Turbo Expo, Düsseldorf, Germany, 2014, 10.1115/GT2014-27034.. Reprinted with permission from ASME.

The system $\boldsymbol{G}_{JC}$ represents the jump condition over the flame and closes the formulation. It relates the following properties

$$\boldsymbol{G}_{JC}: \begin{bmatrix} f_2 \\ g_3 \\ \dot{q}' \end{bmatrix} \mapsto \begin{bmatrix} g_2 \\ f_3 \end{bmatrix} \qquad (13)$$

A specific structure of this system can be derived from the Rankine-Hugoniot jump equations [25].

Grey-box Modeling of the Flame Dynamics

In the previous section the flame is treated as black-box model. However, there are different grey-box and white-box models for the flame dynamics. As an FIR model it can be described as

$$\boldsymbol{G}_F: \dot{q}'(t) = \sum_{k=0}^{L} h_k u'(t - k\Delta t) \qquad (14)$$

with the sampling time Δt and the coefficients of the impulse response h_k. From a system theoretic point of view the FIR model is typically seen as black-box model. However, Blumenthal et. al. [26] show that a linearized G-equation model of the flame has indeed a finite impulse response. Furthermore, it can be shown that the flame response can be discussed in terms of perturbations, which are convected along the flame front with distributed time delays [8,27]. The FIR model also accounts for this effect, thus it should be considered as grey-box model of the flame.

The $n-\tau-\sigma$ model [8,27] is a further grey-box model for the flame dynamics. It can be derived from the FIR model. Thereby, the coefficients of the FIR model (14) are calculated according to

$$h_k = \frac{\Delta t}{\sigma\sqrt{2\pi}} exp\left(-\frac{1}{2}\left(\frac{k\Delta t - \tau}{\sigma}\right)^2\right) \qquad (15)$$

Here, τ and σ are the unknown parameters that are to be identified. The occurrence of the time step Δt in equation (15) is discussed in the appendix. The $n-\tau-\sigma$ model is a parameterization of the FIR model and reduces the number of unknown parameters from L to 2. This helps to interpret the model. If both of these parameters are determined by analytic equations, we obtain a white-box model of the flame.

APPLICATION TO A LAMINAR PREMIXED FLAME

In this section we use the grey-box modeling to investigate a 2D CFD simulation of a laminar premixed flame. At first we show the CFD setup and discuss the network model. Afterwards we discuss the results of the identification.

CFD Setup

The CFD configuration is based on an experiment from Le Helley [28]. This experiment was studied numerically in [29] and [30]. With the exception of the inflow and outflow boundary conditions (BCs), we use the 2D CFD model shown in [29,30] utilizing the CFD solver AVBP. With Plane wave masking [31] we obtain boundaries with low reflection. The geometry is shown in Figure 5 and was discretized using a mesh with a minimum cell size of about $3.42 \cdot 10^{-15}\ m^3$. At the inlet we impose a stoichiometric propane-air mixture at $300\ K$ with a mean velocity of $4m/s$. The intake walls are adiabatic non slip walls whereas the chamber walls are modeled as adiabatic slip walls.

In a cross validation study three simulations with different ways of excitation were performed. One simulation with excitation from upstream (case Ex_u), one with excitation from downstream (case Ex_d) and one with a simultaneous excitation at both sides of the flame (case $Ex_{u,d}$). The excitation signal in all cases was a broadband wavelet signal proposed in [22]. In the case $Ex_{u,d}$ with simultaneous excitation both input signals were statistically independent. In all cases the outgoing acoustic waves as well as the fluctuation of the heat release rate were measured as output signals. Each simulation was run for $0.02s$. Using a sampling interval of $2.2 \cdot 10^{-5}s$ this provides 899 data samples.

The characteristic time scale τ_c [26,32] of the configuration is given as

$$\tau_c = \frac{2R}{\bar{u}\ sin(2\alpha)} = 0.7141ms \qquad (16)$$

Here, $R = 0.65mm$ is the radius, $\bar{u} = 4m/s$ is the inlet velocity and $\alpha = 13.536°$ is the flame angle. This time scale is used to normalize all frequencies and times in the subsequent part of this work.

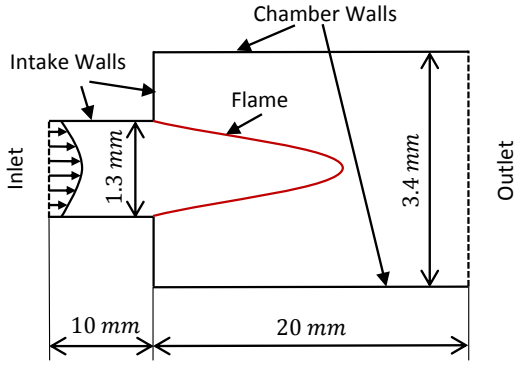

Figure 5: CFD model configuration of the laminar premixed flame

S. Jaensch, T. Emmert, C. F. Silva, and W. Polifke, GT2014-27034, in Proceedings of ASME Turbo Expo, Düsseldorf, Germany, 2014, 10.1115/GT2014-27034.. Reprinted with permission from ASME.

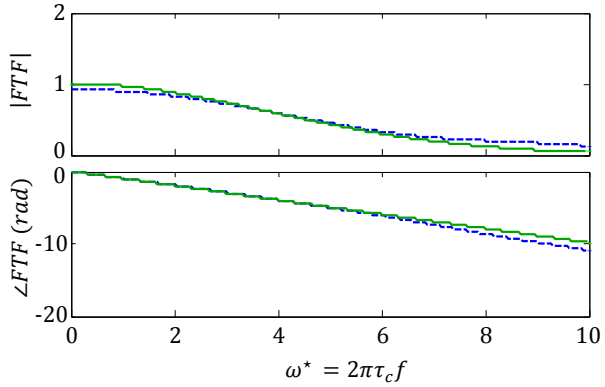

Figure 6: Identified FTF. Solid green lines: $n-\tau-\sigma$ model; Dashed blue lines: FIR model

Direct Identification of the Flame Dynamics

Direct identification of the flame dynamics means to identify the system $\boldsymbol{G}_F$ from the time series of the velocity fluctuations and of the heat release fluctuation. In the previous section we introduced the FIR model and the $n-\tau-\sigma$ model as a grey-box model for the flame. In this section we use the collected time series of velocity and of the heat release rate fluctuation to directly estimate the unknown parameters of the flame models. For the identification of the FIR model we use the Wiener-Hopf inversion. The unknown parameters of the $n-\tau-\sigma$ model are determined in the following way. We start with an initial guess of the parameters and calculate the coefficients h_k of the impulse response according to equation (15). Using this guess and the collected time series of the velocity fluctuation, we can calculate an estimate of the heat release fluctuation with equation (14). With this estimate we can evaluate the cost function (6). In order to minimize the cost function we use the Nelder-Mead optimization algorithm [33].

We used an FIR model with 50 coefficients. The estimated values of the $n-\tau-\sigma$ model are $\tau/\tau_c = 0.9831$ and $\sigma/\tau_c = 0.2597$. In Figure 6 amplitude and phase of the estimated FTF are shown. Polifke and Lawn [34] showed that the low frequency limit of the gain of the FTF of a premixed flame is equal to one. As this knowledge was used to derive the $n-\tau-\sigma$ model, the model exactly fulfills this condition whereas the FIR model slightly violates is. Both models exhibit a linearly decreasing phase angle. This is in agreement with the analytic G-equation model from Schuller et al. [35].

Identification of the Scattering System

As aforementioned, we can model the scattering system of the flame with a black-box and a grey-box ansatz. The grey-box ansatz is very general and consists of several subsystems, which again have to be modeled themselves.

For the acoustic subsystem $\boldsymbol{G}_A$ we need models for the scattering systems $\boldsymbol{G}_S^u$ and $\boldsymbol{G}_S^d$. According to Figure 3, the scattering system $\boldsymbol{G}_S^u$, which relates the acoustic waves upstream of the flame, has to represent a duct-area jump configuration. For the present study we model the duct as a time delay and the area jump as a static gain. However, due to the abstract formulation of the problem the use of less simplistic models for the scattering system is straight forward. The scattering system $\boldsymbol{G}_S^d$ for the waves downstream of the flame we use a simple time delay model.

To model the system $\boldsymbol{G}_{JC}$ we use the Rankine-Hugoniot equations [25] in order to describe this system. In state-space form they are given as

$$\boldsymbol{G}_{RH}: \begin{bmatrix} g_2 \\ f_3 \end{bmatrix} = \frac{1}{\zeta+1} \begin{bmatrix} 1-\zeta & 2 & \vartheta\bar{u}_1 \\ 2\zeta & \zeta-1 & \vartheta\zeta\bar{u}_1 \end{bmatrix} \begin{bmatrix} f_2 \\ g_3 \\ \dot{q}' \end{bmatrix} \qquad (17)$$

with $\zeta = \frac{\bar{\rho}_2\bar{c}_2}{\bar{\rho}_3\bar{c}_3}$ and $\vartheta = \frac{T_3}{T_2} - 1$, where $\bar{\rho}$ denotes the mean density, $\bar{c}$ the mean speed of sound, T the temperature and $\bar{u}_1$ the mean velocity at position 1. The position of the indices is shown in Figure 3. Here again, we use of the Rankine-Hugoniot equations because they describe the investigated configuration sufficiently well. However, the framework allows to consider more complex models for the jump conditions as well. This may be useful when non-compact flames are investigated.

Finally, we need a model for the system $\boldsymbol{G}_F$ describing the dynamics of the flame. We introduced the FIR model and the $n-\tau-\sigma$ model. As the results for both models are very similar we only show the results for the FIR model in this section.

The analytic models for the system $\boldsymbol{G}_A$ and $\boldsymbol{G}_{JC}$ require only parameters that depend on the geometry and on the mean flow properties. Therefore, the unknown parameters of the grey-box model are the coefficients of the impulse response h_k. For these parameters we can either use the estimate we obtained in the previous section or use a grey-box identification algorithm. The latter approach has the advantage that we can directly optimize the scattering behavior of the identified system. Furthermore, it does not require the collected time series of the heat release fluctuation. This is an advantage when experimentally determined time series are analyzed because the measurement of fluctuations of heat release rate with quantitative accuracy is in general very difficult [10]. The procedure of the grey-box identification is similar to the identification of the parameters of the $n-\tau-\sigma$ model. We start with an initial guess for the coefficients h_k. This guess has to fulfill the requirement that the resulting model is stable. Now, by simulating the model with the time series of the incoming acoustic waves, we obtain an estimate of the time series of the outgoing acoustic waves. This enables us to evaluate the cost function (6). Using the state-space representation of the grey-box model, we can directly

S. Jaensch, T. Emmert, C. F. Silva, and W. Polifke, GT2014-27034, in Proceedings of ASME Turbo Expo, Düsseldorf, Germany, 2014, 10.1115/GT2014-27034.. Reprinted with permission from ASME.

apply the algorithms discussed in [23] in order to find parameters that minimize the cost function.

In Figure 7 the resulting estimate of the scattering system are shown in terms of the estimated gain of the scattering matrix. Here, the scattering matrix is defined as

$$\boldsymbol{G}_S: \begin{bmatrix} g_1 \\ f_4 \end{bmatrix} = \begin{bmatrix} S_{11} & S_{12} \\ S_{21} & S_{22} \end{bmatrix} \begin{bmatrix} f_1 \\ g_4 \end{bmatrix} \qquad (18)$$

We compare the following identification results:

1. A black-box estimate using an FIR filter with 150 coefficients for each entry of the scattering matrix. In order to obtain the full scattering matrix on this way from a single CFD run, we have to excite the domain simultaneously from the inlet and the outlet. Therefore, the results shown were based on the data set $\mathrm{Ex_{u,d}}$.
2. A combination of the grey-box model and the FTF that was directly estimated from velocity and heat release fluctuations. This approach allows to determine the full scattering matrix from a CFD run excited only at the inlet or from the outlet. For the results shown in Figure 7 we used the data from CFD case $\mathrm{Ex_u}$, which was excited from the inlet only.
3. We use the grey-box identification routine. This allows us to use our physical understanding of the problem and yet, to directly identify the scattering behavior of the system. Also this approach allows to determine the full scattering matrix from a single CFD run, which was excited only from the inlet or the outlet. In order to perform a cross validation, we used the third data set $\mathrm{Ex_d}$, which was excited from the outlet only.

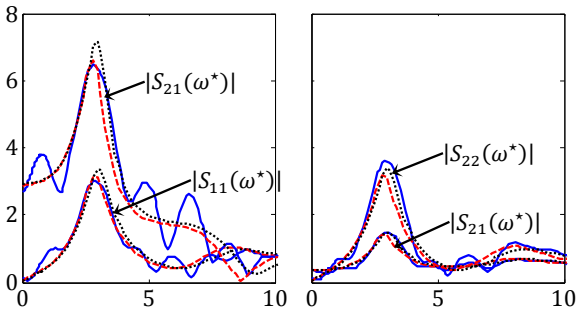

Figure 7: Magnitude of the elements of the scattering matrix. Solid blue lines: black-box FIR model (data: time series of incoming and outgouing acoustc waves of CFD case $\mathrm{Ex_{u,d}}$); Dashed red lines: Combination of directly identified FTF and grey-box model (data: time series of velocity fluctuations and heat release rate fluctuations of CFD case $\mathrm{Ex_u}$); Dotted black lines: grey-box identification (data: time series of incoming and outgouing acoustc waves of CFD case $\mathrm{Ex_d}$);

Each of the models shown in Figure 7 were calculated using a different data set. Nevertheless, all estimates are in good agreement. However, there are oscillations in the curve of the black-box FIR model. The reason is that the black-box model has 600 unknown parameters, whereas the grey-box model has only 50 parameters. The high number of unknown parameters of the FIR model is necessary, as the black-box model has to model the dynamic of the acoustic and of the flame simultaneously. Therefore, the black-box identification of the FIR model requires much longer time series for the same accuracy.

Indirect Identification of the Flame Dynamics

As noted in the previous section, the grey-box identification of the scattering system does not require the time series of the heat release fluctuation. Nevertheless, we obtain an estimate of the impulse response coefficients. Therefore, we can indirectly estimate the flame dynamics. The resulting estimate of the impulse response is plotted in Figure 8. As the first ten parameters of the impulse response could only poorly be estimated, they were fixed to zero.

We can obtain an estimate $\hat{q}'$ of the time series of the heat release rate fluctuations by imposing the measured velocity fluctuation to the identified system $\boldsymbol{G}_F$. In table 1, the real and the estimated heat release fluctuations are compared in terms of the normalized root mean square error, also known as fit value, which is given as

$$\mathrm{fit} = 100\left(1 - \frac{\|\dot{q}' - \hat{\dot{q}}'\|}{\|\dot{q}'\|}\right) \qquad (19)$$

As expected, the highest values are achieved by the direct identification. However, inverting the Rankine-Hugoniot equations by the use of the grey-box identification routine gives almost the same estimate without the usage of $\dot{q}'$, although the corresponding time series was not used for the estimation. Figure 8 shows that the regularization smooth the resulting estimate of the impulse response. This leads according to table 1 to an improvement of about 4% points of the fit value. The regularization parameter λ was choosen to maximize the fit value for the case $\mathrm{Ex_{u,d}}$. The corresponding fit value shows the best improvement we can receive with by regularizing the estimate. Looking at the fit values for the other two regularized cases we can state that the regularization indeed improves the results. However, choosing the regularization parameter in this way is only possible, if the time series of the heat release fluctuation is known.

excitation	direct	Grey-box	Grey-box + regularization
$\mathrm{Ex_u}$	84.88	77.63	81.23
$\mathrm{Ex_d}$	80.49	71.18	76.23
$\mathrm{Ex_{u,d}}$	81.83	75.45	78.55

table 1: fit values for the different CFD cases and identification methods

S. Jaensch, T. Emmert, C. F. Silva, and W. Polifke, GT2014-27034, in Proceedings of ASME Turbo Expo, Düsseldorf, Germany, 2014, 10.1115/GT2014-27034.. Reprinted with permission from ASME.

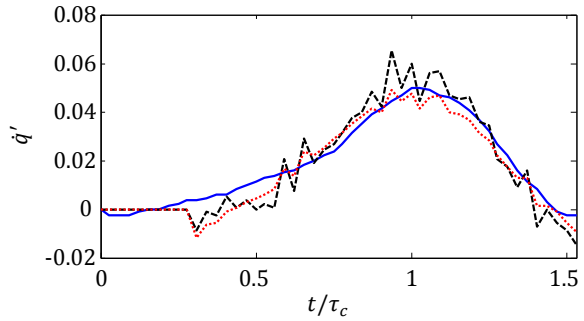

Figure 8: Impulse response of the FTF. Solid blue line: direct SI; dashed black line: grey-box SI; dotted red line: grey-box SI with regularization

CONCLUSION

The low order modelling of the scattering behavior of a laminar flame stabilized in a duct was analyzed. Starting from a black-box description we showed that the scattering behavior can be represented by three interconnected subsystems. One subsystem models the acoustic part, a second subsystem models the flame dynamics and third subsystem models the jump condition over the flame. Each of these subsystems can either be identified as a black-box model or be modeled using first principles. This allows to validate physical assumptions separately. The approach was validated by means of a CFD model of a laminar conical flame.

We showed that grey-box identification allows to exploit the physical knowledge for the identification. This allows to directly optimize the scattering behavior of the identified system and still use the relationships of the network modelling. Furthermore, the approach allows to indirectly estimate the fluctuation of the heat release rate from the acoustic field.

The grey-box approach was introduced in a very general way and therefore, it can easily be extended to more complex configurations. It is also possible to adjust the identification routine depending on the quantity of interest and the data available.

ACKNOWLEDGEMENT

Financial support from the Research Association for Combustion Engines (Forschungsvereinigung Verbrennungs-kraftmaschinen e.V. – FVV) is gratefully acknowledged. The CFD solver AVBP was kindly provided by CERFACS. The authors would like to thank Prof. Arun Tangirala (IIT Madras) for his explanations of the theory of system identification during his stay in Munich.

APPENDIX

The following derivation is based on [19]. In continuous time the impulse response $\bar{h}(t)$ of the $n-\tau-\sigma$ model is given as

$$\bar{h}(t) = \frac{1}{\sigma\sqrt{2\pi}} exp\left(-\frac{1}{2}\left(\frac{t-\tau}{\sigma}\right)^2\right) \qquad (20)$$

According to [19] the impulse response characterizes a linear time invariant causal system. The output $\dot{q}'(t)$ of the system can be calculated by convoluting the input signal $u'(t)$ with the impulse response $\bar{h}(t)$. This is

$$\dot{q}'(t) = \int_0^\infty \bar{h}(\tau)\, u'(t-\tau) d\tau \qquad (21)$$

Sampling this equation with a time step Δt yields after k intervals

$$\dot{q}'(k\Delta t) = \int_0^\infty \bar{h}(\tau)\, u'(k\Delta t-\tau) d\tau \qquad (22)$$

Assuming $h(t)$ and $u'(t)$ to be constant over a time interval Δt gives

$$\dot{q}'(k\Delta t) \approx \sum_{k=0}^{\infty} \bar{h}(k\Delta t) u'(k\Delta t-\tau)\Delta t \qquad (23)$$

Comparing the equations (14) and (23) the coefficients of the discrete impulse response of the $n-\tau-\sigma$ model are

$$h_k = \bar{h}(k\Delta t)\Delta t \qquad (24)$$

This yields the factor Δt in equation (15).

S. Jaensch, T. Emmert, C. F. Silva, and W. Polifke, GT2014-27034, in Proceedings of ASME Turbo Expo, Düsseldorf, Germany, 2014, 10.1115/GT2014-27034.. Reprinted with permission from ASME.

REFERENCES

[1] Lieuwen T., and Yang V., 2005,"Combustion Instabilities in Gas Turbine Engines," **210**, American Institute of Aeronautics and Astronautics, Inc.

[2] Dowling A. P., 1995,"The Calculation of Thermoacoustic Oscillations," Journal of Sound and Vibration, **180**(4), pp. 557–581.

[3] Keller J. J., 1995,"Thermoacoustic oscillations in combustion chambers of gas turbines," AIAA Journal, **33**(12), pp. 2280–2287.

[4] Schuermans B., Bellucci V., and Paschereit C. O., 2003,"Thermoacoustic Modeling and Control of Multi Burner Combustion Systems," ASME Conference Proceedings, **2003**(36851), pp. 509–519.

[5] Bothien M. R., Moeck J. P., Lacarelle A., and Paschereit C. O., 2007,"Time Domain Modelling and Stability Analysis of Complex Thermoacoustic Systems," Proceedings of the Institution of Mechanical Engineers, Part A: Journal of Power and Energy, **221**(5), pp. 657–668.

[6] Bohn D., and Deuker E., 1993,"An acoustical model to predict combustion driven oscillations," *20th International Congress on Combustion Engines*.

[7] Poinsot T., and Veynante D., 2005. *Theoretical and Numerical Combustion*, 2nd ed., R T Edwards Inc.

[8] Polifke W., Kopitz J., and Serbanovic A., 2001,"Impact of the Fuel Time Lag Distribution in Elliptical Premix Nozzles on Combustion Stability," *7th AIAA/CEAS Aeroacoustics Conference*, Maastricht, The Netherlands.

[9] Lawn C. J., and Polifke W., 2004,"A Model for the Thermoacoustic Response of a Premixed Swirl Burner, Part Ii: The Flame Response," Combustion Science and Technology, **176**(8), pp. 1359–1390.

[10] Schuermans B., Bellucci V., Paschereit C., Guethe F., Meili F., and Flohr P., 2004,"A Detailed Analysis of Thermoacoustic Interaction Mechanisms in a Turbulent Premixed Flame," *Proceedings of ASME Turbo Expo 2004 Power for Land, Sea, and Air*.

[11] Polifke W., Poncet A., Paschereit C. O., and Döbbeling K., 2001,"Reconstruction of Acoustic Transfer Matrices by Instationary Computational Fluid Dynamics," Journal of Sound and Vibration, **245**(3), pp. 483–510.

[12] Emmert T., Bomberg S., and Polifke W.,"Intrinsic Thermoacoustic Instability of Premixed Flames," submitted to Combustion and Flame.

[13] Polifke W., Paschereit C., and Doebbeling K., 2001,"Constructive and Destructive Interference of Acoustic and Entropy Waves in a Premixed Combustor with a Choked Exit," International Journal of Acoustics and Vibration, **6 (3)**, pp. 135–146.

[14] Munjal M. L., 1987. *Acoustics of ducts and mufflers with application to exhaust and ventilation system design*, Wiley, New York.

[15] Kierkegaard A., Boij S., and Efraimsson G., 2012,"Simulations of the scattering of sound waves at a sudden area expansion," Journal of Sound and Vibration, **331**(5), pp. 1068–1083.

[16] Gentemann A., Hirsch C., Kunze K., Kiesewetter F., Sattelmayer T., and Polifke W., 2004,"Validation of Flame Transfer Function Reconstruction for Perfectly Premixed Swirl Flames," *Int'l Gas Turbine and Aeroengine Congress & Exposition*, Vienna, Austria.

[17] Polifke W., and Gentemann A., 2004,"Order and Realisability of Impulse Response Filters for Accurate Identification of Acoustical Multi-Ports from Transient CFD," Int. J. of Acoustics and Vibration, **9**(3), pp. 139–148.

[18] Tay-Wo-Chong L., Komarek T., Kaess R., Foeller S., and Polifke W., 2010,"Identification of Flame Transfer Functions from LES of a Premixed Swirl Burner," *Proceedings of ASME Turbo Expo 2010: Power for Land, Sea and Air*.

[19] Ljung L., 1999. *System identification - theory for the user*, 2nd ed., Prentice Hall PTR, New Jersey.

[20] Isermann R., and Münchhof M., 2010. *Identification of dynamical systems: An introduction with applications*, Springer-Verlag, Berlin, Heidelberg.

[21] Verhaegen M., and Verdult V., 2012. *Filtering and system identification: A least squares approach*, Cambridge University Press, Cambridge.

[22] Föller S., and Polifke W., 2011,"Advances in Identification Techniques for Aero-Acoustic Scattering Coefficients from Large Eddy Simulation," *18th International Congress on Sound and Vibration (ICSV18)*, Rio de Janeiro.

[23] Wills A., and Ninness B., 2008,"On Gradient-Based Search for Multivariable System Estimates," IEEE Trans. Automat. Contr., **53**(1), pp. 298–306.

[24] Chen T., Ohlsson H., and Ljung L., 2012,"On the estimation of transfer functions, regularizations and Gaussian processes—Revisited," Automatica, **48**(8), pp. 1525–1535.

[25] Chu B.-T., 1953,"On the generation of pressure waves at a plane flame front," Symposium (International) on Combustion, Elsevier, **4**, pp. 603–612.

[26] Blumenthal R. S., Subramanian P., Sujith R. I., and Polifke W., 2013,"Novel perspectives on the dynamics of premixed flames," Combustion and Flame, **160**(7), pp. 1215–1224.

[27] Komarek T., and Polifke W., 2010,"Impact of Swirl Fluctuations on the Flame Response of a Perfectly Premixed Swirl Burner," J. Eng. Gas Turbines Power, **132**(6), pp. 061503-1,7.

S. Jaensch, T. Emmert, C. F. Silva, and W. Polifke, GT2014-27034, in Proceedings of ASME Turbo Expo, Düsseldorf, Germany, 2014, 10.1115/GT2014-27034.. Reprinted with permission from ASME.

[28]P. Le Helley, 1994,“Etude théorique et expérimentale des instabilités de combustion et de leur contrôle dans un brûleur laminaire prémélangé,” PhD. Thesis, Ecole Centrale Paris.
[29]Kaufmann A., Nicoud F., and Poinsot T., 2002,“Flow forcing techniques for numerical simulation of combustion instabilities,” Combustion and Flame, **131**(4), pp. 371–385.
[30]C. Silva, 2010,“Numerical study of combustion noise in gas turbines,” PhD. Thesis, Siences et techniques du languedoc, University of Montpellier II.
[31]Polifke W., Wall C., and Moin P., 2006,“Partially reflecting and non-reflecting boundary conditions for simulation of compressible viscous flow,” Journal of Computational Physics, **213**(1), pp. 437–449.
[32]Ducruix S., Durox D., and Candel S., 2000,“Theoretical and experimental determinations of the transfer function of a laminar premixed flame,” Proceedings of the Combustion Institute, **28**(1), pp. 765–773.
[33]Nocedal J., and Wright S. J., 2006. *Numerical optimization*, 2nd ed., Springer, New York.
[34]Polifke W., and Lawn C., 2007,“On the low-frequency limit of flame transfer functions,” Combustion and Flame, **151**(3), pp. 437–451.
[35]Schuller T., Durox D., and Candel S., 2003,“A unified model for the prediction of laminar flame transfer functions: comparisons between conical and V-flame dynamics,” Combustion and Flame, **134**(1–2), pp. 21–34.

S. Jaensch, T. Emmert, C. F. Silva, and W. Polifke, GT2014-27034, in Proceedings of ASME Turbo Expo, Düsseldorf, Germany, 2014, 10.1115/GT2014-27034.. Reprinted with permission from ASME.

Journal of Computational Physics 314 (2016) 145–159

Contents lists available at ScienceDirect

Journal of Computational Physics

www.elsevier.com/locate/jcp

On the robust, flexible and consistent implementation of time domain impedance boundary conditions for compressible flow simulations

S. Jaensch *, C. Sovardi, W. Polifke

Professur für Thermofluiddynamik, Technische Universität München, 85747 Garching, Germany

ARTICLE INFO

Article history:
Received 26 May 2015
Received in revised form 10 November 2015
Accepted 3 March 2016
Available online 10 March 2016

Keywords:
Boundary condition
Acoustics
State-space
Impedance
Reflection coefficient
NSCBC

ABSTRACT

The accurate simulation of compressible flows requires the appropriate modeling of the reflection of acoustic waves at the boundaries. In the present study we discuss time domain impedance boundary conditions (TDIBC). The formulation proposed allows to impose a desired reflection coefficient at the inflow and outflow boundaries. Our formulation is an extension of the well known Navier–Stokes characteristic boundary conditions. The frequency dependent reflections at the boundaries are implemented with a state-space model in the time domain. We provide a comprehensive discussion on how such state-space models can be constructed and interpreted. This discussion shows that the state-space description allows a robust and flexible implementation. It allows to consider complex reflection coefficients and account for non-constant CFD time steps in a straight forward manner. Furthermore, we prove analytically and demonstrate numerically that the formulation proposed is consistent, i.e. the formulation ensures that the flow simulation exhibits the reflection coefficient imposed accurately, as long as the waves impinging on the boundary are plane, and it prohibits drift of the mean flow variables. Finally, the boundary conditions are tested successfully for laminar and turbulent flows.

1. Introduction

The simulation of unsteady compressible flows in particular by large eddy simulation (LES) or by direct numerical simulation (DNS) requires the appropriate modeling of the reflection of acoustic waves at the boundaries. Otherwise, the simulation results will be unphysical and will not match experimental data or numerical instabilities occur. Except for some special cases (a chocked inlet, say), the acoustic reflection coefficient depends on the frequency of the acoustic waves. This dependency is a property of the configuration investigated. The boundary conditions discussed in the present work provide a solution to this issue as they allow to impose a frequency dependent reflection coefficient. The concept is known as “time domain impedance boundary conditions” (TDIBC).

For example, the TDIBC formulation proposed in the present work, can facilitate an LES simulation of a gas turbine combustion chamber, which accounts for the acoustic feedback of compressor and turbine. A sketch of such a configuration and the corresponding LES model is shown in Fig. 1. The combustion chamber is resolved with an LES. Simultaneously,

* Corresponding author.
E-mail address: jaensch@tfd.mw.tum.de (S. Jaensch).

http://dx.doi.org/10.1016/j.jcp.2016.03.010
0021-9991/

S. Jaensch, C. Sovardi, and W. Polifke, Journal of Computational Physics, vol. 314, pp. 145–159, 2016, http://dx.doi.org/10.1016/j.jcp.2016.03.010.. Reprinted with permission from Elsevier.

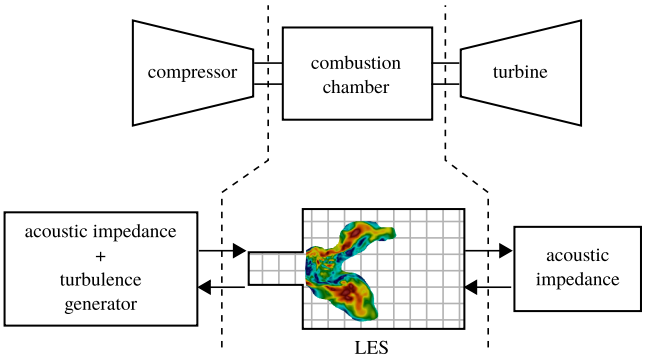

Fig. 1. Schematic diagram of a gas turbine (top) and the corresponding LES model using a TDIBC formulation (bottom).

a TDIBC accounts for the acoustic feedback by imposing the acoustic impedance at the inlet and the outlet. Additionally, turbulence created upstream of the combustion chamber is modeled by a turbulence generator. This modeling reduces the computational costs, significantly, and makes an LES of a gas turbine combustion chamber, which accounts for the acoustic feedback, possible even with today's computational resources. A similar scenario can be considered for rocket engine combustion chambers. Here, the influence of a large number of injectors can be modeled via a TDIBC formulation, efficiently.

A TDIBC formulation has to solve two problems: (1) A time-domain model of the frequency dependent reflection coefficient or of the impedance is required and (2) this model has to be coupled with the flow simulation. The time-domain model has to be robust and flexible so that complex reflection coefficients can be modeled with a reasonable effort. The coupling of the flow simulation and the time-domain model has to ensure that the formulation is consistent. This means that the flow simulation exhibits the reflection coefficient imposed, accurately, without introducing artificial reflections, and that drift of the mean flow variables is avoided. Furthermore, the TDIBC should not constrain the flow simulation, e.g. by requiring a constant time step. In the present work we review existing TDIBC formulations and propose a formulation that is robust, flexible and consistent at the same time.

The time-domain model can either model the acoustic impedance or the acoustic reflection coefficient. The former relates primitive acoustic variables and the latter uses characteristic wave amplitudes. One can show that formally both expressions are equivalent. For TDIBC a time-domain model of one of the expressions is required. Several authors [1–9] suggested to apply an inverse Laplace- or z-transform to the reflection coefficient or the impedance. This yields a convolution integral in the time domain, which can be integrated in a CFD code. Schuermans et al. [10] proposed, independently, to use discrete-time state-space models. State-space models are inherently causal, numerically more robust and more flexible. Furthermore, as discussed in section 4.1, they allow a physical meaningful interpretation.

The coupling of the time-domain model with the flow simulation can be done based on primitive variables or on characteristic wave amplitudes. Formulations based on primitive variables use a, possible simplified, version of Myers's condition [11] in the time domain in combination with a time-domain model for the impedance [4,5,8,9]. These formulations work well for solvers of perturbation equations. However, when applied as inflow or outflow boundary condition (BC) to an LES or DNS this coupling yields drift of the mean variables. Therefore, Schuermans et al. [10] proposed to stabilize the simulation with a high pass filter. This method was also utilized by Huber et al. [7]. However, as we will show analytically in the present work, it yields an incorrect reflection coefficient for low frequencies. Kaess et al. [6] proposed to extend "plane wave masking" (PWM) [12] to a TDIBC. PWM itself is an extension of the low-reflective Navier–Stokes characteristic boundary conditions (NSCBC) [13,14]. It minimizes the reflection of plane acoustic waves propagating in the direction perpendicular to the boundary surface. Therefore, this formulation is suitable for configurations which are ducted in the region close to the boundary condition (see Fig. 2). In this case waves with a frequency below the cut-off frequency of the first higher order mode are plane.

In the present work we combine the formulation of Kaess et al. [6] with state-space description of the reflection coefficient as proposed by Schuermans et al. [10]. Therefore, we call the BC proposed **C**haracteristic **B**ased **S**tate-space **B**oundary **C**ondition (CBSBC). We prove analytically and demonstrate numerically that when PWM is used for the coupling drift is avoided and the flow simulation exhibits the reflection behavior imposed, accurately. We show that the coupling based on primitive variables yields drift of the mean flow variables and that the use of a high pass filter avoids the drift but yields incorrect results for low frequencies. In contrast to [10] we use continuous time state-space models this allows to use non-constant time steps in a straight forward manner. Furthermore, we propose to use a state-space model with two inputs. The first input is the characteristic amplitude of the outgoing wave and the second input is an external excitation signal. The latter allows e.g. to consider a loud speaker or a turbulent noise source inside the region of the acoustic model. We demonstrate by a numerical example that CBSBC works well with unstable state-space models. We discuss how state-space models can be determined in most practically relevant situations. CBSBC was implemented in the fully compressible explicit

S. Jaensch, C. Sovardi, and W. Polifke, Journal of Computational Physics, vol. 314, pp. 145–159, 2016, http://dx.doi.org/10.1016/j.jcp.2016.03.010.. Reprinted with permission from Elsevier.

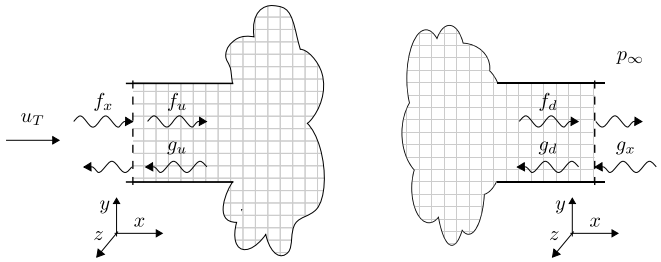

Fig. 2. LES/DNS configuration considered and characteristic wave amplitudes. Left: inflow. Right: outflow.

density-based solvers AVBP (Cerfacs and IFP) and LESLIE (Computational Combustion Lab, Georgia Institute of Technology). To the best of our knowledge the formulation proposed should work also with implicit pressure-based codes.

The paper is organized as follows: In the next section we recapitulate the separation of the flow variables in mean field and turbulent and acoustic fluctuation. In section 3 we recall NSCBC and PWM. How PWM can be extended to TDIBC is shown in section 4. In subsection 4.1 we give a comprehensive introduction to the modeling of the acoustic reflection coefficients in the state-space form. The advantages of the state-space formulation are discussed in subsection 4.2. In subsection 4.3 we provide a pseudo-code example of CBSBC. In subsection 4.4 the properties of the BC proposed and of other formulations are discussed. Finally, in section 5 we illustrate the theory discussed in the previous sections with numerical examples and demonstrate that CBSBC works well for laminar as well as for turbulent flows.

2. Plane acoustic waves

As shown in Fig. 2, we consider configurations that are ducted in regions close to the inlet/outlet BC at which CBSBC are applied. In these configurations waves with a frequency lower then the cut-off frequency of the first higher order mode will be plane. In this situation the flow field can be separated in

$$p(t,x,y,z) = \bar{p}(x,y,z) + p'_T(t,x,y,z) + p'_A(t,x), \tag{1a}$$

$$u(t,x,y,z) = \bar{u}(x,y,z) + u'_T(t,x,y,z) + u'_A(t,x), \tag{1b}$$

with pressure p and velocity u. Variables with bar $\bar{(\cdot)}$ are temporal averaged fields and the indexes "T" and "A" denote the turbulent and the acoustic fluctuations, respectively. The argument t is the time and x, y, z are spatial coordinates as given in Fig. 2. Please note, as we assumed that only plane waves are propagating the acoustic fluctuation depends only on time and axial coordinate (along the length of the duct section).

Plane acoustic waves can be described by the characteristic wave amplitudes f and g

$$f = \frac{1}{2}\left(\frac{p'_A}{\bar{\rho}\bar{c}} + u'_A\right), \quad g = \frac{1}{2}\left(\frac{p'_A}{\bar{\rho}\bar{c}} - u'_A\right). \tag{2}$$

Here, ρ and c are the density and the speed of sound, respectively. As shown in Fig. 2, f corresponds to the wave traveling in downstream direction and g is traveling in upstream direction.

In order to determine f and g from a compressible flow simulation we have to determine the acoustic fluctuations p'_A and u'_A. As the spatial correlation length of the turbulent fluctuations is very small these fluctuations vanish if a spatial average is applied. Therefore, the acoustic fluctuations are given as

$$p'_A = \langle p - \bar{p} \rangle, \tag{3a}$$

$$u'_A = \langle u - \bar{u} \rangle. \tag{3b}$$

Here, $\langle\cdot\rangle$ represents a spatial average of a plane perpendicular to the traveling direction of the acoustic waves.

For highly turbulent flows this area average might not be sufficient. The separation can be improved with characteristic based filtering (CBF) [10,15]. At first f and g are determined locally at n planes, which are perpendicular to the traveling direction of the acoustic wave. Considering the time lags resulting form the speed of propagation of the waves one can average over the local values of f and g

$$f(t,x) = \frac{1}{n}\sum_{i=0}^{n-1} f\left(t + \frac{\Delta x_i}{\bar{c}+\bar{u}}, x + \Delta x_i\right), \tag{4a}$$

$$g(t,x) = \frac{1}{n}\sum_{i=0}^{n-1} g\left(t - \frac{\Delta x_i}{\bar{c}-\bar{u}}, x + \Delta x_i\right). \tag{4b}$$

S. Jaensch, C. Sovardi, and W. Polifke, Journal of Computational Physics, vol. 314, pp. 145–159, 2016, http://dx.doi.org/10.1016/j.jcp.2016.03.010.. Reprinted with permission from Elsevier.

with $\Delta x_i = x_i - x$ and x_i is the axial position of the plane. As demonstrated in [15], this additional filtering allows to determine f and g in highly turbulent flows. For the reminder of this work $\langle\cdot\rangle$ denotes an CBF average, which simplifies to a plane average for $n = 1$.

3. Non-reflective BC with plane wave masking

The boundary conditions proposed in the present work are based on plane wave masking (PWM) [12]. Therefore, we recapitulate PWM in the present section.

The NSCBC framework [13,14] defines the boundary conditions for pressure and velocity as

$$\frac{\partial p}{\partial t} + \frac{1}{2}\bar{\rho}\bar{c}\left(\mathcal{L}_5 + \mathcal{L}_1\right) = 0, \quad \frac{\partial u}{\partial t} + \frac{1}{2}\left(\mathcal{L}_5 - \mathcal{L}_1\right) = 0. \tag{5}$$

Here, $\mathcal{L}_1$ and $\mathcal{L}_5$ are locally (on the boundary patch) defined derivatives of the characteristic wave amplitudes traveling in the up- and downstream direction, respectively. A spatial average over the $\mathcal{L}$-waves yields the derivatives of f and g

$$\frac{\partial f}{\partial t} = \frac{1}{2}\left\langle\mathcal{L}_5\right\rangle, \quad \frac{\partial g}{\partial t} = \frac{1}{2}\left\langle\mathcal{L}_1\right\rangle. \tag{6}$$

Using the original NSCBC a low-reflective outflow BC can be constructed as follows. $\mathcal{L}_5$ leaves the domain and can be determined from the internal field

$$\mathcal{L}_5 = (u + c)\left(\frac{\partial p}{\partial x} + \rho c\frac{\partial u}{\partial x}\right). \tag{7}$$

$\mathcal{L}_1$ is entering the domain and has to be imposed

$$\mathcal{L}_1 = \frac{\sigma}{\bar{\rho}\bar{c}}\left(p - p_\infty\right), \tag{8}$$

with the desired pressure at the outflow p_∞. σ is the relaxation parameter and the term $(p - p_\infty)$ is known as linear relaxation term. An inflow boundary condition can be constructed on a similar way [14].

This BC is partially reflective. As shown by Selle et al. [16] and Polifke et al. [12] the resulting reflection coefficient $R(\omega)$ is a first-order low pass filter

$$R(\omega) = \frac{\hat{g}_d}{\hat{f}_d} = \frac{-1}{1 + 2i\omega/\sigma}, \tag{9}$$

with the angular frequency ω. The hat $\hat{(\cdot)}$ labels variables in the frequency domain. The relaxation parameter σ determines the cut-off frequency of the filter. Using this formulation it is not possible to control phase and magnitude of the reflection coefficient independently from each other. A small value of σ yields a low cut-off frequency and thus, lower reflections. However, if σ is chosen too low, drift of the mean variables is observed.

Polifke et al. extended the NSCBC with PWM, in order to minimizes the reflection of plane acoustic waves at the boundaries [12]. The idea is "to identify outgoing plane waves at the boundary, and then explicitly eliminate outgoing wave contributions from the linear relaxation term" [12].

According to PWM the linear relaxation term for a outflow BC is modified

$$\mathcal{L}_1 = \frac{\sigma}{\bar{\rho}\bar{c}}\left(p - \bar{\rho}\bar{c}\left(f_d + g_x\right) - p_\infty\right) + 2\frac{\partial g_x}{\partial t}. \tag{10}$$

Here, $\bar{\rho}\bar{c}\left(f + g_x\right) = p'_A$ represents the acoustic part of the pressure fluctuation. This term compensates any plane-wave acoustic fluctuation at the boundary condition. The external excitation g_x is the amplitude of an imposed plane wave entering the domain.

As in the NSCBC formulation, the relaxation term of PWM avoids drift of the mean values. PWM yields non-reflective boundary conditions, if (1) all waves close to the boundary are plane and (2) one can accurately separate between mean field, turbulent fluctuations and acoustic fluctuations. As discussed in section 2 the first assumption limits the BC to the low frequency regime and to ducted configurations. CBF allows to separate the flow field, accurately. In summary, one can state that PWM yields very low reflection coefficients for plane acoustic waves, as demonstrated in [12].

A non-reflective inflow boundary condition can be constructed, analogously. Here, the wave $\mathcal{L}_1$ leaves the domain and can be calculated from the internal field

$$\mathcal{L}_1 = (u - c)\left(\frac{\partial p}{\partial x} - \rho c\frac{\partial u}{\partial x}\right). \tag{11}$$

According to PWM the ingoing wave $\mathcal{L}_5$ is given as

$$\mathcal{L}_5 = \sigma\left(u - \left(f_x - g_u\right) - u_T\right) + 2\frac{\partial f_x}{\partial t}, \tag{12}$$

where f_x is the amplitude of a plane wave imposed at the boundary.

S. Jaensch, C. Sovardi, and W. Polifke, Journal of Computational Physics, vol. 314, pp. 145–159, 2016, http://dx.doi.org/10.1016/j.jcp.2016.03.010.. Reprinted with permission from Elsevier.

A.2 PAPER-CBSBC

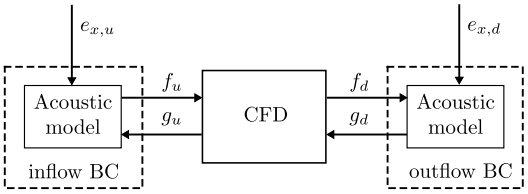

Fig. 3. System theoretic perspective of the impedance boundary conditions.

4. Characteristic based state-space boundary conditions (CBSBC)

In the previous section the wave amplitudes f_x and g_x were considered to be independent external excitation signals. In order to impose a specific reflection behavior this excitation has to be calculated from the characteristic wave leaving the domain according to a proper acoustic model (compare Fig. 3).

In the sake of better readability we restrict the discussion in this section to an outflow BC. The corresponding expressions for an inflow boundary can be derived, analogously. The necessary changes for the implementation are briefly summarized in section 4.3.

For many configurations of practical interest the reflection of acoustic waves can be assumed to be linear and causal. Hence, it can be described with a linear state space model

$$\dot{\mathbf{x}} = A\mathbf{x} + B\underbrace{\begin{bmatrix} f_d \\ e_{x,d} \end{bmatrix}}_{\mathbf{u}} \tag{13a}$$

$$\underbrace{g_d}_{y} = C\mathbf{x} + D\underbrace{\begin{bmatrix} f_d \\ e_{x,d} \end{bmatrix}}_{\mathbf{u}} \tag{13b}$$

Here, $\mathbf{u}$ denotes the input vector of the model. Its first element f_d is the amplitude of the wave leaving the CFD-domain. The second element is the external excitation signal $e_{x,d}$. This signal is also filtered by the state-space model and can describe e.g. an excitation with a loud speaker or turbulent sound production inside the acoustic domain. The output signal y of the acoustic model is the amplitude g_d of the wave imposed to the CFD simulation. The matrices A, B, C and D are the state space matrices and $\mathbf{x}$ is state vector.

The state-space model given in (13) is a complete mathematical representation of any linear causal system. Depending on the choice of the matrices A, B, C and D it can represent, e.g. a linear acoustic solver, a measured reflection coefficient or a thermoacoustic network model. The only restriction made by using the (linear) state-space structure as such is its linearity. Therefore, the state-space representation allows a very general implementation of TDIBCs. In the remainder of this section, we will first explain by examples how a state-space model for TDIBC can be determined in situations of practical interest. Afterwards, we discuss the advantages of using state-space models compared to other model structures that are found in the literature. Then we present a pseudo code implementation of CBSBC. We conclude the section with a discussion of the properties of CBSBC and other TDIBC formulations found in the literature.

4.1. Examples of state-space models for acoustic boundary conditions

In this subsection we give examples how a state-space model for the acoustic can be constructed. The results of this subsection are probably familiar to readers with a profound background in control theory. However, in order to apply the boundary condition proposed in practical application, a good understanding of the state space description of acoustic models is mandatory. Therefore, we discuss in this section how such state space models can be determined and interpreted in detail.

The best way to determine the parameters of a state space model depends on the information available. We identify three situations that typically occur: (1) A set of linear partial differential equations (PDE) is known to model the acoustic reflections. (2) Measurements of the reflection coefficient at several distinct frequencies are available. (3) Different modeling approaches are combined using an acoustic network model as discussed by Schuermans et al. [17] and Bothien et al. [18].

4.1.1. State-space models deduced from linear partial differential equations

In many situations the reflection of acoustic waves is well described by a set of linear PDEs, e.g. the linearized Euler or Navier–Stokes equations. In this subsection we discuss how an exhaust duct can be modeled. This is a pedagogical example of how PDEs can be casted in state space form. The same procedure can be extended to three dimensional PDEs and to more sophisticated discretization schemes.

As shown in Fig. 4, the exhaust is discretized with a homogeneous one-dimensional mesh. Please compare the notation in Fig. 3 and Fig. 4.

S. Jaensch, C. Sovardi, and W. Polifke, Journal of Computational Physics, vol. 314, pp. 145–159, 2016, http://dx.doi.org/10.1016/j.jcp.2016.03.010.. Reprinted with permission from Elsevier.

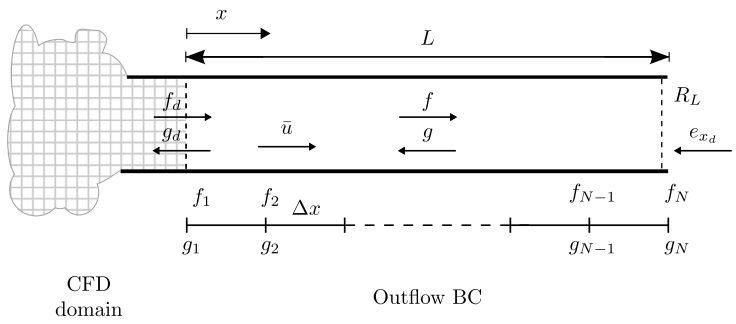

Fig. 4. Discretization of the exhaust section.

The plane-wave acoustic inside the exhaust section can be modeled with the one dimensional Euler equations. Neglecting mean flow gradients they are given as

$$\frac{\partial f}{\partial t} + (\bar{u} + \bar{c}) \frac{\partial f}{\partial x} = 0, \tag{14a}$$

$$\frac{\partial g}{\partial t} + (\bar{u} - \bar{c}) \frac{\partial g}{\partial x} = 0. \tag{14b}$$

The problem is closed with the boundary conditions

$$f\,(x = 0, t) = f_1 = f_d, \tag{15a}$$

$$g\,(x = L, t) = g_N = R_L f\,(x = L, t) + e_{x,d}. \tag{15b}$$

The meaning of all variables is given in Fig. 4. The Dirichlet boundary condition at $x = 0$ couples the acoustic model with the CFD simulation. The boundary condition at $x = L$ describes the reflection of an acoustic wave at the boundary with a scalar (real valued) reflection coefficient R_L. Additionally, it models an excitation with an acoustic source $e_{x,d}$, e.g. a loud speaker.

We apply a linear upwind finite difference scheme for the spatial discretization. This yields for (14a)

$$\frac{\partial f_i}{\partial t} = -(\bar{u} + \bar{c}) \frac{f_i - f_{i-1}}{\Delta x} \qquad \text{for } i = 2, \cdots, N \tag{16}$$

and for (14b)

$$\frac{\partial g_i}{\partial t} = -(\bar{u} - \bar{c}) \frac{g_{i+1} - g_i}{\Delta x} \qquad \text{for } i = 1, \ldots, N-1. \tag{17}$$

The boundaries (15) are included according to

$$\frac{\partial f_2}{\partial t} = -(\bar{u} + \bar{c}) \frac{f_2 - f_d}{\Delta x}, \tag{18a}$$

$$\frac{\partial g_{N-1}}{\partial t} = -(\bar{u} - \bar{c}) \frac{R_L f_N + e_{x,d} - g_{N-1}}{\Delta x}. \tag{18b}$$

Now, a state-space model can easily be derived by rewriting the equations (16) to (18b) in matrix vector form

$$\underbrace{\frac{\partial}{\partial t}\begin{bmatrix} f_2 \\ f_3 \\ \vdots \\ f_N \\ g_1 \\ \vdots \\ g_{N-2} \\ g_{N-1} \end{bmatrix}}_{\dot{\mathbf{x}}} = \underbrace{\begin{bmatrix} -\alpha_+ & 0 & & & & & & & \\ \alpha_+ & -\alpha_+ & & & & & & & \\ & \ddots & \ddots & & & & & & \\ & & \alpha_+ & -\alpha_+ & & & & & \\ & & & & \alpha_- & -\alpha_- & & & \\ & & & & & \ddots & \ddots & & \\ & & & & & & \alpha_- & -\alpha_- \\ & & & -R_L\alpha_- & & & 0 & \alpha_- \end{bmatrix}}_{A} \underbrace{\begin{bmatrix} f_2 \\ f_3 \\ \vdots \\ f_N \\ g_1 \\ \vdots \\ g_{N-2} \\ g_{N-1} \end{bmatrix}}_{\mathbf{x}}$$

S. Jaensch, C. Sovardi, and W. Polifke, Journal of Computational Physics, vol. 314, pp. 145–159, 2016, http://dx.doi.org/10.1016/j.jcp.2016.03.010.. Reprinted with permission from Elsevier.

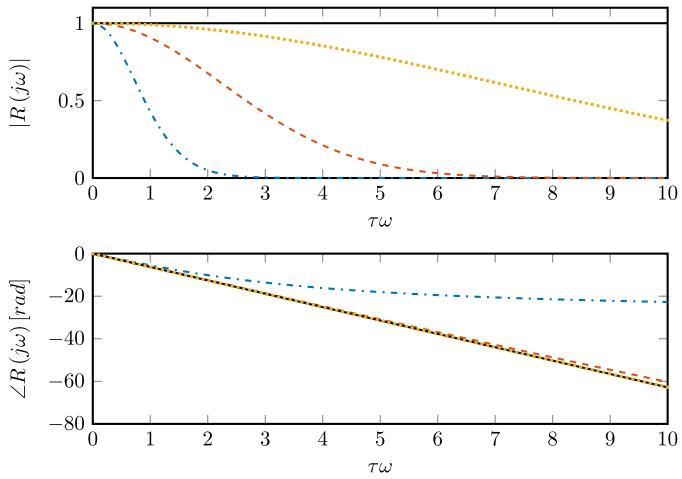

Fig. 5. Reflection coefficient of the quarter wave resonator. Determined by discretizing the one dimensional Euler equations with a mesh of 10 nodes (·-·-·), of 100 nodes (- - -) and of 1000 nodes (·) and analytical solution (——).

$$+\underbrace{\begin{bmatrix} \alpha_+ & 0 \\ 0 & 0 \\ \vdots & \vdots \\ 0 & 0 \\ 0 & -\alpha_- \end{bmatrix}}_{B} \underbrace{\begin{bmatrix} f_d \\ e_{x,d} \end{bmatrix}}_{\mathbf{u}} \tag{19a}$$

$$\underbrace{g_d}_{y} = g_1 = \underbrace{\begin{bmatrix} 0 & \cdots & 0 & 1 & 0 & \cdots & 0 \end{bmatrix}}_{C}\mathbf{x} + \underbrace{\begin{bmatrix} 0 & 0 \end{bmatrix}}_{D}\mathbf{u}, \tag{19b}$$

with $\alpha_+ = (\bar{u}+\bar{c})/\Delta x$ and $\alpha_- = (\bar{u}-\bar{c})/\Delta x$. In this form the meaning of the parameters of the state space model becomes evident. The state vector $\mathbf{x}$ consists of the values of f and g at the nodes of the mesh. The state matrix A is a linear operator. The elements at the diagonal band are determined by the discretization scheme. The off diagonal element couples the state values f_N and g_{n-1} and thus, describes the reflection at the outlet of the resonator. The input matrix B models how the input signal $\mathbf{u}$ acts on the temporal derivative of the state vector. Again, its elements are determined by the discretization scheme. All but one element of the output vector C are equal to zero. One element is equal to unity and by multiplying the output vector C with the state vector $\mathbf{x}$ one obtains the output signal $y = g_d$. The feed through D is a null vector in the case considered.

The corresponding reflection coefficient is the transfer function of the state-space model. It can be determined by applying a Laplace transform to equation (19)

$$R_d(s) = \frac{\hat{g}_d}{\hat{f}_d} = C\,(sI - A)^{-1}\,B_1. \tag{20}$$

Here, $\hat{g}_d$ and $\hat{f}_d$ denotes the Laplace transform of the respective signals, B_1 is the first column vector of B, I the identity matrix and s is the complex frequency. Restricting s to purely imaginary values yields the well known interpretation of the reflection coefficient, as the response of the model to a harmonic forcing signal. The result with $R_L = 1$ is shown in Fig. 5. ω is the real valued angular frequency of the excitation signal. The frequency is normalized by the propagation time of the acoustic signal

$$\tau = \frac{L}{\bar{c}+\bar{u}} + \frac{L}{\bar{c}-\bar{u}}. \tag{21}$$

In Fig. 5 the results are compared against the analytical solution

$$R_d(s) = e^{-\tau s}. \tag{22}$$

The figure shows that the state-space model behaves as an acoustic solver of the one dimensional advection equation which utilizes the first order upwind scheme. Looking at the gain one can clearly see the dissipative behavior of the scheme. The error increases with the frequency of the excitation and with the time lag of the resonator. It decreases when a finer grid is chosen. It is interesting to note that the linear upwind scheme captures the phase quite well, which is of particular importance for stability analysis.

S. Jaensch, C. Sovardi, and W. Polifke, Journal of Computational Physics, vol. 314, pp. 145–159, 2016, http://dx.doi.org/10.1016/j.jcp.2016.03.010.. Reprinted with permission from Elsevier.

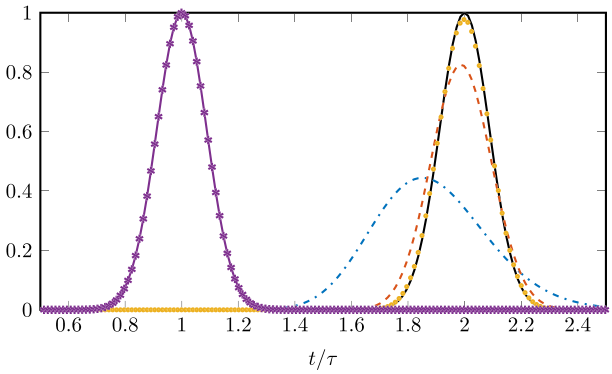

Fig. 6. Time response $g_d(t)$ of the model (19) with a mesh of 10 nodes (· - · -), of 100 nodes (- - -) and of 1000 nodes (·) and analytical solution (——). The full line (—•—) is the excitation signal $f_d(t)$.

We can also determine the response of the model (19) to a Gaussian impulse signal. For this we consider the state-space model as set of ordinary differential equation (ODE), which is to be discretized in time. Fig. 6 shows the results with a Euler forward scheme and a CFL number of 0.3. Again, the results of the state-space model are identical to the results expected from an acoustic solver of the same problem.

Considering that the state-space model is a set of ODEs, it becomes evident that the stability of the state-space model is determined by the eigenvalues of the matrix A. The model is stable, if the real part of all eigenvalues is smaller then zero.

A exhaust duct, as sketched in the present example, may also be modeled efficiently within a LES/DNS by coarsening the mesh towards the outline. This approach, however, has a number of disadvantages compared to a TDIBC. A TDIBC formulation allows to impose an arbitrary reflection coefficient at the end of the exhaust and to add an external excitation signal. With the latter one can model e.g. loudspeaker or a turbulent sound source. Furthermore, a TDIBC formulation can also be applied at the inlet. Here, the additional difficulty arises that besides the acoustic field also a mean velocity profile and possibly turbulence has to be imposed. In particular the imposition of a proper turbulence statistics requires a good mesh. In contrast to TDIBC, a coarse grid cannot maintain these properties, accurately.

The main take away message of the example is that a state-space model can be *interpreted* as a complete and exact representation of an acoustic solver. The procedure can also be applied to a more complex set of PDEs, e.g. the linearized Navier–Stokes equations, and to three dimensional meshes. Modeling errors are introduce due to the choice of a specific set of PDEs or of a specific discretization scheme. The state-space representation as such does not introduce any additional error.

However, developing suitable models is a time consuming task and the discretization of linearized Navier–Stokes equations is prone to numerical instabilities. As these instabilities are unphysical they will yield unphysical results when imposed as boundary condition. Therefore, in practical application it is often more convenient to determine the model based on measured reflection coefficients, as discussed in the next section.

4.1.2. Determining state-space models from measured reflection coefficients

Often, the reflection coefficient is known at several distinct frequencies, e.g. from experimental measurements or from an analytical solution. This information can be used to construct a state space model. For the sake of better readability and without loss of generality, we neglect the source term in this subsection.

At first we apply an algorithm which fits the coefficients a_i and b_i of the rational polynomial

$$R_d(s) = \frac{\hat{g}_d}{\hat{f}_d} = \frac{b_{n_b} s^{n_b} + \cdots + b_1 s + b_0}{s^{n_a} + a_{n_a-1} s^{n_a-1} + \cdots + a_1 s + a_0}, \tag{23}$$

with $n_a \geq n_b$ to the complex frequency response. A robust algorithm for this fitting is given in [19]. The next step is to apply the inverse Laplace transform to (23). Considering the relation $\mathcal{L}\left(y^{[n]}\right) = s^n \hat{y}$ this yields an ODE of order n_a

$$g_d^{[n_a]} + a_{n_a-1} g_d^{[n_a-1]} + \cdots + a_1 g_d^{[1]} + a_0 g_d = b_{n_b} f_d^{[n_b]} + \cdots + b_1 f_d^{[1]} + b_0 f_d \tag{24}$$

where $g_d^{[i]}$ and $f_d^{[i]}$ are the ith temporal derivatives of the respective signals. This ODE can be rewritten in the so-called controllability normal form of a state space model (see e.g. [20])

S. Jaensch, C. Sovardi, and W. Polifke, Journal of Computational Physics, vol. 314, pp. 145–159, 2016, http://dx.doi.org/10.1016/j.jcp.2016.03.010.. Reprinted with permission from Elsevier.

A.2 PAPER-CBSBC

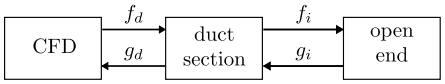

Fig. 7. Acoustic network model of the example case shown in Fig. 1.

$$\underbrace{\frac{d}{dt}\begin{bmatrix} g_d \\ g_d^{(1)} \\ \vdots \\ g_d^{(n_a-2)} \\ g_d^{(n_a-1)} \end{bmatrix}}_{\dot{\mathbf{x}}} = \underbrace{\begin{bmatrix} 0 & 1 & & & \\ & 0 & 1 & & \\ & & \ddots & \ddots & \\ & & & 0 & 1 \\ -a_0 & -a_1 & \cdots & -a_{n_a-2} & -a_{n_a-1} \end{bmatrix}}_{A} \underbrace{\begin{bmatrix} g_d \\ g_d^{(1)} \\ \vdots \\ g_d^{(n_a-2)} \\ g_d^{(n_a-1)} \end{bmatrix}}_{\mathbf{x}} + \underbrace{\begin{bmatrix} 0 \\ \vdots \\ 0 \\ 1 \end{bmatrix}}_{B} \mathbf{u} \tag{25a}$$

$$\underbrace{g_d}_{y} = \underbrace{\begin{bmatrix} b_0 - b_{n_a}a_0, & b_1 - b_{n_a}a_1, & \cdots, & b_{n_a-1} - b_{n_a}a_{n_a-1} \end{bmatrix}}_{C} \mathbf{x} + \underbrace{b_{n_a}}_{D} \mathbf{u} \tag{25b}$$

In this form the elements of the state vector consists of higher order temporal derivatives of the output signal g_d. The first $n_a - 1$ lines of (25a) are trivial. The last line of equation (25a) and equation (25b) can be verified in a straight forward manner if $b_i = 0$ for $i > 0$. The remaining terms follow from the linearity of the ODE and the Laplacian transform (compare e.g. [20]).

Once a state space model has been constructed in this way, we can validate its quality by comparing the measured frequency response with the frequency response of the model. The frequency response of the model is given in (20). Integrating equation (25) in times allows to determine its response in the time domain.

4.1.3. State-space representation of acoustic network models

Determining a state space model for an acoustic BC by fitting its frequency response to a given reflection coefficient, is a method which is of particular importance for complex configurations, where the reflection coefficient is known only from experiment. The drawback of this approach is that changes in the experimental setup can be considered only by new experiments. Acoustic network models overcome this drawback with a divide and conquer approach. At first a given complex configuration is divided into subsystems. For each of these subsystems a model is determined. Finally, all theses models are interconnected in order to obtain a single model describing the whole configuration. The state space representation of acoustic network models is discussed in detail by Schuermans et al. [17] and Bothien et al. [18].

Again the ducted exhaust section as already discussed in section 4.1.1 is a good example where network models can be very useful. A network model of this configuration is shown in Fig. 7. The network model consists of two elements. The first element models a duct section. For this part an analytical model can be derived analogously to the model shown in section 4.1.1. The second element is an open end. Here, analytical models are available. However, the reflection at an open end depends on the geometry behind the open end, which is difficult to model in a general way. Therefore, it is beneficial to describe this part with a fitted model. This network model clearly combines the advantages of analytical and fitted models. A change of the length of the duct section can be considered easily as this is a parameter of the analytical duct model and still an accurate model of the open end can be used.

4.2. The advantage of using continuous time state space models

Discretizing the continuous-time state-space model (13) in time with a constant time step Δt yields a discrete time state-space model

$$\mathbf{x}((k+1)\Delta t) = \tilde{A}\mathbf{x}(k\Delta t) + \tilde{B}\mathbf{u}(k\Delta t) \tag{26a}$$

$$y(k\Delta t) = \tilde{C}\mathbf{x}(k\Delta t) + \tilde{D}\mathbf{u}(k\Delta t) \tag{26b}$$

with $t = k\Delta t$. The discrete state-space matrices are market with $\tilde{(\cdot)}$. Schuermans et al. [10] proposed to utilize this form of a state-space model. The drawback of this formulation is that it requires an interpolation to account for non-constant CFD time steps. Furthermore, transforming a continuous-time state-space model into discrete-time, explicitly, may (depending on the scheme used) yield dense matrices and thus be extremely inefficient. In order to overcome this drawback we propose to use a continuous time state-space model, directly, and to integrated it with an ODE solver. This has the advantage that the behavior of an ODE solver is much better understood, which simplifies a general and efficient implementation.

A discrete-time state-space model can be transformed into an IIR model

$$y(k\Delta t) = \sum_{i=1}^{n_a} \tilde{a}_i\, y\left((k-i)\Delta t\right) + \sum_{i=0}^{n_b} \tilde{b}_i u\left((k-i)\Delta t\right) \tag{27}$$

S. Jaensch, C. Sovardi, and W. Polifke, Journal of Computational Physics, vol. 314, pp. 145–159, 2016, http://dx.doi.org/10.1016/j.jcp.2016.03.010.. Reprinted with permission from Elsevier.

with n_a coefficients $\tilde{a}_i$ and n_b coefficients $\tilde{b}_i$. This form is utilized in many TDIBC formulations [1–3,5–7]. There exists a transformation from the IIR model (27) to a time-discrete state-space model, similar to the transformation discussed in section 4.1.2. Therefore, IIR models can also be imposed if a implementation of TDIBC is based on the state-space representation. As IIR models utilizes a fixed time step, an interpolation scheme is necessary in order to account for non-constant time steps. However, the main problem when using the convolution formulation is that the coefficients $\tilde{a}_i$ and $\tilde{b}_i$ are on the one hand hardly ever known, directly, and on the other hand that the response of the model can be extremely sensitive to a small change of the coefficients. This difficulties arise because the transformation from a state-space model, which can be interpreted as a one-to-one representation of an acoustic solver, to an IIR model is poorly conditioned. Paige [21] demonstrated that this transformation can become problematic for a system of order 10 and should not be used.

Therefore, the only general way to determine the coefficients of an IIR model is to fit them to a given frequency response. As discussed in 4.1.2, this is also possible for state space models. Therefore, there exits no situation where IIR models are superior to state-space models. Hence, a general implementation of TDIBC should be based on continuous time state-space models, as proposed in the present work.

In summary continuous state-space model have the following advantages: They can be understood as one-to-one correspondence to an acoustic solver In section 4.1.1 we have demonstrated this with a simplistic example, but more sophisticated discretization schemes or 3D formulations are also possible. State-space models allow to account for non-constant CFD time steps in a robust and general way. When only the frequency response of the reflection coefficient is known, a state-space model can be determined using a fitting algorithm, which induces the same numerical error as when an IIR model is utilized (see section 4.1.2). As discussed in section 4.1.3, it is also possible to obtain a state-space model by interconnecting several state-space models. This is useful in many situations of practical interest.

4.3. Implementation of CBSBC

A schematic implementation of CBSBC as outflow BC is given in Listing 1. In a pre-processing step the matrices A, B, C and D of the state space model are loaded from data file. Additionally, an external excitation $e_{x,d}(t)$ is read as a time series from a data file. The variables $x^{(n-1)}$, $e_{x,d}^{(n-1)}$ and $f_d^{(n-1)}$ are necessary in order to perform a clean restart. Here, the exponent $(n-1)$ denotes values at the last final sub-time step. In contrast, the exponent (n) in Listing 1 corresponds to values at the current time or sub-time step.

In the processing step at first the values of the input signals $e_{x,d}^{(n)}$ and $f_d^{(n)}$ of the state space model are calculated. The current value of the external excitation $e_{x,d}^{(n)}$ is determined by interpolating the corresponding time series. The wave leaving the CFD-domain $f_d^{(n)}$ is determined by characteristic based filtering according to equation (4a). This is represented by calling the function `cbf()`.

The second step is to calculate the amplitude $g_d^{(n)}$ of the wave imposed to the CFD domain according to the output equation (13b) of the state space model (13).

In order to determine $\mathcal{L}_1$ according to (10) the time derivative of the wave amplitude entering the domain has to be calculated. Therefore, at first the derivative in time of the output equation (13b) is taken

$$\dot{g}_d = C\dot{\mathbf{x}} + D\dot{\mathbf{u}}. \tag{28}$$

The derivative of the state vector $\dot{\mathbf{x}}$ is determined according to the state equation (13a). The derivative of the input $\dot{\mathbf{u}}$ is calculated by a finite difference approximation, which yields the expression in line 7 in Listing 1.

The next step is to calculate $\mathcal{L}_1$ according to (10).

Finally, at the final sub-time step of the current CFD time step, the state space model is integrated in time for the time instance Δt. This is indicated by calling the function `integrateODE()`. The implementation used in the present study utilizes a forward Euler scheme for this integration. Additionally, the values at time $(n-1)$ are updated.

As LES/ DNS time steps are typically much smaller then the time step required to integrate the acoustic model, the error created by the forward Euler scheme is small. Nevertheless, higher order time integration schemes for the state space models can be applied, if necessary.

For an inflow BC one has to exchange the following variables in Listing 1 (compare Fig. 3)

$$e_{x,d} \rightarrow e_{x,u},\ f_d \rightarrow g_u,\ g_d \rightarrow f_u. \tag{29}$$

Furthermore, at the inflow the wave $\mathcal{L}_5$ has to be calculated according to (12).

In comparison to the original NSCBC, CBSBC is changing only the way in which incoming waves are calculated. Hence, they can be implemented in a straight forward way on any solver, which already includes NSCBC.

4.4. Properties of the boundary condition

The most important property of CBSBC is that the reflection coefficient imposed is captured accurately, provided that all assumptions made for PWM hold. That is the acoustic waves impinging on the BC have to be plane and one is able to distinguish between acoustic and turbulent fluctuations with a negligible error. Following [12] we can prove this property

S. Jaensch, C. Sovardi, and W. Polifke, Journal of Computational Physics, vol. 314, pp. 145–159, 2016, http://dx.doi.org/10.1016/j.jcp.2016.03.010.. Reprinted with permission from Elsevier.

A.2 PAPER-CBSBC

1 `Pre-processing:`
2 `load` $A, B, C, D, \omega(t), x^{(n-1)}, e_{x,d}^{(n-1)}, f_d^{(n-1)}$ `from file`
3 `Processing: Calculate incoming` $\mathcal{L}$`-wave`
4 $e_{x,d}^{(n)} = \texttt{interpolation}\left(e_{x,d}(t), t^{(n)}\right)$
5 $f_d^{(n)} = \texttt{cbf}()$
6 $g_d^{(n)} = C\mathrm{x}^{(n-1)} + D\begin{bmatrix} f_d^{(n)} \\ e_{x,d}^{(n)} \end{bmatrix}$
7 $\dot{g}_d^{(n)} = CA\mathrm{x}^{(n-1)} + CB\begin{bmatrix} f_d^{(n)} \\ e_{x,d}^{(n)} \end{bmatrix} + \frac{1}{\Delta t^{(n)}} D\begin{bmatrix} f_d^{(n)} - f_d^{(n-1)} \\ e_{x,d}^{(n)} - e_{x,d}^{(n-1)} \end{bmatrix}$
8 $\mathcal{L}_1^{(n)} = \sigma\left(p^{(n)} - \bar{\rho}\bar{c}\left(f_d^{(n)} + g_d^{(n)}\right) - p_\infty\right) + \dot{g}_d^{(n)}$
9 `if final sub-time step`
10 $\mathrm{x}^{(n-1)} = \texttt{integrateODE}\left(\mathrm{x}^{(n-1)}, \Delta t, A, B, \begin{bmatrix} f_d^{(n)} \\ e_{x,d}^{(n)} \end{bmatrix}\right)$
11 $f_d^{(n-1)} = f_d^{(n)}, \quad e_{x,d}^{(n-1)} = e_{x,d}^{(n)}$
12 `end if`

Listing 1: Implementation of CBSBC as outflow BC.

$$
\begin{aligned}
R_d(s) &= \frac{\hat{g}_d(s)}{\hat{f}_d(s)} = \frac{\left\langle \hat{\mathcal{L}}_1(s) \right\rangle / 2}{\left\langle s\hat{f}_d(s) \right\rangle} \\
&= \frac{1}{2s\hat{f}_d(s)} \left\langle \left[\frac{\sigma}{\bar{\rho}\bar{c}} \left(\hat{p}(s) - \bar{\rho}\bar{c}\left(\hat{f}_d(s) + \hat{g}_d(s) \right) - p_\infty \right) + 2s\hat{g}_d(s) \right] \right\rangle \\
&= \underbrace{\frac{\sigma}{2s\bar{\rho}\bar{c}} \left(\underbrace{\left\langle \hat{p}(s) - p_\infty \right\rangle}_{\approx p'_A} - \underbrace{\left\langle \bar{\rho}\bar{c}\left(\hat{f}_d(s) + \hat{g}_d(s) \right) \right\rangle}_{\approx p'_A} \right)}_{\approx 0} + \underbrace{\frac{\left\langle \hat{g}_d(s) \right\rangle}{\left\langle \hat{f}_d(s) \right\rangle}}_{= R_d(s)}
\end{aligned}
\tag{30}
$$

As we assumed that the turbulent length scales are much smaller than the acoustic length scales, the CBF average $\langle\cdot\rangle$ separates the turbulent and the acoustic fluctuations. Hence, in this case the relaxation term vanishes and the CFD simulation will exhibit the reflection behavior imposed.

In [4,5] it was proposed to impose an impedance, directly. The velocity is calculated from the internal field and the pressure BC is given as

$$
p = p_\infty + Z_d * \langle u - \bar{u} \rangle . \tag{31}
$$

Here, $*$ denotes a convolution. For the further analysis of the BC please recall the transformation from impedance to reflection coefficient and vice versa

$$
R(s) = \frac{Z(s) - \bar{\rho}\bar{c}}{Z(s) + \bar{\rho}\bar{c}} \iff Z(s) = \bar{\rho}\bar{c}\frac{1 + R(s)}{1 - R(s)} \tag{32}
$$

Applying the Laplace transform to (31) yields the reflection coefficient

$$
R_d(s) = \frac{\hat{g}_d(s)}{\hat{f}_d(s)} = \frac{\left\langle \left(\hat{p}(s) - p_\infty \right) - \bar{\rho}\bar{c}\left(\hat{u}(s) - \bar{u} \right) \right\rangle}{\left\langle \left(\hat{p}(s) - p_\infty \right) + \bar{\rho}\bar{c}\left(\hat{u}(s) - \bar{u} \right) \right\rangle} = \frac{Z_d(s) - \bar{\rho}\bar{c}}{Z_d(s) + \bar{\rho}\bar{c}} = R_d(s), \tag{33}
$$

which seems to be exactly the behavior desired. However, comparing (33) with (30) it becomes evident that imposing an impedance directly implies a relaxation coefficient equal to zero. Hence, the BC given in (31) can be imposed only to linearized Navier–Stokes equations, as they will cause a drift of the mean quantities otherwise.

In [10] it was proposed to apply a high pass filter in order to avoid drift

$$
p = \bar{p} + F_{HP} * Z_d * \langle u - \bar{u} \rangle . \tag{34}
$$

Here, F_{HP} denotes the high pass filter. Its properties are $F_{HP}(\omega = 0) = 0$ and $F_{HP}(\omega \to \infty) = 1$. The resulting reflection coefficient is

$$
R_d(s) = \frac{\hat{g}_d(s)}{\hat{f}_d(s)} = \frac{F_{HP}(s)Z_d(s) - \bar{\rho}\bar{c}}{F_{HP}(s)Z_d(s) + \bar{\rho}\bar{c}} \neq R_d(s). \tag{35}
$$

S. Jaensch, C. Sovardi, and W. Polifke, Journal of Computational Physics, vol. 314, pp. 145–159, 2016, http://dx.doi.org/10.1016/j.jcp.2016.03.010.. Reprinted with permission from Elsevier.

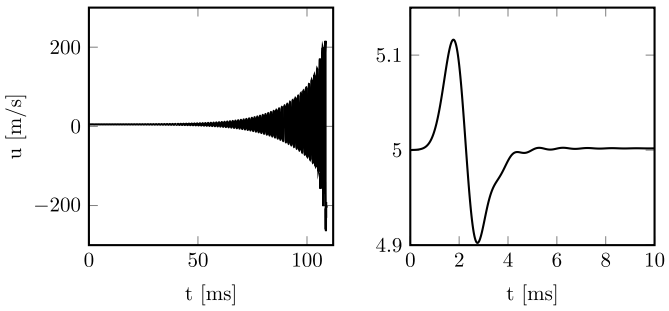

Fig. 8. Velocity probe in the center of the CFD model with an unstable outflow BC. Left: With non-reflective inflow BC. Right: With a reflective inflow BC.

As $F_{HP}(\omega = 0) = 0$ the reflection coefficient for this formulation is equal to unity for low frequencies. This avoids drift, however, the CFD will not exhibit the reflection behavior desired for low frequencies. For high frequencies $F_{HP}(\omega \to \infty) = 1$ holds and thus, in this limit the formulation is equivalent to the formulation proposed in the present study.

Please note, it is possible to impose a impedance using CBSBC. Therefore, we assume a model of the impedance in state space form is available

$$\dot{\mathbf{x}} = A_Z \mathbf{x} + B_Z u'_A, \tag{36a}$$

$$\frac{p'_A}{\bar{\rho}\bar{c}} = C_Z \mathbf{x} + D_Z u'_A. \tag{36b}$$

It has to be transformed into a state space model of the reflection coefficient. This is done by inserting (2) into (36). Reformulating the equations obtained yields

$$\dot{\mathbf{x}} = \underbrace{\left(A_Z + \frac{1}{1+D_Z} B_Z C_Z\right)}_{A} \mathbf{x} + \underbrace{B_Z \left(1 - \frac{D_Z - 1}{D_Z + 1}\right)}_{B} f \tag{37a}$$

$$g = \underbrace{\frac{1}{1+D_Z} C_Z}_{C} \mathbf{x} + \underbrace{\frac{D_Z - 1}{D_Z + 1}}_{D} f. \tag{37b}$$

We neglected the source term without essential loss of generality, it can be included in a straight forward manner. $D_Z = -1$ implies an infinite reflection coefficient and thus is unphysical.

Please, note the transformation modifies the A matrix of the state space model. Therefore, it may change the stability of the model from stable to unstable or vice versa. Fortunately, as will be demonstrated in the subsequent example, CBSBC works well with both stable and unstable state-space models.

The example case is a 3D CFD model of a 70 mm long cylindrical pipe, with slip walls and a mean flow of 5 m/s. At the outlet we impose CBSBC with the reflection coefficient

$$R_d = \frac{K}{(s - p_1)(s - p_2)}, \tag{38}$$

where $K = 2.5 \cdot 10^7$ and $p_{1,2} = 50 \pm 5000i$. As the real part of the poles are larger than zero, the model is unstable.

Using this setup, we performed two simulations: (1) a non-reflective inflow according to PWM was applied and (2) the inflow boundary condition was changed to a constant reflection coefficient of $R_u = 0.5$. This value was determined by a stability analysis. A network model of the whole setup i.e. the CFD model with both boundary conditions as depicted in Fig. 3 was configured. This model predicts that the CFD setup should be unstable for $R_u = 0$ and stable for $R_u = 0.5$.

The results of both simulations are shown in Fig. 8. The amplitudes in the first case grow rapidly, as there is no stabilization mechanism. Please note, this simulation shows the robustness of our formulation as the simulation did not diverge up to reverse flow with a Mach number larger than 0.7 at the outflow BC. In the second case the reflective inflow BC stabilizes the simulation and the initial oscillation decays.

As mentioned above, the transformation of the state space model for the impedance (36) to a state space model for the reflection coefficient (37) can change the stability of the model. However, considering that the state-space representation is inherently causal, it is interesting to notice that both the impedance and the reflection coefficient can be represented in the state-space representation. From this we can deduce that if the reflection coefficient is causal the impedance is causal, too, and vice versa.

S. Jaensch, C. Sovardi, and W. Polifke, Journal of Computational Physics, vol. 314, pp. 145–159, 2016, http://dx.doi.org/10.1016/j.jcp.2016.03.010.. Reprinted with permission from Elsevier.

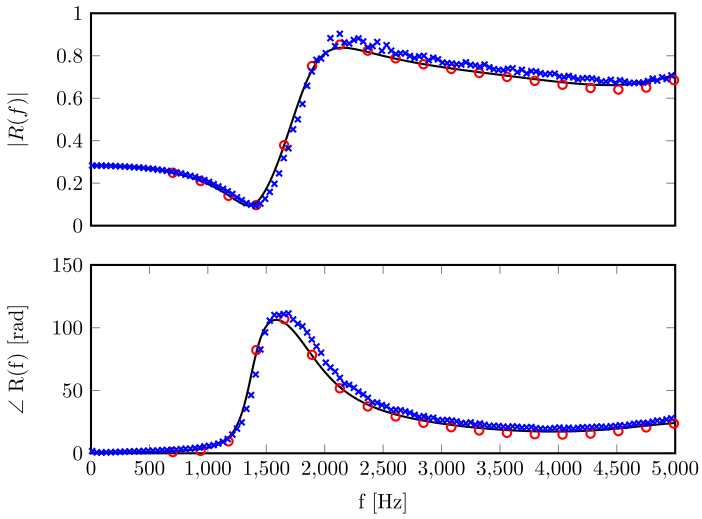

Fig. 9. Comparison of imposed (——) and measured (Euler scheme (○) and TTGC scheme (×)) reflection coefficients for the laminar case.

5. Numerical examples

As discussed above, CBSBC is based on the same assumptions as PWM i.e. all waves impinging on the boundary are plane and one can determine their amplitude accurately. PWM itself was used for LES of highly turbulent and reactive flows (see e.g. [22]). It is expected that also CBSBC yields accurate results in these situations.

In the scope of the present work we implemented CBSBC in the solver AVBP and LESLIE. The results presented in the present paper were obtained with AVBP.

Please note, the example shown could not have been achieved by any of the other TDIBC formulation mentioned in this paper. The formulations discussed in [7,10] yield a reflection coefficient equal to 1 for flow frequencies. The method proposed in [5] is valid only for linearized solver. The formulation discussed [6] is based on IIR model, which has several drawbacks as discussed in section 4.2. An implementation of this approach accounting for non-constant time steps and higher order time integration would be very complicated. Therefore, a constant time-step and a one-step time integration scheme has been used in [6].

5.1. Laminar test case

The domain of the laminar test case is cylindrical duct of 70 mm length with an diameter of 30 mm. The mesh is three dimensional and consists of 40 320 hexahedral cells. At the wall we impose isothermal slip boundary conditions. The mean flow velocity is 5 m/s. The CFL-number was set to 0.7. Four planes at the inlet and the outlet, respectively, were utilized for the CBF.

At the inlet as well as at the outlet, we use CBSBC. The state space matrices imposed at the inlet are

$$A = 0,\ B = \begin{bmatrix} 0 & 0 \end{bmatrix},\ C = 0,\ D = \begin{bmatrix} 0 & 1 \end{bmatrix}. \tag{39}$$

As the first element of B and D, which correspond to the wave leaving the CFD domain (compare Eq. (13)), are equal to zero, this choice yields a non-reflective BC. The value 1 in the D vector corresponds to the external source term and allows to impose an external acoustic excitation. We use this functionality to analyze the reflection coefficient at the outlet BC by harmonic forcing. The time series required for the post processing are sampled by a probe located at the center line of the cylinder at the outlet. The use of probes ensures that the sampling is independent of any modifications made in the source code of AVBP in order to implement the boundary conditions.

At the outflow BC we impose a state-space model which describes the upstream reflection coefficient of the orifice investigated in [23]. The reflection coefficient itself was determined using the LES/SI approach, see [22,24,25] and transformed into state-space form.

We performed the simulation using a forward Euler scheme and the Taylor–Galerkin scheme TTGC. The results are shown in Fig. 9. The imposed and measured reflection coefficients are in very good agreement.

5.2. Turbulent test case

The turbulent test case is a three dimensional cylindrical duct with an diameter of 30 mm and a length of 150 mm. It was discretized with 518 400 hexahedral cells. The mean flow velocity is 9 m/s and the CFL-number was set to 0.7. At the

S. Jaensch, C. Sovardi, and W. Polifke, Journal of Computational Physics, vol. 314, pp. 145–159, 2016, http://dx.doi.org/10.1016/j.jcp.2016.03.010.. Reprinted with permission from Elsevier.

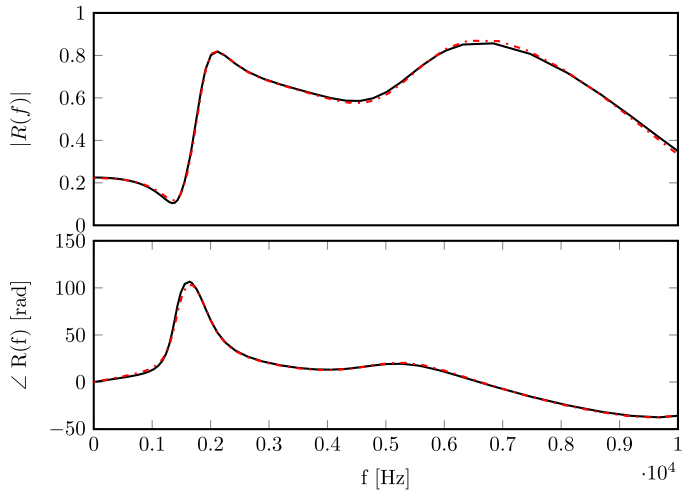

Fig. 10. Comparison of imposed (——) and measured (· - - -) reflection coefficients for the turbulent case.

wall we apply an isothermal non-slip BC. In order to impose turbulence CBSBC was combined with a turbulent inflow BC, which created a homogeneous isotropic turbulence (HIT) with a RMS value of 1 m/s. Therefore, the turbulent fluctuation was added to $\mathcal{L}_5$. A WALE model was used for the LES.

Again, we impose the TDIBC at the inlet and the outlet. The boundary at the outlet is non-reflective and the matrices are given in (39). At the inflow we impose the downstream reflection coefficient of the orifice investigated in [23]. Again, a state-space model for this reflection coefficient was determined with the LES/SI approach.

In order to evaluate the actual reflection coefficient at the inflow we imposed a broadband forcing signal at the outflow BC. Again, the data was collected with a probe located at the inflow boundary and hence, independently from our modifications of the source code. For the post processing we applied system identification [22].

The results are shown in Fig. 10. The imposed and measured reflection coefficients are in excellent agreement. Please note, for these results we imposed CBSBC and a turbulence generator, simultaneously, at the inflow BC.

6. Conclusion

CBSBC may be considered as a combination of the TDIBC formulations of Kaess et al. [6] and Schuermans et al. [10]. The coupling of the acoustic model and the flow simulation is done by plane wave masking (PWM) [12]. We proved analytically that with this coupling the CFD exhibits the reflection behavior imposed, accurately, provided all acoustic waves impinging on the boundary are plane. Our analysis made evident that the coupling proposed in [4,5] and [10] yields ill posed problems if applied to LES/ DNS or incorrect result for low frequencies, respectively.

Following Schuermans et al. [10], we utilize a continuous-time state-space model to describe the frequency dependent reflection of acoustic waves. It was discussed that it allows a general and robust implementation. A comprehensive overview on the modeling of acoustic reflection coefficients in state-space form was provided. We identified and discussed by way of examples three ways to determine a state-space model used for CBSBC: (1) A set of linear partial differential equations (PDE) is known to model the acoustic reflections. (2) Complex values of the reflection coefficient at several distinct frequencies are available. (3) Different modeling approaches are combined using an acoustic network model. The state-space formulation also allows to add an external excitation. E.g. it allows to consider a loud speaker or a turbulent sound source within the impedance domain. The formulation proposed allows a simple yet general implementation. A pseudo-code example of an implementation which accounts for non-constant CFD time steps and which is independent from the time integration schemes of the flow simulation was provided.

Finally, we demonstrated numerically that our formulation handles complex and possibly unstable reflection coefficients and that it works well with laminar as well as turbulent flows.

Acknowledgements

The financial support for the first author by the Research Association for Combustion Engines (Forschungsvereinigung Verbrennung e.V. – FVV, project number: 6011150) and for the second author by the Marie Curie People program FlowAirs of the European Union (grant number FP7-PEOPLE-2011-ITN-289352) is gratefully acknowledged. We thank CERFACS and IFP for providing the solver AVBP and in particular for the access to the source code. The authors gratefully acknowledge the Gauss Centre for Supercomputing e.V. (www.gauss-centre.eu) for funding this project by providing computing time on the GCS Supercomputer SuperMUC at Leibniz Supercomputing Centre (LRZ, www.lrz.de).

S. Jaensch, C. Sovardi, and W. Polifke, Journal of Computational Physics, vol. 314, pp. 145–159, 2016, http://dx.doi.org/10.1016/j.jcp.2016.03.010.. Reprinted with permission from Elsevier.

A.2 PAPER-CBSBC

We also like to thank Prof. Suresh Menon (Georgia Institute of Technology) for inviting the first author to a short term visit to his department, where a first version of CBSBC was implemented.

References

[1] R. Luebbers, F. Hunsberger, K.S. Kunz, R. Standler, M. Schneider, A frequency-dependent finite-difference time-domain formulation for dispersive materials, IEEE Trans. Electromagn. Compat. 32 (3) (1990) 222–227, http://dx.doi.org/10.1109/15.57116.
[2] J. Maloney, G. Smith, The use of surface impedance concepts in the finite-difference time-domain method, IEEE Trans. Antennas Propag. 40 (1) (1992) 38–48, http://dx.doi.org/10.1109/8.123351.
[3] D.M. Sullivan, Frequency-dependent FDTD methods using z transforms, IEEE Trans. Antennas Propag. 40 (10) (1992) 1223–1230, http://dx.doi.org/10.1109/8.182455.
[4] Y. Özyörük, L.N. Long, A time-domain implementation of surface acoustic impedance condition with and without flow, J. Comput. Acoust. 5 (3) (1997) 277–296.
[5] Y. Özyörük, L.N. Long, M.G. Jones, Time-domain numerical simulation of a flow-impedance tube, J. Comput. Phys. 146 (1998) CP985919.
[6] R. Kaess, A. Huber, W. Polifke, A time-domain impedance boundary condition for compressible turbulent flow, in: 14th AIAA/CEAS Aeroacoustics Conference, 29th AIAA Aeroacoustics Conference, Vancouver, Canada, 2008.
[7] A. Huber, P. Romann, W. Polifke, Filter-based time-domain impedance boundary conditions for CFD applications, in: Proceedings of ASME Turbo Expo 2008: Power for Land, Sea and Air, Berlin, Germany, 2008.
[8] K.-Y. Fung, H. Ju, B. Tallapragada, Impedance and its time-domain extensions, AIAA J. 38 (1) (2000) 30–38, http://dx.doi.org/10.2514/2.950.
[9] K.-Y. Fung, H. Ju, Broadband time-domain impedance models, AIAA J. 39 (8) (2001) 1449–1454, http://dx.doi.org/10.2514/2.1495.
[10] B. Schuermans, H. Luebcke, D. Bajusz, P. Flohr, Thermoacoustic analysis of gas turbine combustion systems using unsteady CFD, in: Proc. of ASME Turbo Expo 2005 Power for Land, Sea and Air, ASME, 2005.
[11] M.K. Myers, On the acoustic boundary condition in the presence of flow, J. Sound Vib. 71 (3) (1980) 429–434.
[12] W. Polifke, C. Wall, P. Moin, Partially reflecting and non-reflecting boundary conditions for simulation of compressible viscous flow, J. Comput. Phys. 213 (2006) 437–449.
[13] T. Poinsot, S.K. Lele, Boundary conditions for direct simulation of compressible viscous flows, J. Comput. Phys. 101 (2) (1992) 104–129, http://dx.doi.org/10.1016/0021-9991(92)90227-P.
[14] T. Poinsot, Theoretical and Numerical Combustion, 2nd edition, Edwards, Philadelphia, 2005.
[15] J. Kopitz, E. Bröcker, W. Polifke, Characteristics-based filter for identification of planar acoustic waves in numerical simulation of turbulent compressible flow, in: 12th Int. Congress on Sound and Vibration, 2005.
[16] L. Selle, F. Nicoud, T. Poinsot, Actual impedance of nonreflecting boundary conditions: implications for computation of resonators, AIAA J. 42 (5) (2004) 958–964.
[17] B. Schuermans, V. Bellucci, C.O. Paschereit, Thermoacoustic modeling and control of multi burner combustion systems, in: Proc. of ASME Turbo Expo 2003 Power for Land, Sea and Air, ASME, 2003.
[18] M. Bothien, J. Moeck, A. Lacarelle, C.O. Paschereit, Time domain modelling and stability analysis of complex thermoacoustic systems, Proc. Inst. Mech. Eng. A, J. Power Energy 221 (5) (2007) 657–668, http://dx.doi.org/10.1243/09576509JPE384.
[19] B. Gustavsen, A. Semlyen, Rational approximation of frequency domain responses by vector fitting, IEEE Trans. Power Deliv. 14 (3) (1999) 1052–1061, http://dx.doi.org/10.1109/61.772353.
[20] J. Lunze, Regelungstechnik 1, Springer Vieweg, Berlin, 2014.
[21] C.C. Paige, Properties of numerical algorithms related to computing controllability, IEEE Trans. Autom. Control 26 (1) (1981) 130–138.
[22] W. Polifke, Black-box system identification for reduced order model construction, Ann. Nucl. Energy 67C (2014) 109–128, http://dx.doi.org/10.1016/j.anucene.2013.10.037.
[23] P. Testud, Y. Aurégan, P. Moussou, A. Hirschberg, The whistling potentiality of an orifice in a confined flow using an energetic criterion, J. Sound Vib. 325 (4–5) (2009) 769–780, http://dx.doi.org/10.1016/j.jsv.2009.03.046.
[24] C. Sovardi, S. Jaensch, C. Silva, W. Polifke, Identification of sound sources in internal ducted flows: a large eddy simulation–system identification approach, in: 21st International Congress on Sound and Vibration, ICSV21, 2014.
[25] C. Sovardi, S. Jaensch, W. Polifke, Concurrent identification of aero-acoustic scattering and noise sources at a flow duct singularity in low Mach number flow, J. Sound Vib. (2016), submitted for publication.

S. Jaensch, C. Sovardi, and W. Polifke, Journal of Computational Physics, vol. 314, pp. 145–159, 2016, http://dx.doi.org/10.1016/j.jcp.2016.03.010.. Reprinted with permission from Elsevier.

Available online at www.sciencedirect.com

ScienceDirect

Proceedings of the Combustion Institute 36 (2017) 3827–3834

Proceedings of the Combustion Institute

www.elsevier.com/locate/proci

Hybrid CFD/low-order modeling of nonlinear thermoacoustic oscillations

S. Jaensch [a], M. Merk [a], E.A. Gopalakrishnan [b], S. Bomberg [a], T. Emmert [a], R.I. Sujith [b], W. Polifke [a,*]

[a] *Professur für Thermofluiddynamik, Fakultät für Maschinenwesen, Technische Universität München, Boltzmannstr. 15, D-85748 Garching, Germany*

[b] *Department of Aerospace Engineering, Indian Institute of Technology Madras, Chennai 600036, India*

Received 3 December 2015; accepted 1 August 2016
Available online 5 October 2016

Abstract

This paper proposes and compares two nonlinear time-domain models of self-excited thermoacoustic oscillations of laminar premixed flames. Both models are hybrid formulations, where the flame and its immediate vicinity are resolved with a reactive flow simulation, while the acoustic field is modeled with a low-order model that is coupled to the reactive flow simulation. Firstly, a flame model based on the fully compressible Navier–Stokes equations is investigated. In this case, the flame simulation is coupled to the low-order model via the characteristic wave amplitudes at the inlet boundary. Secondly, the flame is resolved with a low Mach number reactive flow simulation. In order to include two-way thermoacoustic feedback, this flame model is coupled with an acoustic network model via the global heat release rate and the fluctuation of the axial velocity at a reference position upstream of the flame. A bifurcation analysis using the plenum length as bifurcation parameter is conducted. Both models exhibit complex nonlinear oscillations and are in good agreement with each other. Therefore, we conclude that the coupling of a linear acoustic model and a nonlinear flame model via reference velocity and global heat release rate is sufficient to accurately capture thermoacoustic oscillations of the configuration investigated. This implies that the most important nonlinearities can be attributed to hydrodynamic effects and flame kinematics. Furthermore, the study corroborates that premixed flames respond predominantly to fluctuations of the upstream flow velocity.

Keywords: Nonlinear combustion dynamics; Premixed flame; Causality; State-space; Nonlinear time series analysis

1. Introduction

The development of gas turbines or rocket engines is often impeded by thermoacoustic instabilities. Feedback between the unsteady heat release rate of the combustion and the acoustic field

* Corresponding author.
E-mail address: polifke@tfd.mw.tum.de (W. Polifke).
URL: http://www.tfd.mw.tum.de (W. Polifke)

http://dx.doi.org/10.1016/j.proci.2016.08.006
1540-7489 © 2016 by The Combustion Institute. Published by Elsevier Inc.

S. Jaensch, M. Merk, E. A. Gopalakrishnan, S. Bomberg, T. Emmert, R. I. Sujith, W. Polifke, Proceedings of the Combustion Institute, vol. 36, pp. 3827-3834, 2017, http://dx.doi.org/10.1016/j.proci.2016.08.006.. Reprinted with permission from Elsevier.

results in very large oscillations of pressure, heat release and velocity. These oscillations can reach amplitude levels at which gas turbines have to be shut down, or rockets are destroyed. To decide whether a thermoacoustic instability reaches such amplitude levels, nonlinear models are required.

This modeling is a challenging task, as complex nonlinear phenomena are involved. Durox et al. [1] studied the response of various laminar flame configurations to fluctuations of the inflow velocity. It was observed that the fluctuations of the global heat release rate saturate for high forcing amplitudes. Correspondingly, Kabiraj et al. [2] studied self-excited thermoacoustic oscillations of a laminar flame and observed periodic, aperiodic, or chaotic oscillations as well as hysteresis. In order to obtain qualitative and quantitative agreement with these experimental results, a model of thermoacoustic instabilities has to account for all effects observed. Dowling [3] proposed to model the nonlinear flame dynamics with a flame describing function (FDF). Noiray et al. [4] showed that the FDF combined with an acoustic network model provides a useful estimate of limit cycle amplitudes in many cases. However, it is a frequency domain approach and considers only a single unstable acoustic mode. Therefore, it can only predict harmonic oscillations. The advantage of time-domain models is that they can account for multi-modal coupling, which is necessary to describe complex types of oscillations. A time-domain model that has enjoyed recent interest uses a *G*-equation based flame model coupled with a low-order acoustic model [3,5–7]. This model shows complex nonlinear oscillations. However, the results depend strongly on the velocity model used [8,9]. Indeed, the *G*-equation models found in the literature do not account for vortex shedding or vortex-flame interaction. Additionally, gas expansion and shear layer effects were reported to have a significant influence on the flame response [10]. These effect are also not considered by state-of-the-art *G*-equation implementations. Therefore, quantitative agreement with experiment is not obtained and more sophisticated models are needed.

A suitable low-order model has to account for the complex interactions between flame, flow and acoustics. The present study compares two models which account for these effects: Firstly, a model which resolves the flame and its vicinity with a fully compressible, reactive flow simulation. As shown in Fig. 1, the simulation is coupled to the acoustic low order model via the characteristic wave amplitudes in order to model the full acoustic field of the plenum. In the following we denote this simulation "C-fg". Secondly, a model as proposed by Moeck et al. [11] that utilizes a low Mach number, reactive flow simulation. Here, the density depends only on the temperature, but not on pressure. As shown in Fig. 2, this model is coupled to a low-order network model via a reference velocity and the global heat release rate. Consequently, we denote this model "LM-uq".

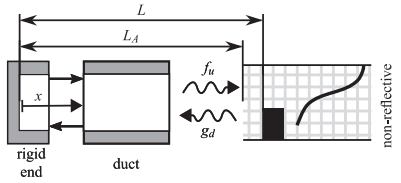

Fig. 1. Coupling of the fully compressible simulation and the corresponding acoustic model (Model: C-fg).

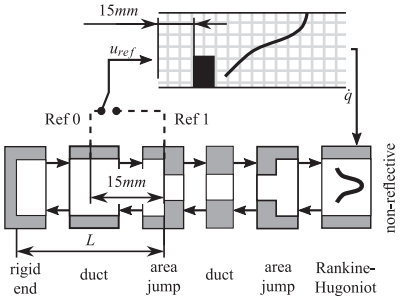

Fig. 2. Coupling of the low Mach number simulation and the corresponding acoustic model. The reference velocity is measured at two different locations (compare Table 1) (Model: LM-uq).

Please note that in the literature [12–14] other hybrid models for thermoacoustic oscillations have been proposed. However, the coupling used by these hybrid models has not been cross-validated in a systematic manner against a fully compressible simulation. This cross-validation allows to directly verify the coupling between flame, hydrodynamics and acoustics.

In the following section, the two formulations are explained in detail. Thereafter, in Section 3 the results of the two models are compared via a bifurcation analysis. Although, complex thermoacoustic oscillations are observed, the two models are in good agreement with each other. Thus we conclude that the coupling of a nonlinear flame model and a linear acoustic model is sufficient to describe the thermoacoustic oscillation of the configuration investigated.

2. Numerical setup

The laminar slit burner considered in the present study is shown in Fig. 3. Kornilov et al. [15] and Duchaine et al. [16] investigated the linear dynamics of this configuration by experiment and simulation, respectively. Good agreement between experimental and numerical results was found. The CFD setup used in the present work corresponds to that

S. Jaensch, M. Merk, E. A. Gopalakrishnan, S. Bomberg, T. Emmert, R. I. Sujith, W. Polifke, Proceedings of the Combustion Institute, vol. 36, pp. 3827-3834, 2017, http://dx.doi.org/10.1016/j.proci.2016.08.006.. Reprinted with permission from Elsevier.

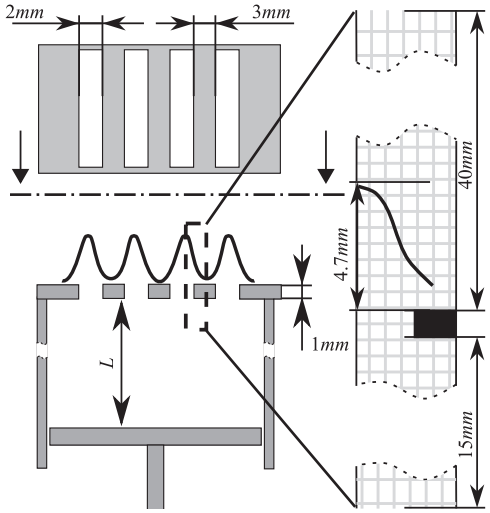

Fig. 3. Left: sketch of the experimental configuration considered. Right: truncated CFD domain.

of Duchaine et al. [16]. As sketched in Fig. 3, symmetry boundary conditions are imposed, such that only one half of one flame is resolved within the two dimensional CFD domain. A structured grid with 122,300 cells was used. In the region of the steady-state position of the flame and of the area contractions, the grid is uniform with a cell size of 0.025 mm. This corresponds to about 18 grid points in the reactive zone. Outside this region the cells were stretched in the axial direction. At the inflow, we impose a mean velocity of 0.4 m/s and a temperature of 293 K. The plate on which the flame is stabilized is modeled as a no-slip wall with a fixed temperature of 373 K, as measured in experiment [15]. The fuel is methane with an equivalence ratio of 0.8. For a detailed description of the two-step reaction mechanism we refer to [16].

Fully non-reflective outlet acoustic boundary conditions are imposed, as indicated in Figs. 1 and 2. This simplistic treatment does not represent faithfully the acoustic radiation by a collection of unconfined flames, but is completely adequate for the purpose of cross-comparison of the two hybrid approaches. Note that a more realistic radiation boundary condition such as the one proposed by Noiray et al. [4] could be implemented without essential difficulty in the low-order model as well as the fully compressible flow simulation. For the latter, one would employ the CBSBC formulation of time-domain impedance boundary conditions [17], see below. The transmission and reflection of acoustic waves at the burner plate is modeled explicitly in the compressible simulation by including the plate within the CFD domain. On the other hand, in the low Mach number simulation the plate is an element of the low-order acoustic model. The treatment of the inlet acoustic boundary conditions in models C-fg and LM-uq is explained in the following subsections.

2.1. Compressible simulation – plenum modeled via acoustic boundary conditions

By its nature, the compressible simulation used by the model C-fg captures the coupling between combustion, hydrodynamics and acoustics. However, the plenum length L determines the acoustic impedance at the burner plate and thus, is crucial for the thermoacoustic stability of the configuration. In order to capture thermoacoustic instabilities, the full plenum length has to be modeled. The most straight-forward way to model the plenum is to resolve it within the CFD domain. However, this approach has two important drawbacks: (1) with standard boundary conditions, the acoustic impedance at the inlet of the extended CFD domain can be imposed only with limited flexibility. (2) Changing the length of the plenum requires to create a new mesh. In order to overcome these drawbacks, in the present study Characteristics-Based State-Space Boundary Conditions (CBSBC), as proposed in Jaensch et al. [17], are utilized to effectively extend the plenum to the full plenum length (compare Fig. 1).

CBSBC provide a robust and consistent implementation of time-domain impedance boundary conditions. This formulation allows to impose a frequency-dependent impedance and ensures that the CFD simulation exhibits with good accuracy the desired impedance values. CBSBC are based on a model of the reflection coefficient, which can be considered as equivalent to the acoustic impedance. The reflection coefficient has to be provided in state-space representation. We will first explain how the state-space model for the present study is determined. Afterward, we show how the model is coupled with the compressible CFD simulation.

Plane acoustic waves can be described by means of the characteristic wave amplitudes

$$f = \frac{1}{2}\left(p'/\bar{\rho}\bar{c} + u'\right), \quad g = \frac{1}{2}\left(p'/\bar{\rho}\bar{c} - u'\right), \tag{1}$$

with density $\bar{\rho}$, speed of sound $\bar{c}$. p' and u' are the acoustic pressure and velocity fluctuations, respectively. f corresponds to the wave traveling in the downstream direction and g to the wave traveling in the upstream direction. The one-dimensional, linearized Euler equations

$$\frac{\partial f}{\partial t} + (\bar{u} + \bar{c})\frac{\partial f}{\partial x} = 0 \text{ and } \frac{\partial g}{\partial t} + (\bar{u} - \bar{c})\frac{\partial g}{\partial x} = 0, \tag{2}$$

describe the propagation of the acoustic wave amplitudes. At the inlet of the acoustic model the boundary condition

$$u'(x = 0) = 0 \Leftrightarrow f(x = 0) = g(x = 0), \tag{3}$$

S. Jaensch, M. Merk, E. A. Gopalakrishnan, S. Bomberg, T. Emmert, R. I. Sujith, W. Polifke, Proceedings of the Combustion Institute, vol. 36, pp. 3827-3834, 2017, http://dx.doi.org/10.1016/j.proci.2016.08.006.. Reprinted with permission from Elsevier.

represents a rigid wall. At the outlet of the acoustic model the boundary condition

$$g(t, x = L_A) = g_u(t), \tag{4}$$

allows to impose an arbitrary incoming wave $g_u(t)$. The discretization of Eq. (2) with a third-order upwind scheme in space under consideration of the boundary conditions (3) and (4) can be written in state-space form

$$\dot{\mathbf{x}}_{\text{C-fg}} = A_{\text{C-fg}}\mathbf{x}_{\text{C-fg}} + B_{\text{C-fg}}g_u \tag{5a}$$

$$f_u = C_{\text{C-fg}}\mathbf{x}_{\text{C-fg}}, \tag{5b}$$

with the state-space matrices $A_{\text{C-fg}}$, $B_{\text{C-fg}}$ and $C_{\text{C-fg}}$ and the state-vector $x_{\text{C-fg}}$. The index "C-fg" emphasizes that the state-space model belongs to the model C-fg. For a tutorial explanation of how these matrices can be determined we refer to [17].

The second step is to couple the model (5) with the CFD simulation. CBSBC extends the well-known Navier–Stokes characteristic boundary conditions (NSCBC) [18]. As in the NSCBC framework, CBSBC define the derivative of pressure p and velocity u according to

$$\frac{\partial p}{\partial t} + \frac{1}{2}(\mathcal{L}_5 + \mathcal{L}_1) = 0, \quad \frac{\partial u}{\partial t} + \frac{1}{2}(\mathcal{L}_5 - \mathcal{L}_1) = 0. \tag{6}$$

Here, $\mathcal{L}_5$ and $\mathcal{L}_1$ are the temporal derivatives of the characteristic wave amplitudes f and g, respectively. With a setup as shown in Fig. 1, $\mathcal{L}_1$ corresponds to the wave leaving the CFD domain and is given as

$$\mathcal{L}_1 = (u - c)\left(\frac{\partial p}{\partial x} - \rho c \frac{\partial u}{\partial x}\right). \tag{7}$$

$\mathcal{L}_5$ corresponds to the f-wave entering the domain and has to be imposed

$$\mathcal{L}_5 = \sigma(u - (f_u - g_d) - u_T) + 2\frac{\partial f_u}{\partial t}, \tag{8}$$

The term $(f_u - g_d)$ is equal to the acoustic velocity fluctuation. Including this term in the relaxation term avoids artificial reflections at the boundaries of the CFD domain, as it compensates the effect of the acoustic fluctuation on the relaxation term. The term $\partial f_u/\partial t$ allows to impose an ingoing wave. Please note that Eq. (8) is equal to the formulation given in Polifke et al. [19].

Solving Eqs. (5)–(8) at every time step allows to extend the acoustic domain to the full plenum length. By changing the length L_A we can change the plenum length without the requirement of a new mesh. At the outlet of the compressible simulation we impose non-reflective boundary conditions as proposed by Polifke et al. [19]. The fully compressible simulations were conducted using AVBP [1] (Cerfacs and IFP). The Lax–Wendroff scheme was used for the discretization. This scheme is second-order accurate in both time and space. The time step was set to ensure an acoustic CFL number less than 0.7.

[1] http://cerfacs.fr/en/computational-fluid-dynamics-softwares/

2.2. Low Mach number simulation – coupled to acoustics via Rankine–Hugoniot

The model LM-uq is based on a low Mach number simulation. With such a formulation, which is also called *weakly compressible*, the density depends only on the temperature, but not on pressure. In this way acoustic waves and hence, thermoacoustic feedback inside the CFD domain is suppressed. In order to account for the thermoacoustic feedback, the low Mach number simulation is coupled with an acoustic network model via the linearized Rankine–Hugoniot equations [20] for a compact heat source. As shown in Fig. 2, the network model and the low Mach number simulation are coupled via the global heat release rate $\dot{q}'$ and a reference velocity u_{ref}. It can be shown that the coupling is equivalent to the one proposed by Moeck et al. [11]. As the acoustic model is linear it can be written in state-space form

$$\dot{\mathbf{x}}_{LM-uq} = A_{\text{LM-uq}}\mathbf{x}_{\text{LM-uq}} + B_{\text{LM-uq}}\dot{q}' \tag{9a}$$

$$u_{ref} \quad = C_{\text{LM-uq}}\mathbf{x}_{\text{LM-uq}} + D_{LM-uq}\dot{q}', \tag{9b}$$

with the state-space matrices $A_{\text{LM-uq}}$, $B_{\text{LM-uq}}$ and, $C_{\text{LM-uq}}$ and the state-vector $x_{\text{LM-uq}}$. Here, the index "LM-uq" emphasizes that the state-space model belongs to the low Mach number simulation. A detailed description of how these matrices may be formulated can be found in Emmert et al. [21–23]. The elements of the network model are shown in Fig. 2. As for the C-fg case the duct sections are modeled using the linearized Euler equations. The model for the area jump is based on the continuity equation and does not include acoustic losses. The inlet BC of the acoustic network model is a reflection coefficient of 1, which corresponds to a rigid wall. The outlet BC is a non-reflective boundary condition. The temperature ratio across the flame is 6.1. Overall, both the models LM-uq and C-fg describe the configuration shown in Fig. 3.

The Rankine–Hugoniot equations assumes that the flame is compact with respect to the acoustic wavelength. Considering the height of the flame of about 5 mm and the length of the plenum which is the characteristic dimension of the acoustics for longitudinal modes, varying between 200 and 1000 mm, this assumption is fulfilled with good accuracy. The flame acts as an acoustic point source while the real flame has some spacial extent. The exact position of this source is a model parameter. In the present study this position was chosen 2.6 mm after the burner plate. Additionally, it is assumed that the flame responds only to fluctuations of the reference velocity. Again, due to the spatial extent

S. Jaensch, M. Merk, E. A. Gopalakrishnan, S. Bomberg, T. Emmert, R. I. Sujith, W. Polifke, Proceedings of the Combustion Institute, vol. 36, pp. 3827-3834, 2017, http://dx.doi.org/10.1016/j.proci.2016.08.006.. Reprinted with permission from Elsevier.

Table 1
Model settings considered. Compare Fig. 2 for the reference position of the model LM-uq. Abbreviation: perturbation (pert.).

Case name	Model	Initial condition	Reference position
C-fg-low	C-fg	Low pert.	—
C-fg-high	C-fg	High pert.	—
LM-uq-low-0	LM-uq	Low pert.	0
LM-uq-high-0	LM-uq	High pert.	0
LM-uq-high-1	LM-uq	High pert.	1

of the real flame, the position at which this reference velocity is extracted is a model parameter. As indicated in Fig. 2, two different positions were investigated: (1) 15 mm upstream of the burner plate. This position coincides with the inlet boundary of the low Mach number simulation and is denoted as reference 0 (compare Fig. 2 and Table 1). (2) The reference velocity was chosen at the upstream side of the burner plate. In Fig. 2 and Table 1 this position is denoted as reference 1.

The open-source finite volume code OpenFOAM[2] was used as low Mach number CFD solver. For the temporal integration the implicit Euler scheme with a (hydrodynamic) CFL number of 0.3 was employed. Gaussian integration is applied. The gradient operator is discretized with the linear scheme and the divergence operator with limited linear differencing scheme. A transient SIMPLEC algorithm [24] was used, which stopped iterating once the residuals were lower than 10^{-6}.

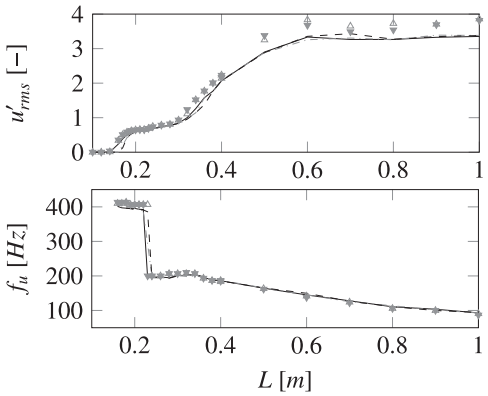

Fig. 4. RMS (top) and dominant frequency (bottom) of the reference velocity for different plenum length. -·-·-: LM-uq-low-0, - - - : LM-uq-high-0, ——: LM-uq-high-1, △: C-fg-low, ▽: C-fg-high.

3. Numerical results

The model settings for which self-excited thermoacoustic instabilities were observed are listed in Table 1. Simulations with two different initial conditions were conducted. (1) The simulations denoted with "low" were started from a converged mean field. Here, only a small initial acoustic excitation was applied. This speeds up the development of a thermoacoustic oscillation and allows to reduce the computational costs significantly. (2) The simulations denoted with "high" were started from a initial condition taken from a snapshot with developed thermoacoustic oscillation. For all values of the plenum length L the same snapshot is used. The two different reference positions for the model LM-uq were explained in the previous section and are shown in Fig. 2. Depending on the complexity of the oscillations observed for each case, time series between 100 and 500 ms were generated. The first part of the time series at which the thermoacoustic oscillations are not yet fully developed were not included in the post-processing. The two models were compared w.r.t. the normalized fluctuation of the reference velocity:

$$u' = \left(u'_{ref} - \bar{u}'_{ref}\right)/\bar{u}'_{ref} \tag{10}$$

Here, u'_{ref} is the area averaged velocity measured at a plane 15 mm upstream of the burner plate. $\bar{u}'_{ref}$ is the temporal average of u'_{ref}. In the remainder of this section the two models are first compared via a bifurcation analysis. Thereafter, the cases with a plenum length of $L = 200$ mm and $L = 700$ mm are investigated in detail.

3.1. Bifurcation analysis

In Figs. 4 (top) and5 the variation of the root mean square (RMS) value with plenum length and the bifurcation diagram are shown, respectively. The amplitudes predicted by the two models are in good agreement with each other. This holds in particular for short plenum lengths L. For long plenum lengths the amplitudes predicted by the model LM-uq are slightly lower than the amplitudes predicted by the model C-fg. The corresponding velocities correspond to Reynolds numbers of about 1000. Thus, the flow is in the transition to turbulence.

At the onset of the thermoacoustic oscillations, we observe what appears to be a supercritical Hopf bifurcation. Note that this assessment is based on a

[2] http://www.openfoam.org/

S. Jaensch, M. Merk, E. A. Gopalakrishnan, S. Bomberg, T. Emmert, R. I. Sujith, W. Polifke, Proceedings of the Combustion Institute, vol. 36, pp. 3827-3834, 2017, http://dx.doi.org/10.1016/j.proci.2016.08.006.. Reprinted with permission from Elsevier.

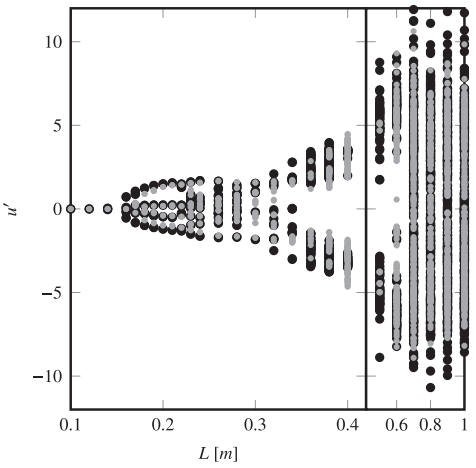

Fig. 5. Bifurcation diagram showing the minima and maxima of the normalized fluctuation of the reference velocity. The black dots show the result obtained with C-fg-low and C-fg-high and the gray dots the one obtained with LM-uq-low-0 and LM-uq-high-0.

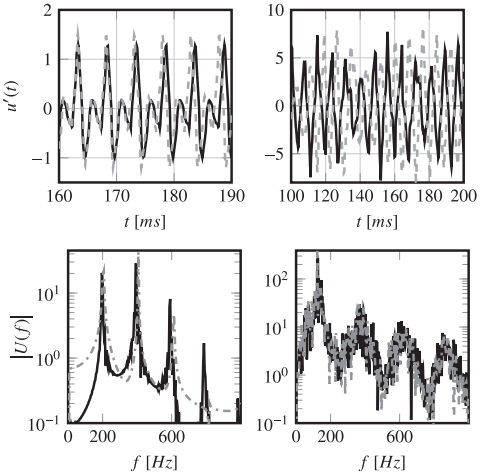

Fig. 6. Time series (top), power spectrum (bottom) of the velocity signal for $L = 200$ mm (left) and $L = 700$ mm (right). Dashed gray line: compressible simulation (case: C-fg-low), full black line: low Mach number simulation (case: LM-uq-low-0).

resolution $\Delta L = 10$ mm of the bifurcation parameter L around the bifurcation point. A smaller step size ΔL may reveal a weakly pronounced subcritical Hopf bifurcation.

The models C-fg and the LM-uq with reference position 1 (compare Fig. 2) become unstable at a plenum length of $L = 160$ mm. The model LM-uq with reference position 0, however, exhibits a thermoacoustic instability starting at a plenum length of 170 mm. Therefore, the less intuitive coupling using a reference position right before the burner plate is more accurate than the coupling using a reference position that coincides with the inlet boundary of the low Mach number simulation. The reason is that due to the low Mach number formulation, a velocity fluctuation imposed at the inlet will act immediately on the whole CFD domain. In the low-order acoustic model, on the other hand, the fluctuations propagate with the speed of sound. Therefore, the reference position at which the acoustic velocity is extracted from the low-order acoustic model should be chosen at the location where acoustic fluctuations create hydrodynamic fluctuations. In the present configuration, this position is at the burner plate.

In Fig. 5 bifurcation diagrams of the two models are shown. In Fig. 4 (bottom) the dominant frequencies f_u predicted with the different setups investigated are shown. The comparison shows that also the nature of the oscillations predicted by the two models is in good agreement with each other. A significant difference is observed at a plenum length of $L = 500$ mm.

3.2. Comparison of time series

In Fig. 6 the time series (top plots) and the power spectrum (bottom plots) of the unsteady velocity for a plenum length of 200 mm and 700 mm are shown. Both plots show that the simulations are in good agreement with each other. Consistent with the bifurcation diagram, the amplitude at a plenum length of 700 mm is significantly larger than the amplitude at $L = 200$ mm. In the power spectrum for $L = 700$ mm a noise content is observed, which can be attributed to the onset of turbulence due to the high oscillation amplitudes. The corresponding maximum Reynolds number observed inside the slit of the burner plate is about 1000.

The nonlinear dynamics of the thermoacoustic instabilities observed can be better understood with the help of phase portraits. Phase portraits represent the asymptotic state of the system in the phase space. We reconstruct the phase space by applying Takens' embedding theorem [25]. The delay τ is chosen to correspond to the first minima of the average mutual information and the minimum embedding dimension is found using the method of false nearest neighbors. A detailed description of the techniques involved in the phase space reconstruction in the context of a thermoacoustic system can be found in Kabiraj and Sujith [26]. As shown in Fig. 7, also the phase portraits are in good agreement with each other. From the phase portrait we can also deduce the nature of the oscillation observed: We are observing Period-2 oscillations at $L = 200$ mm and limit cycle oscillations at $L = 700$ mm.

S. Jaensch, M. Merk, E. A. Gopalakrishnan, S. Bomberg, T. Emmert, R. I. Sujith, W. Polifke, Proceedings of the Combustion Institute, vol. 36, pp. 3827-3834, 2017, http://dx.doi.org/10.1016/j.proci.2016.08.006.. Reprinted with permission from Elsevier.

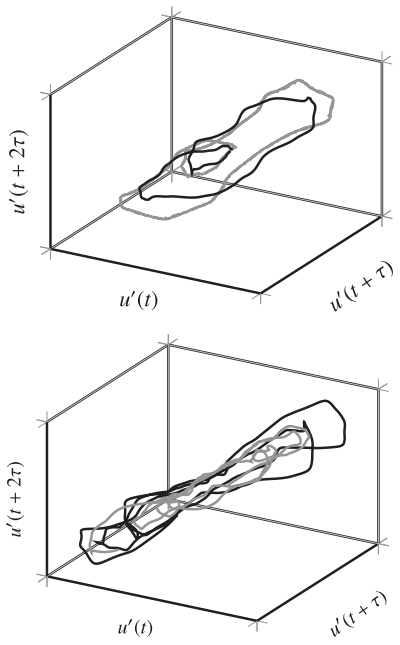

Fig. 7. Phase portraits of the velocity signal for $L = 200$ mm (top) and $L = 700$ mm (bottom). Colors as in Fig. 6.

4. Summary and conclusion

Two nonlinear, hybrid, time-domain models of self-excited thermoacoustic instabilities of a laminar premixed flame (see Fig. 3) were implemented and cross-validated. The model C-fg – see Fig. 1 – resolves the flame with a fully compressible and reactive simulation. A low-order model of the plenum of the burner is coupled to the simulation via the characteristic wave amplitudes. This allows to change the length of the plenum without modifying the computational grid. Alternatively, the model LM-uq – see Fig. 2 – uses a low Mach number formulation of the Navier–Stokes equations to describe the flame dynamics. In order to account for the thermoacoustic feedback this simulation is coupled to an acoustic network model. Here, the two-way coupling is based on the Rankine–Hugoniot equations and uses a reference velocity measured upstream of the flame and the global heat release rate.

A bifurcation analysis with the plenum length as bifurcation parameter was conducted. The two models were in good agreement with each other. The compressible simulation on which the model C-fg is based on resolves the flame acoustic interaction, possible nonlinear scattering of acoustic waves and hydrodynamic effects. On the other hand, the low Mach number simulation utilized by the model LM-uq, suppresses all acoustic effects inside the CFD domain. Thus, in this model the acoustic field is acting on the flame only via fluctuations of the reference velocity. The bifurcation analysis shows good agreement of the two models, thus we conclude that the flame investigated indeed responds predominantly to fluctuations of the reference velocity. This holds even while the flame exhibits complex thermoacoustic oscillations. Consequently, the acoustic pressure p' and acoustic waves f, g act on the flame only indirectly, as they cause fluctuations of the reference velocity u'. This sequence of cause and effect has been questioned in the context of the recent discussion on the intrinsic thermoacoustic feedback [27–32]. Furthermore, the comparison shows that the nonlinearities observed can be attributed to hydrodynamic effects or to the flame kinematics.

The models investigated in the present study form a basis for further research. On the one hand the two models can be extended in a straightforward manner to take into account effects such as conjugate heat transfer or three dimensional effects. This is expected to be necessary in order to obtain models which reproduce experimental results with quantitative accuracy. Here, the most critical limitations are that both models are restricted to the low-frequency regime and that the model LM-uq is valid only for velocity sensitive heat sources. On the other hand the models can serve as reference for nonlinear reduced-order models for the dynamics of laminar flames. In Jaensch and Polifke [33] results of the model LM-uq are compared against predictions made with artificial neural networks. Furthermore, both coupling methods also work with LES and therefore, allow a detailed numerical study of thermoacoustic oscillations of turbulent flames. This is of significant applied interest and will be the subject of future investigations.

Acknowledgment

The financial support for S. Jaensch has been provided by the Research Association for Combustion Engines (Forschungsvereinigung Verbrennung e.V - FVV, project number: 6011150). Financial support for M. Merk and E. A. Gopalakrishan was provided by the German Research Foundation (DFG) via the project PO 710/16-1 and the SFB/TRR40 summer program, respectively. Financial support for S. Bomberg was provided by Technische Universität München / Institute for Advanced Study, funded by the German Excellence Initiative, and DFG, project PO 710/12-1. This support is gratefully acknowledged. We thank CERFACS and IFP for providing the solver AVBP. The authors gratefully acknowledge the Gauss Centre for Supercomputing e.V. (www.gauss-centre.eu) for funding this project by providing computing time

S. Jaensch, M. Merk, E. A. Gopalakrishnan, S. Bomberg, T. Emmert, R. I. Sujith, W. Polifke, Proceedings of the Combustion Institute, vol. 36, pp. 3827-3834, 2017, http://dx.doi.org/10.1016/j.proci.2016.08.006.. Reprinted with permission from Elsevier.

on the GCS Supercomputer SuperMUC at Leibniz Supercomputing Centre (LRZ, www.lrz.de).

References

[1] D. Durox, T. Schuller, N. Noiray, S. Candel, *Proc. Combust. Inst.* 32 (1) (2009) 1391–1398, doi:10.1016/j.proci.2008.06.204.

[2] L. Kabiraj, R. Sujith, P. Wahi, *J. Eng. Gas Turbines Power* 134 (2012) 031502.

[3] A.P. Dowling, *J. Fluid Mech.* 394 (394) (1999) 51–72.

[4] N. Noiray, D. Durox, T. Schuller, S. Candel, *J. Fluid Mech.* 615 (2008) 139–167, doi:10.1017/S0022112008003613.

[5] K. Kashinath, S. Hemchandra, M.P. Juniper, *J. Eng. Gas Turbines Power* 135 (2013) 061502.

[6] K. Kashinath, I.C. Waugh, M.P. Juniper, *J. Fluid Mech.* 761 (2014) 399–430, doi:10.1017/jfm.2014.601.

[7] A. Orchini, S. Illingworth, M. Juniper, *J. Fluid Mech.* 775 (2015) 387–414.

[8] T. Schuller, S. Ducruix, D. Durox, S. Candel, *Proc. Combust. Inst.* 29 (1) (2002) 107–113.

[9] K. Kashinath, S. Hemchandra, M.P. Juniper, *Combust. Flame* 160 (12) (2013) 2856–2865.

[10] S. Schlimpert, S. Hemchandra, M. Meinke, W. Schröder, *Combust. Flame* (2014) 1–23, doi:10.1016/j.combustflame.2014.08.001.

[11] J. Moeck, C. Scharfenberg, O. Paschereit, R. Klein, in: Notes on Numerical Fluid Mechanics and Multidisciplinary Design, 108, 2010, pp. 291–306.

[12] S.R. Chakravarthy, C. Balaji, R.K.R. Katreddy, A. Nath, in: Proceedings of International Summer School and Workshop on Non-Normal and Nonlinear Effects In Aero- and Thermoacoustics (2013), Munich, Germany, 2013,, p. 12.

[13] B. Schuermans, H. Luebcke, D. Bajusz, P. Flohr, in: Proceedings of ASME Turbo Expo, GT2005-68393, 2005, doi:10.1115/GT2005-68393.

[14] C.T. Wall, *Numerical Methods for Large Eddy Simulation of Acoustic Combustion Instabilities* Ph.D. thesis, Stanford University, 2005.

[15] V.N. Kornilov, R. Rook, J.H.M. ten Thije Boonkkamp, L.P.H. de Goey, *Combust. Flame* 156 (10) (2009) 1957–1970. http://dx.doi.org/10.1016/j.combustflame.2009.07.017.

[16] F. Duchaine, F. Boudy, D. Durox, T. Poinsot, *Combust. Flame* 158 (12) (2011) 2384–2394, doi:10.1016/j.combustflame.2011.05.013.

[17] S. Jaensch, C. Sovardi, W. Polifke, *J. Comput. Phys.* 314 (2016) 145–159. http://dx.doi.org/10.1016/j.jcp.2016.03.010.

[18] T. Poinsot, S.K. Lele, *J. Comput. Phys.* 101 (1) (1992) 104–129.

[19] W. Polifke, C. Wall, P. Moin, *J. Comput. Phys.* 213 (2006) 437–449, doi:10.1016/j.jcp.2005.08.016.

[20] B.T. Chu, in: Proceedings of the 4th Symposium (International) on Combustion (1953), vol. 4, 1953, pp. 603–612, doi:10.1016/S0082-0784(53)80081-0.

[21] T. Emmert, S. Jaensch, C. Sovardi, W. Polifke, in: Proceedings of the 7th Forum Acusticum, DEGA, Krakow, 2014.

[22] T. Emmert, M. Meindl, S. Jaensch, W. Polifke, *Acta Acustica United Acustica* 102 (5) (2016) 824–833, doi:10.3813/AAA.918997.

[23] M. Meindl, T. Emmert, W. Polifke, in: Proceedings of ICSV23 Congress Proceeding, 2016.

[24] H.K. Versteeg, W. Malalasekera, *An Introduction to Computational Fluid Dynamics: The Finite Volume Method*, 2nd edition, Pearson Education Ltd, Harlow, England; New York, 2007.

[25] F. Takens, *Detecting Strange Attractors in Turbulence*, Springer, Berlin Heidelberg, 1981.

[26] L. Kabiraj, R. Sujith, *J. Fluid Mech.* 713 (2012) 376–397.

[27] M. Hoeijmakers, V. Kornilov, I. Lopez Arteaga, P. de Goey, H. Nijmeijer, *Combust. Flame* 161 (2014) 2860–2867, doi:10.1016/j.combustflame.2014.05.009.

[28] M. Hoeijmakers, V. Kornilov, I.L. Arteaga, P. de Goey, H. Nijmeijer, *Proc. Combust. Inst.* 35 (1) (2015) 1073–1078, doi:10.1016/j.proci.2014.06.059.

[29] S. Bomberg, T. Emmert, W. Polifke, in: Proc. Combust. Inst., 35, 2015, pp. 3185–3192, doi:10.1016/j.proci.2014.07.032.

[30] E. Courtine, L. Selle, T. Poinsot, *Combust. Flame* 162 (11) (2015) 4331–4341, doi:10.1016/j.combustflame.2015.07.002.

[31] T. Emmert, S. Bomberg, W. Polifke, *Combust. Flame* 162 (1) (2015) 75–85, doi:10.1016/j.combustflame.2014.06.008.

[32] C.F. Silva, T. Emmert, S. Jaensch, W. Polifke, *Combust. Flame* 162 (9) (2015) 3370–3378, doi:10.1016/j.combustflame.2015.06.003.

[33] S. Jaensch, W. Polifke, in: Proceedings of International Symposium on Thermoacoustic Instabilities in Gas Turbines and Rocket Engines, Garching, Germany, 2016.

S. Jaensch, M. Merk, E. A. Gopalakrishnan, S. Bomberg, T. Emmert, R. I. Sujith, W. Polifke, Proceedings of the Combustion Institute, vol. 36, pp. 3827-3834, 2017, http://dx.doi.org/10.1016/j.proci.2016.08.006.. Reprinted with permission from Elsevier.

Original Research Article

International journal of spray and combustion dynamics

International Journal of Spray and Combustion Dynamics
0(0) 1–13

DOI: 10.1177/1756827716687583
journals.sagepub.com/home/scd
SAGE

Uncertainty encountered when modelling self-excited thermoacoustic oscillations with artificial neural networks

Stefan Jaensch and Wolfgang Polifke

Abstract

Artificial neural networks are a popular nonlinear model structure and are known to be able to describe complex nonlinear phenomena. This article investigates the capability of artificial neural networks to serve as a basis for deducing nonlinear low-order models of the dynamics of a laminar flame from a Computational Fluid Dynamics (CFD) simulation. The methodology can be interpreted as an extension of the CFD/system identification approach: a CFD simulation of the flame is perturbed with a broadband, high-amplitude signal and the resulting fluctuations of the global heat release rate and of the reference velocity are recorded. Thereafter, an artificial neural network is identified based on the time series collected. Five data sets that differ in amplitude distribution and length were generated for the present study. Based on each of these data sets, a parameter study was conducted by varying the structure of the artificial neural network. A general fit-value criterion is applied and the 10 artificial neural networks with the highest fit values are selected. Comparing of these 10 artificial neural networks allows to obtain information on the uncertainty encountered. It is found that the methodology allows to capture the forced response of the flame reasonably well. The validation against the forced response, however, depends strongly on the forcing signal used. Therefore, an additional validation criterion is investigated. The artificial neural networks are coupled with a thermoacoustic network model. This allows to model self-excited thermoacoustic oscillations. If the training time series are sufficiently long, this coupled model allows to predict the trend of the root mean square values of fluctuations of the global heat release rate. However, the prediction of the maximal value of the fluctuation amplitude is poor. Another drawback found is that even if very long-time series are available, the behaviour of artificial neural networks cannot be guaranteed. It is concluded that more sophisticated nonlinear low-order models are necessary.

Keywords

System identification, nonlinear flame dynamics, laminar premixed flames, self-excited thermoacoustic oscillations, artificial neural networks

Date received: 25 April 2016; accepted: 12 December 2017

1 Introduction

Thermoacoustic oscillations limit the development of gas turbines and rocket engines. These oscillations are nonlinear. Hence, in order to decide whether or not a thermoacoustic oscillation reaches critical amplitude levels, nonlinear low-order models are necessary.

Several models have been developed to predict these amplitude levels. The flame describing function (FDF) combined with a one-dimensional model for the acoustics has been proven to give useful estimates of the oscillation amplitudes in many cases.[1–3] It is also possible to deduce an FDF from a CFD simulation.[4–6] The FDF is limited to harmonic oscillations, where higher harmonics in the flame response are unimportant. As shown by Moeck and Paschereit[7] and Orchini et al.,[8] the FDF can be extended to the so-called flame double input describing function (FDIDF). This increases the accuracy of the prediction significantly. However, determining a FDIDF is

Technische Universität München, Fakultät für Maschinenwesen, Garching, Germany

Corresponding author:
Stefan Jaensch, Technische Universität München, Fakultät für Maschinenwesen, D-85747 Garching, Germany.
Email: Jaensch@tfd.mw.tum.de

S. Jaensch, W. Polifke, International Journal of Spray and Combustion Dynamics, 2017, http://dx.doi.org/10.1177/1756827716687583.. Reprinted in terms of Creative Commons licence (CC BY-NC).

prohibitively expensive for practically relevant applications.[8] Another model that has drawn recent interest is the G-equation.[2,8–11] The drawback of G-equation-based models is that the results depend strongly on the velocity model used. Consequently, no quantitative agreement with experiment is obtained. A promising technique is hybrid CFD/low-order models.[12–16] These models have the advantage that they can account for the complex interaction between heat source, flow and acoustics. Additionally, compared to a fully compressible simulation of the whole thermoacoustic configuration, the computational effort can be significantly reduced. However, the computational effort is still high and more efficient non-linear low-order models are needed. A general methodology for deriving low-order models from a CFD simulation is the CFD/system identification (SI) approach.[17] The general idea of the CFD/SI approach is to force a CFD simulation with broadband excitation signal. If the flame dynamics of a premixed flame is to be determined, the resulting fluctuation of the reference velocity and of the global heat release rate is recorded. From these time series low-order models can be deduced by system identification.[18,19] In the linear regime, the CFD/SI approach is known to yield accurate estimates of the flame transfer function (FTF).[17] The CFD/SI approach can be extended to the nonlinear regime.[18,20] Selimefendigil et al.[21–23] used the method to identify nonlinear low-order models for a cylinder in pulsating crossflow. Zhang et al.[24] used Hammerstein–Wiener models to deduce nonlinear low-order models from a G-equation solver.

In the present study, the CFD/SI approach is used to obtain nonlinear low-order models of a laminar flame. The capability of artificial neural networks (ANNs) to serve as the nonlinear model structure is investigated. ANNs have become a very popular black-box model in the last decades. They have been used to predict stock prices to forecast the weather and to model aircrafts. The ANN framework provides a model structure, which can easily be extended in such a way that very complex nonlinearities can be described. Consequently, it is expected that there exists an ANN that describes the nonlinear flame dynamic accurately. Indeed, Blonbou et al.[25,26] and Vaudrey and Saunders[27] showed that ANNs can be used to control combustion instabilities. However, the model structure of an ANN has a large number of parameters and consequently, ANNs are prone to over-fitting. This phenomenon occurs in particular if only short time series are available. In contrast to experimental test rigs, as investigated by Blonbou et al.[25,26] and Vaudrey and Saunders,[27] the time series used for the CFD/SI approach should be as short as possible. Otherwise, no advantage in computational time can be achieved. Therefore, the key question addressed in the present study is whether or not an appropriate ANN can be determined based on the limited information available, i.e. the broadband time series. An ANN is considered to be appropriate if on the one hand it can capture the forced response of the flame. This criterion allows to validate the predicted fluctuation of the global heat release rate in both the time and the frequency domain in a straightforward manner. A drawback of this comparison is that it depends strongly on the forcing signal used. Therefore, on the other hand, an additional validation criterion is investigated. The ANNs identified are combined with a thermoacoustic network model in order to model self-excited thermoacoustic oscillations. The predicted oscillations are compared against the results obtained with the hybrid CFD/low-order models discussed in Jaensch et al.[16] This validation analyses if small errors made by the ANN accumulate and is very close to the application considered. A difficulty of this validation is that thermoacoustic oscillations can be very complex, which makes a direct comparison in the time or frequency domain difficult. In the present study, we compare the oscillations predicted in terms of root mean square (RMS)-values and the maximal fluctuation of the global heat release rate.

In the next section, the CFD setup is introduced, which forms the basis of the present study. Thereafter, we discuss how ANNs can be used for the CFD/SI approach. Then, the methodology is validated in terms of forced response and self-excited oscillations.

2 Numerical setup

The CFD setup is shown in Figure 1 and corresponds to the multi-slit burner investigated by Kornilov et al.[28]

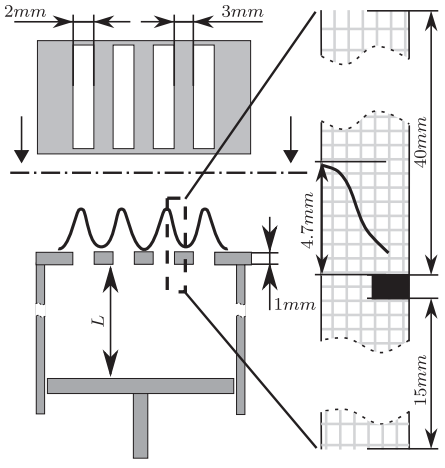

Figure 1. Multi-slit burner and the corresponding CFD domain investigated.[16]

S. Jaensch, W. Polifke, International Journal of Spray and Combustion Dynamics, 2017, http://dx.doi.org/10.1177/1756827716687583..

and Duchaine et al.[29] The numerical settings were chosen as in Duchaine et al.,[29] i.e. equivalence ratio 0.8, inlet velocity 0.4 m/s, inlet temperature, 293 K and wall temperature 373 K. In contrast to Duchaine et al.,[29] a low Mach formulation of the Navier–Stokes equations was solved. This implies that the density depends on the temperature only, but not on the pressure. Consequently, the acoustics inside the computational domain is suppressed. In particular, this modification also suppresses the intrinsic thermoacoustic feedback.[30] It is expected that this simplifies the identification significantly, it allows us to investigate an open-loop problem. OpenFOAM (http://www.openfoam.org/) was used as CFD solver. The CFD setup used in the present study is identical to the low-Mach simulation described in Jaensch et al.[16]

3 ANNs

In the present section, first the structure of ANNs is introduced. Afterward, it is discussed how ANNs can be used as a nonlinear model structure for the CFD/SI approach.

3.1 Structure of ANNs

An ANN consists of interconnected *neurons*. A single neuron is a function $y = \sigma(\mathbf{u}, \mathbf{\Theta})$ with input vector $\mathbf{u}$ and a scalar output y. $\mathbf{\Theta}$ is the parameter vector. The function $\sigma(\cdot)$ is called the activation function. In principle, any function can be used. For practical applications, sigmoid functions and radial basis functions (RBF) have been proven to be useful choices.[20;18] Examples of both functions plotted in Figure 2. A sigmoid function is given as

$$\sigma_{\mathrm{Sig}}(\mathbf{u}, \mathbf{\Theta}) = \frac{2}{1 + \exp\left(-2\mathbf{\Theta}^T \mathrm{u}\right)} - 1 \tag{1}$$

Here, the parameter vector $\mathbf{\Theta}$ weights the inputs. Consequently, the elements Θ_k of $\mathbf{\Theta}$ are called *weights*. A radial basis function is defined as

$$\sigma_{\mathrm{RBF}}(\mathbf{u},\ \mathrm{c},\ \Sigma) = \exp\left(-\frac{1}{2}\|\mathbf{u} - \mathrm{c}\|_{\Sigma}^2\right) \tag{2}$$

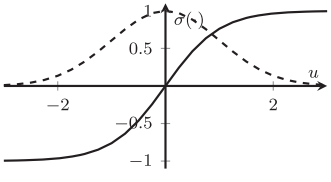

Figure 2. Full line: sigmoid function with $\Theta = 1$, dashed line: radial basis function (RBF) with $\sum = 1$ and $c = 0$.

with the generalized norm

$$\|\mathbf{u} - \mathrm{c}\|_{\Sigma} = \sqrt{(\mathbf{u} - \mathrm{c})^T\ \Sigma(\mathbf{u} - \mathrm{c})} \tag{3}$$

Here, the parameter vector $\mathbf{\Theta}$ is represented by the centre vector c and the norm matrix . These quantities correspond to the mean vector and the covariance matrix of a multivariate normal distribution. In order to reduce the number of parameters, Σ is assumed to be a diagonal matrix.

Several interconnected neurons build an ANN. As depicted in Figure 3, ANNs are structured in several layers. The inputs of the ANN are time-lagged velocity signals $u'(t - i\Delta t)$. Here, i is the time increment and Δt is the time step. The inputs of the ANN are also the inputs of the neurons positioned in the first layer. The inputs of the neurons in the second layer are the outputs of the neurons in the first layer and so on. The last layer consists of a single neuron with a linear activation function. Note that all neurons positioned in the same layer have the same inputs. As only time-lagged input signals and no time-lagged output signals are the inputs of the ANN the impulse response of the ANNs considered is finite and has the length $n\Delta t$. An infinite impulse response would require us to pass the output of the ANN as feedback to its inputs. This is analogue to a finite impulse response (FIR) model used for linear system identification. The finiteness of the impulse response reflects the convective nature of the flame dynamics: an impulse velocity perturbation impinging on the flame causes a perturbation of the flame front and consequently a fluctuation of the global heat release rate. Blumenthal et al.[31] showed for a G-equation flame model that the perturbation of the flame front is convected through the flame and that the original flame front is restored via a convective

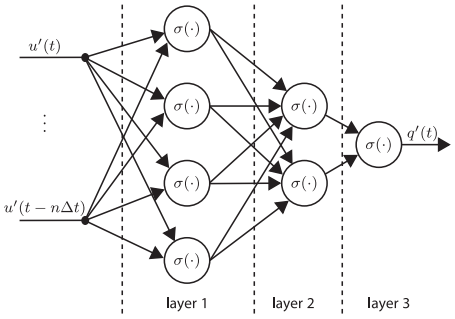

Figure 3. Generic example of a structure of an artificial neural network with four neurons in the first layer, two neurons in the second layer and a single neuron in the third layer.

S. Jaensch, W. Polifke, International Journal of Spray and Combustion Dynamics, 2017, http://dx.doi.org/10.1177/1756827716687583.. Reprinted in terms of Creative Commons licence (CC BY-NC).

restoration mechanism. Once the perturbation and the restoration are convected through the flame, the fluctuation of the global heat release vanishes instantaneously. Thus the impulse response of the flame is finite. Therefore, the FIR model should be considered as a grey-box model of the flame.[32] It is expected that these considerations hold for the nonlinear flame dynamics. In general, the ANN framework allows to additionally consider time-lagged values of the output signal, i.e. the fluctuation of the global heat release rate, as inputs of to the neural network. However, this yields an oscillatory impulse response, which does not correspond to the convective nature of the flame response. Silva et al.[33] show that these so-called *auto-regressive* models are useful for modeling the scattering matrix of a flame, but not for the FTF.

Typically, all activation functions of neurons positioned in the same layer are identical. If RBFs are used, it is advantageous to normalize the output of the k-th neuron in a layer by the output of all neurons in the same layer

$$\sigma_{\mathrm{NRBF},\,k}(\mathbf{u}, \mathrm{c}, \Sigma) = \frac{\sigma_{\mathrm{RBF}}(\mathbf{u}, \mathrm{c}_k, \Sigma_k)}{\sum_{i=0}^{M} \sigma_{\mathrm{RBF}}(\mathbf{u}, \mathrm{c}_i, \Sigma_i)} \tag{4}$$

with M being the number of neurons in the layer. The function $_{\mathrm{NRBF;k}}(\mathrm{u}, \mathrm{c}, \Sigma)$ is called *normalized radial basis function* (NRBF).

3.2 Identification of ANNs

The identification procedure used to determine the unknown parameter vector $\boldsymbol{\Theta}$ of an ANN is similar to the procedure used for linear identification[17,18]:

1. First, a broad band time series is created.
2. The model structure has to be chosen.
3. The unknown parameters are determined by solving an optimization problem.
4. The model identified must be validated.

In order to generate broad band time series, the CFD simulation introduced above was forced with different broadband excitation signals. The signals were generated with the method discussed in Föller and Polifke.[34] As for the linear CFD/SI approach, the frequency content of the signal should be chosen such that all frequencies of interests are excited. For the nonlinear identification, also the amplitude of the signal is important. Therefore, signals with different amplitudes are investigated in the present study. The particular signals used are discussed in detail in the next section.

The second step of the identification procedure is to fix the structure of the ANN. This means choosing the activation function, the number of layers and the number of neurons per layer. Additionally, the maximum delay n has to be fixed. Unfortunately, there exist no general design rules for choosing the structure of an ANN. Typically, one identifies several ANNs with different structures and selects the ANN with the best performance. In the present study, this is done in terms of a large parameter study, which is discussed in the next section.

The third step of the identification procedure is to determine the vector of unknown parameters $\boldsymbol{\Theta}$ of the neural networks. This is done by solving the optimization problem

$$\min_{\boldsymbol{\Theta}} \frac{1}{N} \sum_{i=0}^{N-1} \left(q'_{\mathrm{ANN}}(i\Delta t,\ \boldsymbol{\Theta}) - q'_{\mathrm{CFD}}(i\Delta t) \right)^2 \tag{5}$$

This optimization problem is nonlinear and consequently, nonlinear optimization algorithms are necessary. These algorithms are based on error backpropagation, which allows to calculate the gradient of the cost function analytically. In comparison to the Wiener–Hopf inversion, the computational effort required is significantly larger. However, compared to the computational costs of the CFD simulation, the computational effort is still negligible. A particularity of ANNs is that the optimization is non-deterministic. Recall from the discussion of the structure of ANNs that the inputs and outputs of all neurons positioned in the same layer are equal (see also Figure 3). Hence, neurons positioned in the same layer differ only with respect to their parameter vector. Consequently, if in order to solve the optimization problem all parameters are initialized to zero, after the optimization the parameters of all neurons positioned in the same layer will be equal. The performance of such an ANN would be poor. In order to avoid this behaviour, the parameter vector is initialized to small, random values. Consequently, re-identifying an ANN with the same structure several times can yield ANNs, showing a significantly different performance. Note that only the optimization algorithm is non-deterministic. ANNs are a deterministic model once all parameters have been determined. The number of unknown parameters of an ANN grows rapidly with the number of neurons and layers. This enables ANNs to model complex nonlinearities, however, it creates the risk of over-fitting. If the optimization problem (5) is solved untill convergence, the quality of the ANN obtained would be poor. In order to avoid over-fitting, the data used to identify the parameters of the ANNs is divided into three different data sets: training data, validation data and test data. The optimization algorithm calculates the gradient of the cost function using only the training data set. The optimization stops when the

S. Jaensch, W. Polifke, International Journal of Spray and Combustion Dynamics, 2017, http://dx.doi.org/10.1177/1756827716687583..

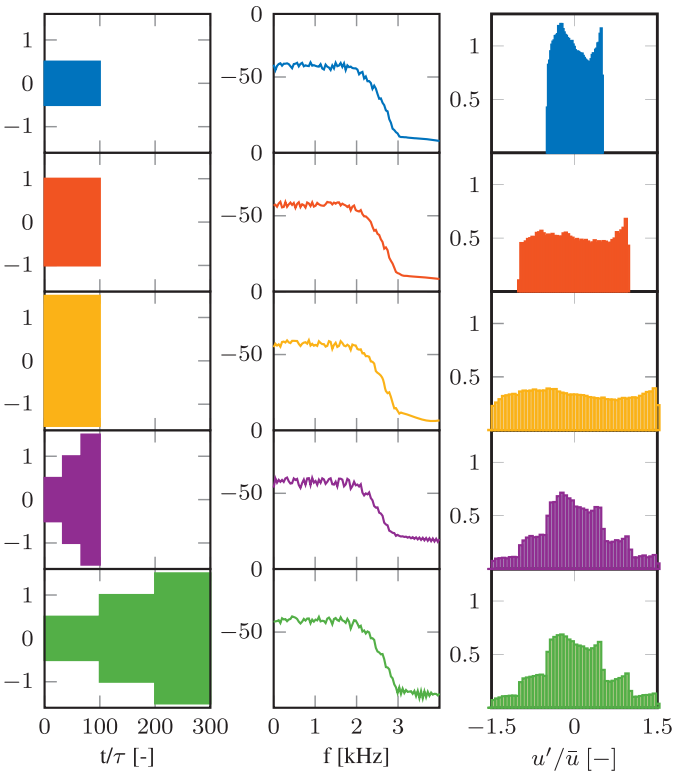

Figure 4. Five different data sets used to generate the ANNs. Left: envelope of the time series $u'/\bar{u}[-]$, middle: power spectral density PSD (dB/Hz), right: empirical probability density function.

error made on the validation data set increases. The test data set is not used during the optimization. In the present work, 70% of the data are used as training data, 15% as validation data and 15% as test data. The data were divided randomly using a fixed seed.

For the present study, the default implementation of ANNs in Matlab (www.mathworks.com, version: R2015b) is used.

4 Numerical results

Unfortunately, there are no general design rules for the structure of neural networks. Indeed, as the training of neural networks is non-deterministic, two ANNs with the same structure can show totally different behaviour. This holds even if the same data set was used to train both networks. In order to use ANNs to model self-excited thermoacoustic oscillations a criterion is necessary, which allows to decide whether or not an ANN identified is a good low-order model of the nonlinear flame dynamics. This criterion should be based on the broadband time series used to identify the network. Otherwise, the computational effort required to find a suitable ANN can make the methodology prohibitively expensive. The criterion investigated in the present work is the fit value defined as

$$\text{fit} = 100\left(1 - \frac{\|q'_{\text{CFD}} - q'_{\text{ANN}}\|}{\|q'_{\text{CFD}} - q'_{\text{CFD}}\|}\right) \tag{6}$$

with the temporal average q'_{CFD} of the fluctuations of the global heat release rate measured in the CFD simulation. This criterion is also known as normalized root mean square error (NRMSE). The criterion is evaluated using the full broadband time series including training data, validation data and test data. Recall that the weights of the ANN are determined via the optimization procedure discussed in the previous section using the validation and the training data. The test data are not used. Considering this data to select the optimal ANNs is an additional method to prevent over-fitting.

In order to increase the generalizability of the results of the present study, a large number of ANNs with different structures were identified using the five data

S. Jaensch, W. Polifke, International Journal of Spray and Combustion Dynamics, 2017, http://dx.doi.org/10.1177/1756827716687583.. Reprinted in terms of Creative Commons licence (CC BY-NC).

sets shown in Figure 4. The 10 ANNs with the greatest fit values on each data set were selected. The underlying parameter study is explained in detail in the next subsection. Thereafter, the ANNs selected are validated against the forced response and against self-excited thermoacoustic oscillations.

4.1 Setup of the parameter study

As shown in Figure 4, five different broadband time series are investigated. These data sets were generated by forcing the inflow velocity u' of the CFD simulation with three different broadband excitation signals. The length of the time series obtained is $100\,\tau$. Here, τ is the length of the impulse response of the flame and is equal to 10 ms. All signals are statistically independent from each other and were generated with the non-Gaussian simulation method described in Föller and Polifke.[34] A small part of the signal is shown in Figure 7. The signals were scaled such that the amplitude $u'/\bar{u}$ of the first signal is 50%, the one of the second signal is 100% and the one of the third signal is 150%. From the three time series obtained, five different data sets were generated. These data sets are shown in Figure 4. The data sets 1, 2 and 3 are the time series directly generated by the CFD simulation. Data set 4 is concatenated and consists of the first third of the data sets 1 to 3, respectively. Data set 5 is concatenated and consists of the full data sets 1 to 3. Data set 4 and 5 are investigated in to analyse whether signals containing several excitation amplitude levels can improve the results. In the linear regime, the length of the time series and its power spectral density are sufficient to characterize the excitation signal used for identification. This is because linearity implies that the response is independent from the excitation amplitude. In the nonlinear regime, however, also the distribution of the amplitudes is important. In Figure 4, this is shown by the empirical probability density function.

In addition to the time series, also the structure of the ANN is varied. The parameters changed are listed in Table 1. All 3780 combinations of these parameters

Table 1. Parameters varied for the parameter study.

$\Delta t/\tau$	0.015, 0.03, 0.06
$n\Delta t/\tau$	1.5, 2, 2.5
# neurons	2 to 20 (step size of 2)
# layers	2, 3
σ (–)	Sigmoid, NRBF

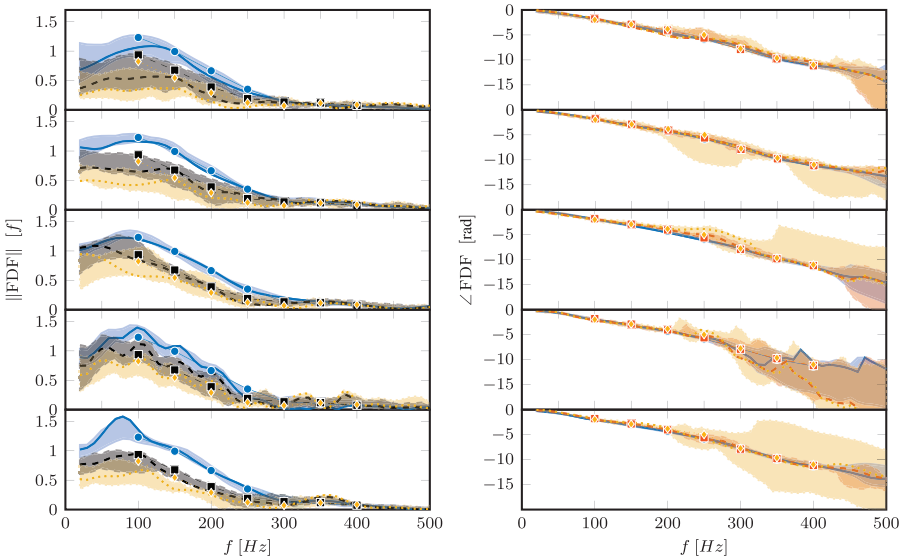

Figure 5. Comparison of the FDF deduced from the optimal ANNs and from the CFD simulation. Left: gain; right: phase; lines: estimate by the ANN with the highest fit value. Shaded area: bounds of the prediction made by the 10 optimal ANNs selected. Markers: reference generated by forcing the CFD with harmonic signals. Excitation amplitudes: A = 50% (full blue line, blue dots), A = 100% (dashed black line, black squares), A = 150% (dotted yellow line, yellow diamonds), training data sets ordered top to bottom as in Figure 4.

S. Jaensch, W. Polifke, International Journal of Spray and Combustion Dynamics, 2017, http://dx.doi.org/10.1177/1756827716687583.. Reprinted in terms of Creative Commons licence (CC BY-NC).

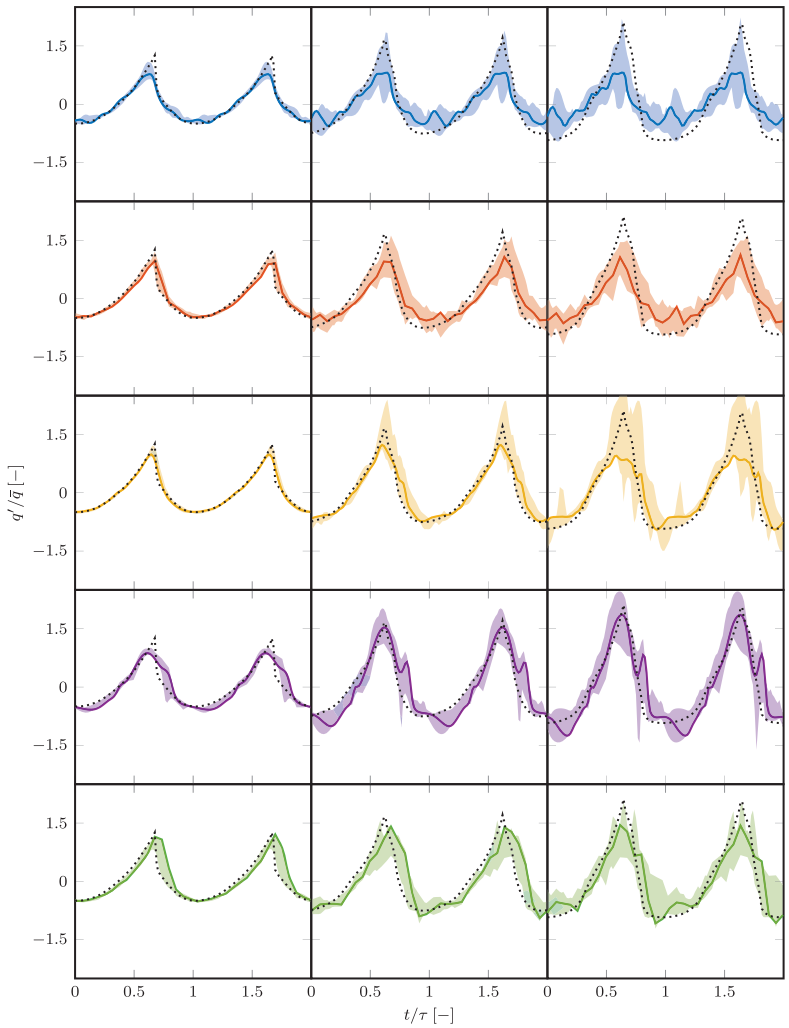

Figure 6. Validation of the response of the 10 optimal ANNs to harmonic forcing in the time domain. Solid line: estimate by the ANN with the highest fit value. Shaded area: bounds of the predictions made by the 10 optimal ANNs. Black dotted line: CFD reference. Forcing frequency: 100 Hz, excitation amplitudes: 50% (left), 100% (middle) and 150% (right), training data sets ordered top to bottom as in Figure 4.

were investigated. The number of unknown parameters of the ANNs varied between 55 and 3801. On each of the five data sets shown in Figure 4, ANNs with the resulting structures were identified. In order to find an optimal ANN for each of the structures, the non-deterministic optimization algorithm was 10 times repeatedly applied. Thereafter, the fit value achieved by each ANN was determined. The 10 ANNs with the highest fit values on each data set were selected. The capability of these optimal ANNs to model the nonlinear flame dynamics is investigated in the next subsections.

4.2 Validation of the forced response

In Figure 5, the FDF deduced from the ANNs is compared against the results obtained from the CFD simulation. An FDF can be deduced from an ANN analogously to the way it is deduced from a CFD simulation or an experiment: at first the ANN is forced with

S. Jaensch, W. Polifke, International Journal of Spray and Combustion Dynamics, 2017, http://dx.doi.org/10.1177/1756827716687583.. Reprinted in terms of Creative Commons licence (CC BY-NC).

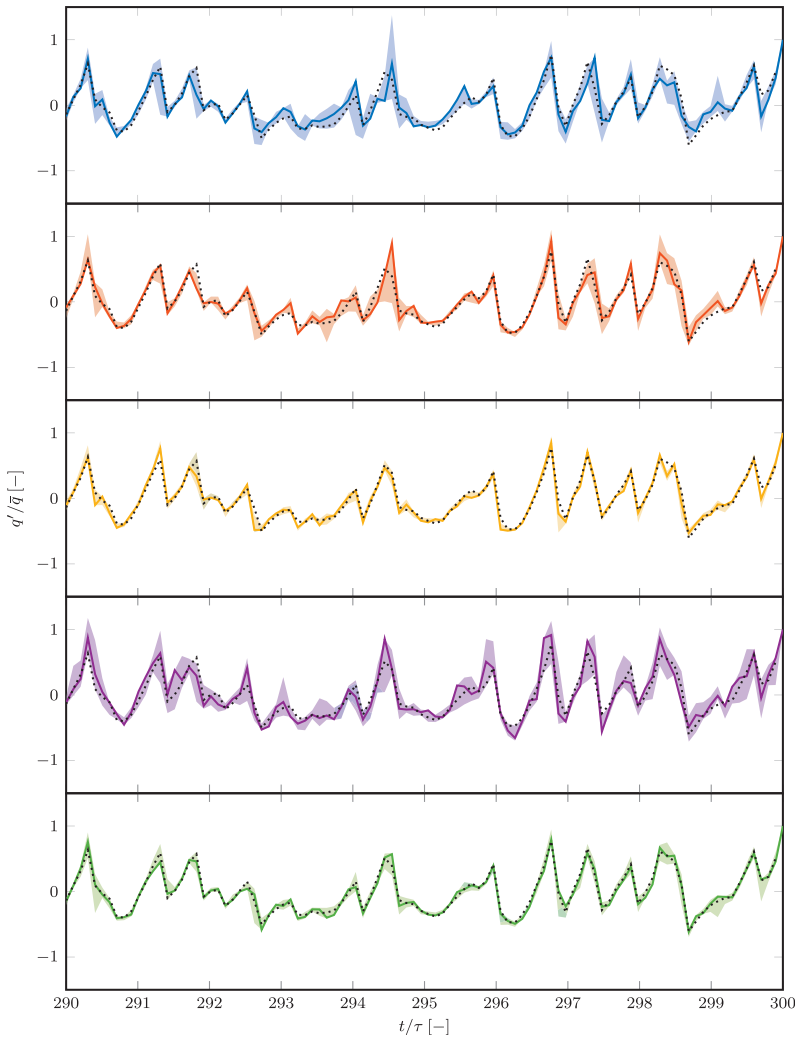

Figure 7. Validation of the forced response of the 10 optimal ANNs against broadband time series. The broadband data are the last 10 t = of data set 5. Solid line: estimate by the ANN with the highest fit value. Shaded area: bounds of the predictions made by the 10 optimal ANNs. Black dotted line: CFD reference. Training data sets ordered top to bottom as in Figure 4.

a harmonic input signal with a specific amplitude and frequency. The output of the ANN is its prediction of the fluctuation of the global heat release rate. The ratio of the Fourier transformed input and output signals at the forcing frequency is the value of the FDF. For frequencies up to 200 Hz, the phases predicted by the ANNS are in excellent agreement with the CFD reference data. Also for higher frequencies, the phase is predicted well. The variance of the results is large only for the highest forcing amplitude considered, i.e. 150% and for the ANNs identified on data set 4. Errors at these high frequencies are expected as the gain of the FDF is very small. The picture is less distinct for the predicted gain. Overall, the low-pass characteristic of the FDF is captured well by the ANNs. The variance of the prediction is quite small for an excitation amplitude of 50% and increases for the higher excitation amplitudes considered. At an excitation amplitude of 50%, a large variance is observed for the ANNs identified on data set 5. This is a problematic observation. It shows that even if very long-time series are available, it cannot be guaranteed that the ANNs identified predict the FDF

S. Jaensch, W. Polifke, International Journal of Spray and Combustion Dynamics, 2017, http://dx.doi.org/10.1177/1756827716687583.. Reprinted in terms of Creative Commons licence (CC BY-NC).

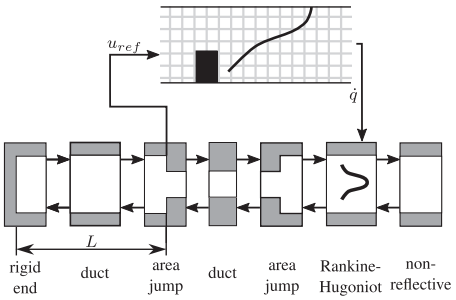

Figure 8. Coupling of the CFD simulation with an acoustic network model to model self-excited thermoacoustic oscillations.

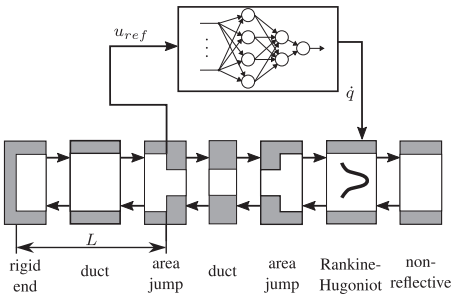

Figure 9. Coupling of an ANN with an acoustic network model to model self-excited thermoacoustic oscillations.

with good accuracy. The results with the ANNs identified on data set 5 improve for higher excitation amplitudes. Here, the prediction is more accurate than the one made by the ANNs identified on the other data sets.

Validating against the FDF allows to compare the results for several different forcing amplitudes and frequencies. However, the analysis is limited to the forcing frequency. This ignores the capability of ANNs to predict also a non-harmonic response of the flame. Therefore, in Figure 6, the response of the optimal ANNs to a harmonic forcing signal is shown in the time domain. The predicted fluctuation of the global heat release rate is validated against the prediction made by the CFD. At an excitation amplitude of 50%, the results are in good agreement with each other and independent from the data set used to identify the ANNs. The variance of the prediction made by the ANNs increases significantly with the excitation amplitude. Up to an amplitude level of 100%, the shape of the response is captured quite well. At 150% amplitude, the peaks of the response are still captured, however, the variance becomes large. The results obtained with data set 4 and data set 5 are slightly more robust. This is expected as these data sets include all excitation amplitudes.

In Figure 7, the ANNS are compared on the last $10t/\tau$ of data set 5. The shape of the response is captured by all sets of ANNs. The ANNs identified on data sets 3 and 5 show the lowest variance. This is because the fit criterion used to select these ANNs contains also the broadband signal shown in Figure 7. The variance of the other sets of optimal neurons is larger. Nevertheless, the main features of the time series are still captured.

4.3 Validation against self-excited oscillations

From the analysis of the forced response, we can conclude that over-fitting was successfully avoided by the procedure applied to obtain the sets of optimal ANNs. However, the analysis depends strongly on the forcing signal used. Therefore, in the present section, the capability of the ANNs identified to predict self-excited thermoacoustic oscillations is investigated.

Both the weakly compressible CFD simulation and the ANNs are models for the flame dynamics of the laminar flame considered. In order to model self-excited thermoacoustic oscillations, they need to be coupled with a model for the acoustics. In Figures 8 and 9, the coupling of the CFD simulation and of an ANN with an acoustic network model is shown, respectively. In Jaensch et al.,[16] the coupling of the CFD and the network model is described in detail. The ANNs are coupled with the acoustic model using Matlab/Simulink.

In Figure 10, the self-excited thermoacoustic oscillations are compared in terms of their RMS values and in terms of the maximal fluctuation of the global heat release rate. The bifurcation parameter is the plenum length, as shown in Figures 1, 8 and 9. At each length investigated, a self-excited oscillation was calculated with all optimal ANNs for $50\,\tau$. As discussed by Jaensch et al.,[16] the thermoacoustic oscillations of the present configurations hardly depend on the initial condition used. In order to minimize the computational effort of the CFD simulation the simulation, was started from a perturbed case. This situation cannot be reproduced with the ANNs. Therefore, we focus the discussion on comparing the fully developed thermoacoustic oscillation. For the results shown in Figure 10, only the last $20\,\tau$ of the $50\,\tau$ time series are used.

At several working points numerical instabilities were observed. One example of such a numerical instability is shown in Figure 11. The oscillation predicted by the ANN develops significantly more slowly than the oscillation predicted by the CFD simulation. This mismatch is due to the different initial conditions used and thus, expected. After about $25\,\tau$, the

S. Jaensch, W. Polifke, International Journal of Spray and Combustion Dynamics, 2017, http://dx.doi.org/10.1177/1756827716687583.. Reprinted in terms of Creative Commons licence (CC BY-NC).

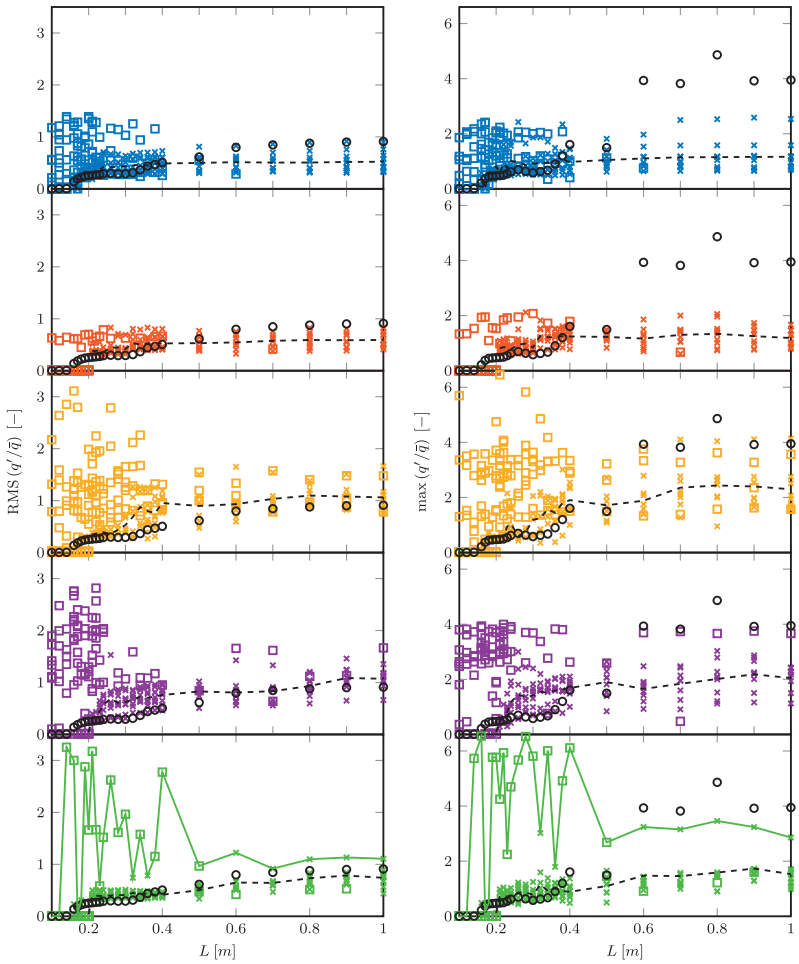

Figure 10. Self-excited thermoacoustic oscillations predicted by the 10 ANNs with the highest fit values on each training set. The training data sets are ordered top to bottom as in Figure 4. Left: comparison in terms of RMS values of the global heat release rate fluctuations; right: comparison in terms of maximum heat release rate fluctuation. Black circles: CFD reference values, colored crosses: solutions oscillating at a dominant frequency f_u in the range of 0 Hz $< f_u <$ 800 Hz predicted by ANNs. These solutions are considered to be physically meaningful. Colored squares: solutions oscillating with a dominant frequency outside of this range. These solutions are considered to be unphysical. Dashed black line: mean value of the physically meaningful solutions predicted by the ANNs. Full green line: connection of the prediction of a selected ANN.

oscillation is in good agreement with the CFD simulation. Unfortunately, numerical errors grow and, after about 35 τ unphysical oscillations are observed. Such numerical instabilities occur irregularly at different plenum lengths and for different ANNs. These oscillations can be identified as its dominant frequency f_u lies outside the interval $0 < f_u < 800$ Hz. In Figure 10, the corresponding data are highlighted with squares.

The variance of the prediction made by the ANNs identified on data set 5 is significantly smaller than the prediction made by the ANNs identified on the other data sets. Only the results of one of these ANNs diverge. This behaviour shows that the prediction of the ANNs improves when longer time series are used to train the ANN. The ANNs identified on data set 5 over-predict the RMS values for short plenum lengths and under-predict the values for long plenum lengths. Nevertheless, the trend of the RMS values is captured. However, the prediction of the maximum heat release fluctuation is poor for long plenum lengths. Only the

S. Jaensch, W. Polifke, International Journal of Spray and Combustion Dynamics, 2017, http://dx.doi.org/10.1177/1756827716687583.. Reprinted in terms of Creative Commons licence (CC BY-NC).

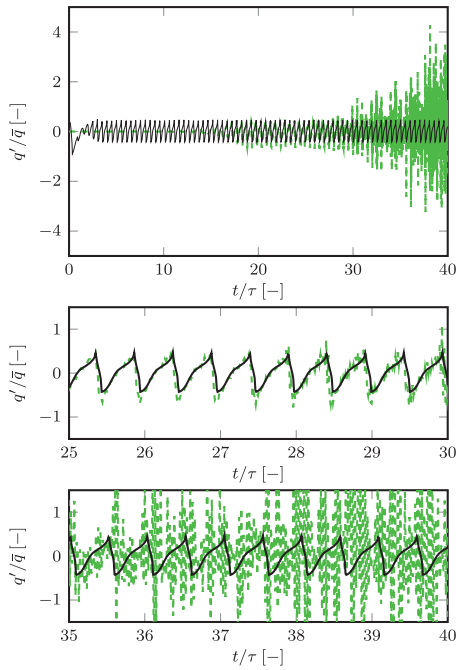

Figure 11. Time series of heat release fluctuation of the self-excited TA oscillations for L = 20 cm. Top: full time series; middle and bottom: zoomed parts of the time series; green-dashed line: prediction of a selected ANN; black line: CFD reference.

prediction of one particular ANN is close to the expected values. In Figure 10, all estimations made by this ANN are connected with a line. This shows that the results of this ANN diverge for short plenum lengths.

5 Conclusion

The capability of ANNs to serve as a model structure in order to deduce nonlinear low-order models of a laminar flame from a CFD simulation was investigated. Via a parameter study a large number of ANNs were identified. A set of 10 optimal ANNs was selected with a fit criterion. The fit criterion only used broadband time series. This allows to evaluate the fit criterion efficiently, since the data used to train the ANNs can be used. Comparing the 10 optimal ANNs allows to estimate the uncertainty of the prediction.

At first the capability of the ANNs to predict the forced response of the flame was analysed. Reasonable agreement was achieved. This shows that over fitting was successfully avoided by the procedure applied to identify and select the optimal ANNs. The validation of the forced response depends strongly on the excitation signal. Therefore, an additional criterion was investigated. The ANNs identified were combined with a thermoacoustic network model in order to model self-excited thermoacoustic oscillations. This comparison is very close to the application. At several working points unphysical numerical instabilities were predicted by the ANNs. It was shown that the variance of the results decreases if very long-time series are used to identify the ANNs. The ANNs identified on the longest of the investigated time series were able to predict the trend of the RMS values. However, the prediction of the maximal fluctuation of the global heat release rate was still poor.

Therefore, we conclude that ANNs, in combination with the identification procedure applied in the present study, do not have the desired properties to deduce nonlinear low-order models from a CFD simulation.

The main problem of the approach is that a good prediction of the forced response does not guarantee a good prediction of self-excited oscillations. This is because the forced response can be analysed for particular excitation signals only. Additionally, in order to obtain an advantage in computational time this signal should be as short as possible. In the present study the longest signal was 30 times longer than a signal needed to determine the FTF. Longer time series would be prohibitively expensive for practical applications.

For the present study the implementation of ANNs provided by Matlab has been used. We consider this implementation as well-established state of the art. The ANN community is rapidly growing and develops a huge number of ANN algorithms, which have their own pros and cons. One of these algorithms may yield better results than the implementation provided by Matlab. This cannot be excluded and is possibly one way to overcome the issues discussed in the present work. Another way to improve the results could be to use different types of excitation signal, e.g. one could use data from simulated self-excited thermoacoustic oscillations. In the author's opinion, however, more sophisticated white- or grey-box models, that account for the physics of the flame dynamics more accurately, are necessary. An additional advantage of grey-box models is that also other information besides the time series of u' and $\dot{q}'$ can be used. For example Jaensch et al.[32] additionally used the acoustic waves emitted by the flame.

Regardless of the way a model was obtained, it should be validated by the systematic procedure proposed in the present study. In particular, the models should be compared in terms of self-excited oscillations.

Acknowledgements

This article has already been published as a non-peer-reviewed publication at the FVV-Frühjahrstagung Turbomaschinen.[35]

S. Jaensch, W. Polifke, International Journal of Spray and Combustion Dynamics, 2017, http://dx.doi.org/10.1177/1756827716687583.. Reprinted in terms of Creative Commons licence (CC BY-NC).

Declaration of Conflicting Interests

The author(s) declared no potential conflicts of interest with respect to the research, authorship, and/or publication of this article.

Funding

The author(s) disclosed receipt of the following financial support for the research, authorship, and/or publication of this article: Research Association for Combustion Engines (Forschungsvereinigung Verbrennung e.V – FVV, project number: 6011150). This support is gratefully acknowledged. The authors also gratefully acknowledge the Gauss Centre for Supercomputing e.V. (www.gauss-centre.eu) for funding this project by providing computing time on the GCS Super-computer SuperMUC at Leibniz Supercomputing Centre (LRZ, www.lrz.de).

References

1. Noiray N, Durox D, Schuller T, et al. A unified framework for nonlinear combustion instability analysis based on the flame describing function. *J Fluid Mech* 2008; 615: 139–167.
2. Dowling AP. A kinematic model of a ducted flame. *J Fluid Mech* 1999; 394: 51–72.
3. Cosic B, Moeck J and Paschereit CO. Prediction of pressure amplitudes of self-excited thermoacoustic instabilities for a partially premixed swirl flame. In: *Proceedings of ASME turbo expo* 2013. San Antonio, Texas, USA: The American Society of Mechanical Engineers GT2013-94160, 2013.
4. Krediet HJ, Beck CH, Krebs W, et al. Saturation mechanism of the heat release response of a premixed swirl flame using LES. *Proc Combust Inst* 2013; 34: 1223–1230.
5. Han X and Morgans AS. Simulation of the flame describing function of a turbulent premixed flame using an open-source LES solver. *Combust Flame* 2015; 162: 1778–1792.
6. Han X, Li J and Morgans AS. Prediction of combustion instability limit cycle oscillations by combining flame describing function simulations with a thermoacoustic network model. *Combust Flame* 2015; 162: 1778–1792.
7. Moeck J and Paschereit C. Nonlinear interactions of multiple linearly unstable thermoacoustic modes. *Int J Spray Combust Dyn* 2012; 4: 1–28.
8. Orchini A, Illingworth S and Juniper M. Frequency domain and time domain analysis of thermoacoustic oscillations with wave-based acoustics. *J Fluid Mech* 2015; 775: 387–414.
9. Kashinath K, Hemchandra S and Juniper MP. Nonlinear phenomena in thermoacoustic systems with premixed flames. *J Eng Gas Turb Power* 2013; 135: 061502.
10. Kashinath K, Waugh IC and Juniper MP. Nonlinear self-excited thermoacoustic oscillations of a ducted premixed flame: bifurcations and routes to chaos. *J Fluid Mech* 2014; 761: 399–430.
11. Kashinath K, Hemchandra S and Juniper MP. Nonlinear thermoacoustics of ducted premixed flames: The influence of perturbation convection speed. *Combust Flame* 2013; 160: 2856–2865.
12. Chakravarthy SR, Balaji C, Katreddy RKR, et al. A framework for numerical simulation of turbulent incompressible unsteady flame dynamics coupled with acoustic calculations in time and frequency domains. In: *n3l – International summer school and workshop on non-normal and nonlinear effects in aero- and thermoacoustics*. Munich, Germany: Technische Universität München, 2013, p.12.
13. Moeck J, Scharfenberg C, Paschereit O, et al. A zero-Mach solver and reduced order acoustic representations for modeling and control of combustion instabilities. In: *Active flow control II, notes on numerical fluid mechanics and multidisciplinary design*, Springer-Verlag Berlin Heidelberg, Germany, Vol. 108, 2010, pp.291–306.
14. Schuermans B, Luebcke H, Bajusz D, et al. Thermoacoustic analysis of gas turbine combustion systems using unsteady CFD. In: *Proceedings of ASME turbo expo 2005*. GT2005-68393. Reno, Nevada: ASME, p.2005.
15. Wall CT. *Numerical methods for large Eddy simulation of acoustic combustion instabilities*. PhD Thesis, Stanford University, 2005.
16. Jaensch S, Merk M, Gopalakrishnan E, et al. Hybrid CFD/ low-order modeling of nonlinear thermoacoustic oscillations. In: *Proceedings of the Combustion Institute*, Vol. 36, 2017, pp. 3827–3834.
17. Polifke W. Black-box system identification for reduced order model construction. *Ann Nucl Energy* 2014; 67C: 109–128.
18. Isermann R and Münchhof M. *Identification of dynamical systems: An introduction with applications*. Advanced textbooks in control and signal processing. Berlin and Heidelberg: Springer-Verlag, 2010.
19. Tangirala AK. *Principles of system identification: Theory and practice*. Boca Raton, Florida, USA: CRC Press, 2014.
20. Nelles O. *Nonlinear system identification: From classical approaches to neural networks and fuzzy models*. Springer-Verlag Berlin Heidelberg, Germany, 2001.
21. Selimefendigil F, Föller S and Polifke W. Nonlinear identification of the unsteady heat transfer of a cylinder in pulsating crossflow. *Comput Fluids* 2012; 53: 1–14.
22. Selimefendigil F and Polifke W. A nonlinear frequency domain system model with coupled modes for limit cycle prediction of thermoacoustic systems. *Int J Spray Comb Dyn* 2011; 3: 303–330.
23. Selimefendigil F. *Identification and analysis of nonlinear heat sources in thermo-acoustic systems*. PhD Thesis, TU München, 2010.
24. Zhang Z, Guan D, Zheng Y, et al. Characterizing premixed laminar flame–acoustics nonlinear interaction. *Energy Convers Manage* 2015; 98: 331–339.
25. Blonbou R, Laverdant A, Zaleski S, et al. Active adaptive combustion control using neural networks. *Combust Sci Technol* 2000; 156: 25–47.
26. Blonbou R, Laverdant A, Zaleski S, et al. Active control of combustion instabilities on a rijke tube using neural networks. *Proc Combust Inst* 2000; 28: 747–755.
27. Vaudrey MA and Saunders WR. Control of combustor instabilities using an artificial neural network. In:

Proceedings of ASME TURBO EXPO, Munich, Germany, 2000-GT-0529, 2000.
28. Kornilov VN, Rook R, ten Thije Boonkkamp JHM, et al. Experimental and numerical investigation of the acoustic response of multi-slit Bunsen burners. *Combust Flame* 2009; 156: 1957–1970.
29. Duchaine F, Boudy F, Durox D, et al. Sensitivity analysis of transfer functions of laminar flames. *Combust Flame* 2011; 158: 2384–2394.
30. Bomberg S, Emmert T and Polifke W. Thermal versus acoustic response of velocity sensitive premixed flames. In: *35th symposium on combustion*. Vol. 35, San Francisco, CA: The Combustion Institute, 2014.
31. Blumenthal RS, Subramanian P, Sujith R, et al. Novel perspectives on the dynamics of premixed flames. *Combust Flame* 2013; 160: 1215–1224.
32. Jaensch S, Emmert T, Silva CF, et al. A grey-box identification approach for thermoacoustic network models. In: *Proceedings of ASME turbo expo*. Düsseldorf, Germany: The American Society of Mechanical Engineers, GT2014-27034, 2014.
33. Silva CF, Jaensch S, Emmert T, et al. On the autoregressive behavior of the intrinsic thermoacoustic feedback loop observed in premixed flames. In: *22nd International congress on sound and vibration (ICSV22)*. Florence, Italy: The International Institute of Acoustics and Vibration (IIAV), 2015.
34. Föller S and Polifke W. Advances in identification techniques for aero-acoustic scattering coefficients from large Eddy simulation. In: *18th International congress on sound and vibration (ICSV18)*. Rio de Janeiro, Brazil: The International Institute of Acoustics and Vibration (IIAV), 2011.
35. Jaensch S and Polifke W. On the uncertainty encountered when modeling self-excited thermoacoustic oscillations with artificial neural networks. In: *International symposium on thermoacoustic instabilities in gas turbines and rocket engines*. Garching, Germany: Technische Universität München (TUM), 2016.

S. Jaensch, W. Polifke, International Journal of Spray and Combustion Dynamics, 2017, http://dx.doi.org/10.1177/1756827716687583..